



Semi-analytical solutions for static and dynamic responses of bi-directional functionally graded nonuniform nanobeams with surface energy effect

Rabab A. Shanab¹ · Mohamed A. Attia²

Received: 1 July 2020 / Accepted: 21 October 2020 / Published online: 12 November 2020
© Springer-Verlag London Ltd., part of Springer Nature 2020

Abstract

In this paper, the bending, buckling, and vibration behaviors of bi-directional functionally graded (BDFG) nonuniform micro/nanobeams are investigated. A new Euler–Bernoulli beam model is developed for BDFG tapered micro/nanobeams using Gurtin–Murdoch surface elasticity theory and modified couple stress theory to capture the effects of surface energy and microstructure stiffening, respectively. The present formulation accounts for the physical neutral surface. The material properties of the bulk and surface continua of the nanobeam are assumed to vary along the thickness and length directions according to power law. Also, the cross section is assumed to vary linearly along the length direction. Hamilton principle is employed to derive the nonclassical equations of motions and boundary conditions. The generalized differential quadrature method (GDQM) is employed to accurately evaluate the variable coefficients of the obtained governing equations. Then after, the Navier’s method is employed for the simply supported BDFG nanobeam for its static bending deflection, critical buckling load, and fundamental frequency. The proposed model is validated by comparing the obtained results with available literature. Effects of different geometrical and material parameters on static and dynamic behaviors of small-scale BDFG nanobeams with the simultaneous effects of microstructure and surface elasticity are comprehensively studied and discussed. Results disclose that the nonuniformity parameters, aspect ratio, dimensionless material length-scale parameter, surface stress, surface elasticity, and gradient indices have a significant effect on the bending, buckling, and free vibration responses of BDFG tapered micro/ nanobeams.

Keywords Bi-directional functionally graded material · Nonuniform nanobeams · Surface elasticity theory · Modified couple stress theory · Semi-analytical solution

1 Introduction

Functionally graded materials (FGMs) are a subclass of composite materials, which are designed to achieve the optimal distribution of constituent materials suitable for certain applications. The superior properties of FGMs such

as designability, lower weight, higher fracture toughness, enhanced thermal properties, lower stress intensity factor, reduced residual thermal stress, reduced interface problems, smaller stress concentration, enhanced corrosion resistance damage resistance, etc., enable them to be suitable candidates for a wide range of different practical fields of engineering and science [1–6]. Based on their application, the spatial variations of the mechanical, thermal, electrical, magnetic, etc. of FGMs are tailored to satisfy particular applications in numerous industrial/medical fields such as energy electronics, aerospace, automotive, military, dentistry, and implants, sensors and thermos-generators [7–10]. In addition, with the rapid advance in nanotechnology, FGMs are currently used in micro/nano-electro-mechanical systems (MEMs/NEMs) such as electrically actuated micro/nano-electromechanical systems [11, 12], atomic force microscopes [13] and also in thin films in the form of shape memory alloys [14]. At small

✉ Rabab A. Shanab
rabab_shanab@yahoo.com

Mohamed A. Attia
mohadlyattia@yahoo.com; madly@zu.edu.eg

¹ Engineering Mathematics Department, Faculty of Engineering, Zagazig University, Zagazig 44519, Egypt

² Department of Mechanical Design and Production Engineering, Faculty of Engineering, Zagazig University, Zagazig 44519, Egypt

scale, both experimental and molecular dynamics simulation results have invariably shown that the small-scale effects cannot be neglected in the analysis of mechanical properties of micro- and nanostructures, especially in micro- and nanobeams applied as sensors and actuators [15–20]. Nowadays, microbeams have been widely used in micro-/nanoelectromechanical systems (MEMS/NEMS) such as micro-engines, micro-turbomachinery, and micro-machining, the ultrasonic piezoelectronic motor, and the development of a micromotor for in vivo medical procedures. However, the classical continuum mechanics theories failed to accurately predict the responses of such small-scale structures.

In the open literature, several size-dependent nonclassical continuum mechanics theories that contain additional material length-scale parameter(s) have been developed to overcome this barrier such as couple stress theory (CST) [21], strain gradient theory (SGT) [22], modified strain gradient theory (MSGT) [20], modified couple stress theory (MCST) [23], nonlocal elasticity theory [24], and nonlocal strain gradient theory (NSGT) [25]. For more details about the nonclassical continuum mechanics theories, the interested readers may refer to the review articles [26–28]. Over these nonclassical continuum mechanics theories, MCST has the merit of involving only one additional higher-order material length-scale parameter to simulate the small-scale effect, in addition to classical material Lamé constants. Based on this feature, the MCST has been employed by many researchers to capture the scale effect on the behavior of microstructures. To evaluate the material length-scale parameter of micro-scale structures, some experiment tests have been performed such as torsion test of slim microcylinders having various diameters [29–31] and bending test of thin microbeams of various thicknesses [20, 32]. However, experimental results proved that different materials have different material length-scale parameters [20, 33]. Furthermore, the surface elasticity theory proposed by Gurtin and Murdoch [34, 35] is widely used to model the surface energy effect for thin and ultrathin structures.

Due to the vast applications of FGM micro/nanostructures, many studies have been performed to investigate the static and dynamic behaviors of FG micro/nanobeams with material variation along the thickness, length, or combination of them. In the framework of the modified couple stress theory, a major part of these studies is focused on microbeams made of transverse functionally graded material (TFG) which are graded along the thickness direction [36–48], and on the axially functionally graded material (AFG) microbeams whose material properties are varied through the length direction [49–55].

As pointed out by Nemat-Ahalla [56], in some engineering applications such as aerospace craft and shuttles, distributions of the stress or thermal field in the structural elements of such advanced machines can be in two or three directions

and thus, the conventional 1D FGMs are not sufficient. As a consequent, there is a need for multi-directional FGMs whose material properties are tailored in two or three directions to obtain more effective high-temperature resistant materials. However, performance of bi-directional (two-dimensional) functionally graded materials (BD-FGMs) beams whose material properties vary along both the thickness and length directions was modeled and investigated by researchers for different mechanical problems. Lü et al. [57] studied the static bending and thermal deformations of BDFG beams with exponential material variation employing the state-space-based differential quadrature method (DQM). Zhao et al. [58] suggested a symplectic framework using the state-space formulation for the static and free vibration analyses of exponential BDFG beams. Şimşek [59] studied the free and forced vibrations of exponential BDFG Timoshenko beam subjected to a moving load using the Lagrange equations and simple polynomial forms. Şimşek [60] also investigated the buckling behavior of BDFG Timoshenko beams with different boundary conditions using Ritz method. Wang et al. [61] investigated the free vibration of BDFG Euler–Bernoulli beam with clamped-free ends employing semi-analytical and semi-numerical methods. Pydah and Sabale [62] analytically studied the flexural response of curved Euler–Bernoulli beams made of power-law BD-FGM. In another study, Pydah and Batra [63] analyzed the static behavior of BDFG thick circular sandwich beam using the shear deformation beam theory. Karamanlı [64] explored the elastostatic behavior of a BDFG beam with different boundary conditions using various beam theories and the symmetric smoothed particle hydrodynamics method. The flexural behavior of BD-FGM sandwich beams is investigated by Karamanlı [65] using a quasi-3D theory and a meshless method. Based on the third-order beam theory, Karamanlı [66] investigated free vibration response of exponential BDFG beams with various boundary conditions using the Lagrange equations. Nguyen et al. [67] used finite element method (FEM) to compute the vibration response of BDFG Timoshenko beams obeying power-law material distribution under a moving concentrated load. Rajasekaran and Khaniki [68] studied the effect of crack type, position, and depth on the dynamic behavior of BDFG cracked Euler–Bernoulli beams using FEM. Li et al. [69] utilized the meshless total Lagrangian corrective smoothed particle method to study the bending behavior of BDFG beams following power-law and exponential distributions in thickness and length directions, respectively. Tang et al. [70] studied the nonlinear free vibration of BDFG Euler–Bernoulli beams by employing the DQM and the homotopy analysis method. Based on the third-order shear deformation and von Kármán nonlinear theories, postbuckling response of BDFG porous beams was investigated by Lei et al. [71] via the DQM. Huang and Ouyang [72] introduced an exact

solution for bending analysis of power-law and exponential BDFG Timoshenko beams based on the classical analysis. The bending and free vibrational behaviors of BDFG cylindrical beams with radially and axially varying material properties based on a high-order beam model are studied by Huang [73]. Chen and Chang [74] studied the free vibration behavior of BDFG Timoshenko beams based on the Chebyshev collocation method. Using the variational iteration method and the Hamiltonian approach, Mohammadian [75] presented closed-form analytical solutions for the nonlinear vibration of damped and undamped BDFG Euler–Bernoulli incorporating higher-order nonlinear terms in the strain field. Using FEM, Nguyen [76] investigated the dynamic behavior of power-law BDFG sandwich beam due to nonuniform motion of a moving point load based on the first-order shear deformation beam theory. Recently, Ghatage et al. [77] presented an exhaustive review on the modeling, analysis, application, and future vision of multi-directional FG structures.

In the framework of nonclassical continuum theories, some studies have been carried for BDFG micro/nanobeams. Using DQM, Nejad et al. [78] and Nejad and Hadi [79] studied the size effects via Eringen's differential nonlocal elasticity theory (EDNET) on the linear buckling and free vibration responses of BDFG Euler–Bernoulli nanobeams with an arbitrary material variation. Karamanlı and Vo [80] developed a finite element model for studying the flexural behavior of BDFG microbeams based on the quasi-3D theory and modified couple stress theory (MCST). In Karamanlı and Vo [81], the size effects on the structural behaviors of BDFG porous microbeams was captured via the MSGT with three material length-scale parameters. Shafiei et al. [82] and Shafiei and Kazemi [83] employed DQM to investigate the influences of the gradation indices, micro-scale, nonlocal parameters, and porosity on the free vibration and buckling responses of porous BDFG microbeams and nanobeams, adopting MCST and EDNET, respectively. In the framework of MCST and quasi-3D deformation theory, Trinh et al. [84] studied the free vibration behavior of exponentially varying BDFG microbeams using the state-space concept. Based on the nonlocal strain gradient theory (NSGT), Li et al. [85] investigated the nonlinear bending response of BDFG Euler–Bernoulli nanobeams with power-law material distribution along thickness using DQM. Yang et al. [86] employed DQM to obtain the nonlinear responses of exponentially varying BDFG Euler–Bernoulli nanobeam based on EDNET and von Kármán geometric nonlinearity. Yu et al. [87, 88] adopted the quasi-3D beam theory and MCST to study the size-dependent bending and free vibration of BDFG microbeams using isogeometric finite element analysis. Based on the Euler–Bernoulli theory and MCST, Khaniki and Rajasekaran [89] used FEM to investigate the mechanical behavior of BDFG nonuniform microbeam whose material properties are arbitrary varied. Forced

vibration analysis of a general nonuniform varying BDFG Euler–Bernoulli microbeam resting on Winkler elastic foundation subjected to a moving harmonic load is presented by Rajasekaran and Khaniki [90]. Utilizing third-order shear beam theory and MCST, Chen et al. [91] investigated the static and dynamic analysis of postbuckling of BDFG microbeams using DQM. This work was extended by Chen et al. [92] to study the free vibration, buckling, and dynamic stability of BDFG microbeams embedded in an elastic medium. Sahmani and Safaei [93, 94] investigated the size-dependent nonlinear free vibration and resonance behaviors of BDFG nanobeams within the context of the hyperbolic shear deformation beam theory and NSGT employing DQM. In another study, Sahmani and Safaei [95] extended this model to study the effect of homogenization scheme of FGM on the nonlinear bending and postbuckling responses of BDFG nanobeams. Rahmani et al. [96] analyzed the vibration response of power-law BDFG rotating porous nanobeams based on Reddy's beam theory and a general nonlocal theory employing DQM. Attia and Mohamed [97, 98] developed a microbeam model based on MCST to explore the static and vibration behaviors of thermal buckling and postbuckling of BDFG nonuniform shear deformable microbeam. Barati et al. [99] investigated the transverse vibration of BDFG nanobeams subjected to a longitudinal magnetic field is investigated via the EDNET. The static bending of Euler–Bernoulli nanobeams made of BDFG material with the method of initial values in the frame of gradient elasticity is studied by Çelik and Artan [100]. The free vibration behavior of BDFG nanobeams is analyzed via EDNET by Dangi et al. [101]. Malik and Das [102] studied the free vibration behavior of rotating BDFG Euler–Bernoulli nanobeam based on EDNET.

According to surface elasticity theory (SET) proposed by Gurtin and Murdoch [34, 35], the surface layers of the bulk continuum material are treated as a two-dimensional membrane of zero thickness with different properties from the bulk continuum. This theory can efficiently incorporate the surface energy effect into the mechanical responses of micro/nanostructures. In recent years, Gurtin–Murdoch surface elasticity theory has been adopted in many studies to explore the surface effects on the bending, buckling, vibration, and instability responses of FGM micro/nanobeam, i.e., [103–112]. Simultaneous effects of surface energy and couple stress have been investigated on the static and dynamic analyses of micro/nanobeams by some authors. Gao and co-workers [113–116] developed a size-dependent model incorporating microstructure and surface energy effects for homogeneous beams using different beam theories. Attia and Mahmoud [117, 118] investigated the mechanics of elastic and viscoelastic Euler–Bernoulli beam on the basis of nonlocal-couple stress elasticity and surface energy theories. Zhang et al. [119] studied the size-dependent behavior of nanobeams incorporating bulk and surface effects. For

FGM micro/nanobeams, Attia [120] and Attia and Rahman [121] explored the mutual effects of microstructure and surface energy on the mechanics of elastic and viscoelastic FG nanobeams. The pull-in stability and freestanding of electromechanically actuated FG nanobeams in the framework of MCST and SET in [122–124]. Shanab et al. [125–127] and Attia et al. [128] presented a comprehensive investigation of nonlinear bending and vibration of TFG Euler–Bernoulli and Timoshenko nanobeams using an integrated couple stress–surface energy model. On the basis of two-phase local/nonlocal formulation, Hosseini-Hashemi et al. [129] studied the damped vibration behavior of viscoelastic Euler–Bernoulli nanobeams in the presence of surface energy. Yin et al. [130, 131] studied the static bending and free vibration behaviors of the nonclassical Bernoulli–Euler and Timoshenko beams based on MCST and SET using isogeometric FE analysis.

From the above literature review, it is noted that most of the researchers are focused on the mechanical behavior of the BDFG microbeams with uniform cross section and in the absence of surface energy effects. To the best of the author’s knowledge, there is no reported work on the mechanics of BDFG micro/nanobeams accounting for the simultaneous effects of cross-section nonuniformity, microstructure, and surface energy. The present study aims to investigate the static bending, buckling, and free vibration behaviors of tapered BDFG nanobeams based on MCST and Gurtin–Murdoch SET to simulate, respectively, the microstructure and surface energy contributions for the first time. All the material properties of the bulk continuum and surface layers including the material length-scale parameter and surface parameters are varies according to power-law in both thickness and length directions. Hamilton’s energy principle has been used to obtain the equations of motion of Euler–Bernoulli nanobeam on the basis of physical neutral surface concept. To this end, the Navier solution in conjunction with GDQM is employed to solve the nonclassical equations for simply supported nanobeams. To authenticate

the preciseness of the developed model and solution procedure, the obtained results are compared with those in the open literature. The influences of different geometrical and material parameters on the static and dynamic responses of nonuniform BDFG micro/ nanobeams are examined and discussed in detail.

2 Theory and formulation

In this section, the size-dependent governing differential equations, and corresponding boundary conditions of a BDFG nonuniform micro/nanoscale beams are exactly derived using the Hamiltonian principle. To model a general micro/nanobeam for mechanical problems, the present formulation considers the simultaneous effect of microstructure and surface energy using the modified couple stress theory and Gurtin–Murdoch surface elasticity theory, respectively, in the framework of continuum mechanics. This is the first time to include the surface energy effects on BDFG tapered nanobeams in the presence of microstructure effect. For this purpose, consider a nonuniform nanobeam whose dimensions with respect to Cartesian coordinate system (x, y, z) are shown in Fig. 1. The middle plane being $z = 0$ with origin at $x = 0$. Both the thickness and width of the nanobeam are assumed to vary along length L as $h(x) = h_0(1 - \beta_h x/L)$ and $b(x) = b_0(1 - \beta_b x/L)$, respectively, where β_h and β_b denote the taperness parameters describing the cross-sectional change along thickness and width directions, respectively; and h_0 and b_0 represent, respectively, the thickness and width at $x = 0$.

2.1 Bi-directional functionally graded material

Due to the continuous grading of the material properties of a BDFG beam along both the axial and transverse directions, the effective material properties are defined in terms of the power law in both directions as follows: [59, 60]

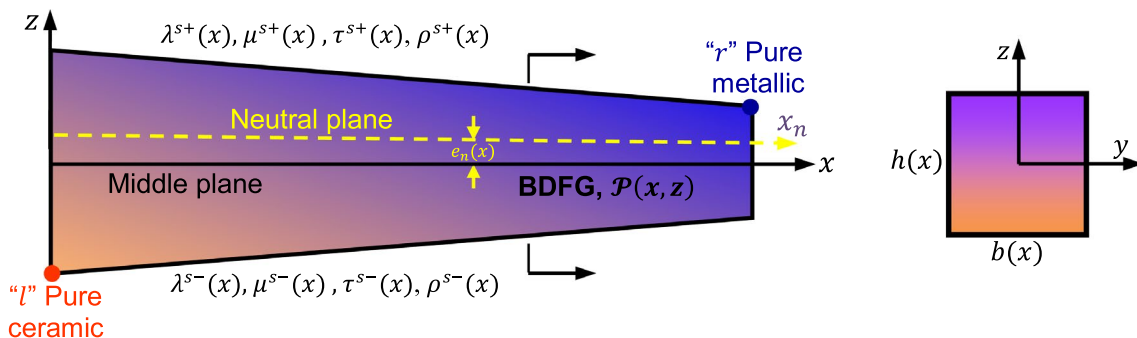


Fig. 1 Schematic sketch of a nonuniform bi-directional functionally graded nanobeam

$$\mathcal{P}(x, z) = \mathcal{P}_l + (\mathcal{P}_r - \mathcal{P}_l)\mathcal{V}_r(x, z), \mathcal{V}_r(z) = \left(\frac{z}{h(x)} + \frac{1}{2}\right)^{k_z} \left(\frac{x}{L}\right)^{k_x}, \mathcal{V}_r(x, z) + \mathcal{V}_l(x, z) = 1, \tag{1}$$

where \mathcal{V}_r is the volume fraction of the constituent at the upper right corner of the beam, and the subscripts l and r represent, respectively, the phases at the lower left and upper right corners of the BDFG beam. In Eq. (1), k_x and k_z stand for non-negative numbers (FGM property gradient indices) that determine the material variation profile through the length and thickness directions, respectively. Following Eq. (1) the variations of the effective Young’s modulus (E^B), mass density (ρ^B), Poisson’s ratio (ν), and variable micro-structure material length-scale (l) of the bulk continuum, can be defined as

$$E^B(x, z) = E_l^B + (E_r^B - E_l^B) \left(\frac{z}{h(x)} + \frac{1}{2}\right)^{k_z} \left(\frac{x}{L}\right)^{k_x}, \tag{2a}$$

$$\rho^B(x, z) = \rho_l^B + (\rho_r^B - \rho_l^B) \left(\frac{z}{h(x)} + \frac{1}{2}\right)^{k_z} \left(\frac{x}{L}\right)^{k_x}, \tag{2b}$$

$$\nu(x, z) = \nu_l + (\nu_r - \nu_l) \left(\frac{z}{h(x)} + \frac{1}{2}\right)^{k_z} \left(\frac{x}{L}\right)^{k_x}, \tag{2c}$$

$$l(x, z) = l_l + (l_r - l_l) \left(\frac{z}{h(x)} + \frac{1}{2}\right)^{k_z} \left(\frac{x}{L}\right)^{k_x}. \tag{2d}$$

The effective surface parameters, surface Lamé’s constants (λ^s and μ^s), surface residual stress (τ^s), and surface mass density (ρ^s) of the BDFG beam are expressed according to the bi-directional power law in Eq. (1), as follows:

$$\lambda^s(x, z) = \lambda_l^s + (\lambda_r^s - \lambda_l^s) \left(\frac{z}{h(x)} + \frac{1}{2}\right)^{k_z} \left(\frac{x}{L}\right)^{k_x}, \tag{3a}$$

$$\mu^s(x, z) = \mu_l^s + (\mu_r^s - \mu_l^s) \left(\frac{z}{h(x)} + \frac{1}{2}\right)^{k_z} \left(\frac{x}{L}\right)^{k_x}, \tag{3b}$$

$$\tau^s(x, z) = \tau_l^s + (\tau_r^s - \tau_l^s) \left(\frac{z}{h(x)} + \frac{1}{2}\right)^{k_z} \left(\frac{x}{L}\right)^{k_x}, \tag{3c}$$

$$\rho^s(x, z) = \rho_l^s + (\rho_r^s - \rho_l^s) \left(\frac{z}{h(x)} + \frac{1}{2}\right)^{k_z} \left(\frac{x}{L}\right)^{k_x}. \tag{3d}$$

Herein and throughout the paper, superscripts “ B ” and “ s ” refer to the bulk and surface continuums, respectively, of the nanobeam.

In Eqs. (1–3a, 3b, 3c, 3d), the position of the midplane (z) is taken as a reference. It is obvious that the variation of the material properties of a BDFG is non-symmetric about the geometric midplane of the beam. Consequently, the associated physical neutral plane deviates from the midplane counterpart [97]. So, it is defined that $e_n = z - z_n$, in which z_n refers to the z -coordinate of the physical neutral plane that can be determined as follows:

$$e_n(x) = \frac{\int_{A(x)} z [\lambda^B(x, z) + 2\mu^B(x, z)] dA}{\int_{A(x)} [\lambda^B(x, z) + 2\mu^B(x, z)] dA}, \tag{4}$$

where e_n is the distance between the midplane and the neutral plane as shown in Fig. 1. It is clear that the position of physical neutral plane is a function of axial direction due to the variations of both the cross section and the material properties along the axial direction. For symmetric variation of the beam material properties about its midplane, the parameter e_n is equal to zero. Lamé’s moduli of the bulk material $\mu^B(x, z)$ and $\lambda^B(x, z)$ are related to Young’s modulus $E^B(x, z)$ and Poisson’s ratio $\nu(x, z)$ of the beam material as follows:

$$\mu^B(x, z) = \frac{E^B(z)}{2(\nu(z) + 1)} \text{ and } \lambda^B(x, z) = \frac{E^B(x, z)\nu(x, z)}{(1 + \nu(x, z))(1 - 2\nu(x, z))}. \tag{5}$$

It is obvious when the Poisson’s ratio effect is neglected, the term $(\lambda^B(x, z) + 2\mu^B(x, z))$ yields to $E^B(x, z)$, as reported in [59, 60, 93, 94].

2.2 Modified couple stress theory

Based on Euler–Bernoulli beam theory, all applied loads and geometry are such that displacement field of a BDFG micro/nanobeam at an arbitrary point at a height (z) measured from the midplane and time (t) can be given as

$$U(x, z, t) = u(x, t) - z_n \frac{\partial w(x, t)}{\partial x}, \tag{6}$$

$$W(x, z, t) = w(x, t),$$

where U and W represent the displacements in axial and transversal directions, respectively, of an arbitrary point (x, y, z) on the beam cross section at time (t). $u(x, t)$ and

$w(x, t)$ are the axial and transverse components of displacement of the point on the physical neutral axis.

In the context of the modified couple stress theory (MCST) proposed by Yang et al. [23], the strain energy of the bulk continuum of deformed micro/nanobeam made of an isotropic linear elastic BDFG is given as

$$\Pi^B = \frac{1}{2} \int_0^L \int_A (\sigma_{ij} \varepsilon_{ij} + m_{ij} \chi_{ij}) dA dx, \quad (7)$$

where ε_{ij} and σ_{ij} are, respectively, the strain tensor and the classical Cauchy stress tensor; and χ_{ij} and m_{ij} are, respectively, the symmetric rotation gradient tensor and deviatoric part of the couple stress tensor. These tensors can be expressed as follows [23]:

$$\varepsilon_{ij} = \frac{1}{2} (u_{i,j} + u_{j,i}), \quad (8a)$$

$$\sigma_{ij} = 2\mu(x, z)\varepsilon_{ij} + \lambda(x, z)\varepsilon_{kk}\delta_{ij}, \quad (8b)$$

$$\chi_{ij} = \frac{1}{2} (\theta_{i,j} + \theta_{j,i}); \theta_i = \frac{1}{2} e_{ijk} u_{k,j}, \quad (9a)$$

$$m_{ij} = 2\mu(x, z)l^2(x, z)\chi_{ij}, \quad (9b)$$

in which, e_{ijk} is the cyclic permutation symbol and δ_{ij} denotes the Kronecker delta. u_i is the displacement vector given by Eq. (6), θ_i is the rotation vector, and $l(x, z)$ denotes the material length-scale parameter which captures the size-effect due to the material microstructures in the nonclassical BDFG beam model. In the aforementioned equations and throughout the paper, the summation convention and standard index notation are used, with the Latin indices running from 1 to 3 and the Greek indices from 1 to 2 unless otherwise indicated.

Based on the kinematic relations of EBBT in Eq. (6), the nonvanishing components of ε_{ij} , σ_{ij} , θ_i , χ_{ij} , and m_{ij} can be, respectively, obtained as

$$\varepsilon_{xx} = \frac{\partial u(x, t)}{\partial x} - z_n \frac{\partial^2 w(x, t)}{\partial x^2}, \quad (10a)$$

$$\sigma_{xx} \equiv (\lambda^B(x, z) + 2\mu^B(x, z)) \left[\frac{\partial u(x, t)}{\partial x} - z_n \frac{\partial^2 w(x, t)}{\partial x^2} \right], \quad (10b)$$

$$\theta_y = -\frac{\partial w(x, t)}{\partial x}, \quad (11a)$$

$$\chi_{xy} = -\frac{1}{2} \frac{\partial^2 w(x, t)}{\partial x^2}, \quad (11b)$$

$$m_{yx} = m_{xy}(x, t) = l(x, z)^2 \mu^B(x, z) \left[-\frac{\partial^2 w(x, t)}{\partial x^2} \right]. \quad (11c)$$

2.3 Surface elasticity theory

In this study, Gurtin–Murdoch theory of surface elasticity is employed to model the interactions between the bulk material and elastic surface of nanoscale structures, Gurtin and Murdoch [33, 34]. In this theory, the surface layer of a bulk elastic material satisfies distinct constitutive equations involving surface elastic constants and surface residual stress. According to the Gurtin–Murdoch surface elasticity theory, the strain energy in the surface layers continuum of deformed micro/nanobeam made of an isotropic linear elastic BDFG can be obtained as [113–115, 117]

$$\Pi^s = \frac{1}{2} \int_0^L \oint_{\partial A} \sigma_{ij}^s(x, t) \varepsilon_{ij}(x, t) dS dx. \quad (12)$$

In accordance with the Gurtin–Murdoch theory of surface elasticity, the surface stress–strain constitutive equations for the surface layers can be introduced as follows [33, 34]:

$$\sigma_{\alpha\beta}^{s\pm} = \tau^{s\pm}(x, z) \delta_{\alpha\beta} + 2(\mu^{s\pm}(x, z) - \tau^{s\pm}(x, z)) \varepsilon_{\alpha\beta}^{\pm} + (\lambda^{s\pm}(x, z) + \tau^{s\pm}(x, z)) \varepsilon_{\gamma\gamma}^{\pm} \delta_{\alpha\beta} + \tau^{s\pm}(x, z) u_{\alpha,\beta}^{\pm}, \quad (13a)$$

$$\sigma_{n\alpha}^{s\pm} = \tau^{s\pm}(x, z) u_{n,\alpha}^{\pm}; (\alpha, \beta = x, y), \quad (13b)$$

where λ^s and μ^s are the surface elastic Lamé's constants and τ^s is the residual surface stress under unstrained conditions (i.e., the surface stress at zero strain). $\sigma_{n\alpha}^s$ is the out-of-plane components of the surface stress tensor. Signs (+) and (−) stand for the upper and lower surface layers at $z = h(x)/2$ and $z = -h(x)/2$, respectively, of the BDFG nanobeam. Following Eqs. (6) and (10a), the nonvanishing components of the surface stresses in terms of the displacement field can be obtained as

$$\sigma_{xx}^s = \tau^{s\pm}(x, z) + (\lambda^{s\pm}(x, z) + 2\mu^{s\pm}(x, z)) \left(\frac{\partial u(x, t)}{\partial x} - z_n \frac{\partial^2 w(x, t)}{\partial x^2} \right), \quad (14a)$$

$$\sigma_{nx}^s = \tau^{s\pm}(x, z) u_{n,x}^s = \tau^{s\pm}(x, z) \frac{\partial w}{\partial x} n_z. \quad (14b)$$

where n_z is the z -component of the unit outward normal vector to the beam lateral surface.

2.4 The equations of motion of BDFG nanobeam based on the surface elasticity

Hamilton’s principle is used to obtain the nonclassical equations of the motion of BDFG tapered nanobeam considering the simultaneous effect of modified couple stress and surface elasticity. Unlike the existing BDFG beam models, the present model accounts for both axial and transverse deformations and the Poisson’s effect is incorporated.

According to Gurtin–Murdoch surface continuum theory of elasticity and modified couple stress theory, the first variation of the total strain energy, including the bulk and surface continuums of a BDFG tapered nanobeam can be given as

$$\delta\Pi^t \equiv \delta\Pi^B + \delta\Pi^s = \frac{1}{2}\delta \int_0^L \left\{ \int_A (\sigma_{xx}\epsilon_{xx} + 2m_{xy}\chi_{xy}) dA + \oint_{\partial A} (\sigma_{xx}^s\epsilon_{xx} + 2\sigma_{nx}^s\epsilon_{nx}) dS \right\} dx, \tag{15}$$

where $\epsilon_{nx} = \frac{1}{2} \frac{\partial w}{\partial x} n_z$. Substitution of Eqs. (10a, 10b), (11a, 11b, 11c), and (14a, 14b), Eq. (15) can be obtained in terms of the stress resultants as follows:

$$\delta\Pi^t = \int_0^L \left[\mathbb{N}(x) \frac{\partial \delta u}{\partial x} - \mathbb{M}(x) \frac{\partial^2 \delta w}{\partial x^2} + \left(C_n^s(x) \frac{\partial w}{\partial x} \right) \frac{\partial \delta w}{\partial x} \right] dx \tag{16}$$

in which,

$$\mathbb{N}(x) = N^B(x) + N^s(x) - \frac{1}{2} C_0^s(x), \tag{17a}$$

$$\mathbb{M}(x) = M^B(x) + M^s(x) + Y^B(x) - \frac{1}{2} C_1^s(x), \tag{17b}$$

The stress and couple-stress resultants of the bulk continuum are given by

$$\begin{Bmatrix} N^B(x) \\ M^B(x) \\ Y^B(x) \end{Bmatrix} \equiv \int_A \begin{Bmatrix} \sigma_{xx} \\ z_n \sigma_{xx} \\ m_{xy} \end{Bmatrix} dA = \begin{Bmatrix} A_{xx}(x) \frac{\partial u}{\partial x} - B_{xx}(x) \frac{\partial^2 w}{\partial x^2} \\ B_{xx}(x) \frac{\partial u}{\partial x} - D_{xx}(x) \frac{\partial^2 w}{\partial x^2} \\ -A_{xz}(x) \frac{\partial^2 w}{\partial x^2} \end{Bmatrix}, \tag{18}$$

where

$$\begin{Bmatrix} A_{xx}(x) \\ B_{xx}(x) \\ D_{xx}(x) \end{Bmatrix} \equiv \int_{b_1(x)}^{b_2(x)} \int_{h_1(x)}^{h_2(x)} (\lambda^B(x, z) + 2\mu^B(x, z)) \begin{Bmatrix} 1 \\ z_n \\ z_n^2 \end{Bmatrix} dz dy, \tag{19a}$$

$$A_{xz}(x) \equiv \int_{b_1(x)}^{b_2(x)} \int_{h_1(x)}^{h_2(x)} \mu(x, z) l^2(x, z) dz dy. \tag{19b}$$

The stress resultants of the surface continuum are given by

$$\begin{Bmatrix} N^s(x) \\ M^s(x) \end{Bmatrix} = \oint_{\partial A} \begin{Bmatrix} \sigma_{xx}^s \\ z_n \sigma_{xx}^s \end{Bmatrix} dS = \begin{Bmatrix} A_{xx}^s(x) \frac{\partial u}{\partial x} - B_{xx}^s(x) \frac{\partial^2 w}{\partial x^2} + C_0^s(x) \\ B_{xx}^s(x) \frac{\partial u}{\partial x} - D_{xx}^s(x) \frac{\partial^2 w}{\partial x^2} + C_1^s(x) \end{Bmatrix}, \tag{20}$$

where

$$\begin{Bmatrix} A_{xx}^s(x) \\ B_{xx}^s(x) \\ D_{xx}^s(x) \end{Bmatrix} \equiv \oint_{\partial A} (\lambda^{s\pm}(x, z) + 2\mu^{s\pm}(x, z)) \begin{Bmatrix} 1 \\ z_n \\ z_n^2 \end{Bmatrix} dS, \tag{21a}$$

$$\begin{Bmatrix} C_0^s(x) \\ C_1^s(x) \\ C_n^s(x) \end{Bmatrix} \equiv \oint_{\partial A} \tau^s(x, z) \begin{Bmatrix} 1 \\ z_n \\ n_z^2 \end{Bmatrix} dS. \tag{21b}$$

In Eqs. (18) and (21a, 21b), dA and dS are the differential area and line elements, respectively.

Performing the partial integration over the time interval $[t_0, t_f]$ and after some mathematical manipulations, the first variation of the strain energy can be obtained as

$$\delta \int_{t_0}^{t_f} \Pi^t = \int_{t_0}^{t_f} \left\{ - \int_0^L \left[\frac{\partial \mathbb{N}(x)}{\partial x} \delta u + \left(\frac{\partial^2 \mathbb{M}(x)}{\partial x^2} + \frac{\partial}{\partial x} \left(C_n^s(x) \frac{\partial w}{\partial x} \right) \right) \delta w \right] dx + \left[\mathbb{N}(x) \delta u + \left(C_n^s(x) \frac{\partial w}{\partial x} + \frac{\partial \mathbb{M}(x)}{\partial x} \right) \delta w - \mathbb{M}(x) \frac{\partial \delta w}{\partial x} \right]_0^L \right\} dt. \tag{22}$$

The first variation of the kinetic energy of the BDFG nanobeam incorporating the effect of surface mass density can be obtained as

$$\begin{aligned} \delta\Pi^k &\equiv \delta \int_0^L \frac{1}{2} \left\{ \int_A \rho^B(x, z) \left(\left(\frac{\partial U}{\partial t} \right)^2 + \left(\frac{\partial W}{\partial t} \right)^2 \right) dA + \oint_{\partial A} \left[\rho^s(x, z) \left(\left(\frac{\partial U}{\partial t} \right)^2 + \left(\frac{\partial W}{\partial t} \right)^2 \right) \right] dS \right\} dx \\ &= \delta \int_0^L \frac{1}{2} \left\{ \int_A \rho^B(x, z) \left(\left(\frac{\partial u}{\partial t} - z_n \frac{\partial^2 w}{\partial x \partial t} \right)^2 + \left(\frac{\partial w}{\partial t} \right)^2 \right) dA + \oint_{\partial A} \left[\rho^s(x, z) \left(\left(\frac{\partial u}{\partial t} - z_n \frac{\partial^2 w}{\partial x \partial t} \right)^2 + \left(\frac{\partial w}{\partial t} \right)^2 \right) \right] dS \right\} dx. \end{aligned} \tag{23}$$

Proceeding the above integration by parts over the time interval $[t_0, t_f]$, one can obtain the following:

$$\begin{aligned} \delta \int_{t_0}^{t_f} \Pi^k dt = & - \int_{t_0}^{t_f} \int_0^L \left\{ \left[I_A(x) \frac{\partial^2 u}{\partial t^2} - I_B(x) \frac{\partial^3 w}{\partial x \partial t^2} \right] \delta u \right. \\ & + \left[I_A(x) \frac{\partial^2 w}{\partial t^2} + I_B(x) \frac{\partial^3 u}{\partial x \partial t^2} + \frac{\partial I_B(x)}{\partial x} \frac{\partial^2 u}{\partial t^2} \right. \\ & \left. \left. - I_D(x) \frac{\partial^4 w}{\partial x^2 \partial t^2} - \frac{\partial I_D(x)}{\partial x} \frac{\partial^3 w}{\partial x \partial t^2} \right] \delta w \right\} dx dt \\ & + \int_{t_0}^{t_f} \left\{ \left[I_B(x) \frac{\partial^2 u}{\partial t^2} - I_D(x) \frac{\partial^3 w}{\partial x \partial t^2} \right] \delta w \right\}_0^L dt \\ & + \int_0^L \left\{ \left[I_A(x) \frac{\partial u}{\partial t} - I_B(x) \frac{\partial^2 w}{\partial x \partial t} \right] \delta u + \left[I_A(x) \frac{\partial w}{\partial t} \right. \right. \\ & \left. \left. - \left[I_B(x) \frac{\partial u}{\partial t} - I_D(x) \frac{\partial^2 w}{\partial x \partial t} \right] \delta \frac{\partial w}{\partial x} \right\}_{t_0}^{t_f} dx, \end{aligned} \tag{24}$$

where the effective mass moments of inertia are given by

$$\begin{Bmatrix} I_A(x) \\ I_B(x) \\ I_D(x) \end{Bmatrix} = \int_{b_1(x)}^{b_2(x)} \int_{h_1(x)}^{h_2(x)} \rho_b(x, z) \begin{Bmatrix} 1 \\ z_n \\ z_n^2 \end{Bmatrix} dz dy + \oint_{\partial A} \rho_s(x, z) \begin{Bmatrix} 1 \\ z_n \\ z_n^2 \end{Bmatrix} dS. \tag{25}$$

From the general expression of the work done by external forces in the modified couple stress theory and in the surface elasticity theory, the virtual work done by the forces applied on the current beam can be written as [46, 113–115, 132]

$$\begin{aligned} \delta \Pi^w = & \int_{\Omega} (\mathbf{f} \cdot \delta \mathbf{u} + \mathbf{f}_{nc} \cdot \delta \boldsymbol{\theta}) d\Omega + \oint_{\partial A} (\bar{\mathbf{t}} \cdot \delta \mathbf{u} + \bar{\mathbf{s}} \cdot \delta \boldsymbol{\theta}) dS \\ & + \int_L P \left(\frac{\partial \delta u}{\partial x} + \frac{\partial w}{\partial x} \frac{\partial \delta w}{\partial x} \right) dx, \end{aligned} \tag{26}$$

where \mathbf{f} and \mathbf{f}_{nc} are, respectively, the body force resultant per unit volume and body couple resultant per unit volume, and $\bar{\mathbf{t}}$ and $\bar{\mathbf{s}}$ are, respectively, the traction resultant per unit area and surface couple resultant per unit area, and S represents the surface of domain Ω . The first variation of work done by the external applied forces on the time interval $[t_0, t_f]$ can be obtained as

$$\begin{aligned} \delta \int_{t_0}^{t_f} \Pi^w = & \int_{t_0}^{t_f} \int_0^L \left\{ \left(f - \frac{\partial P}{\partial x} \right) \delta u \right. \\ & + \left(q - P \frac{\partial^2 w}{\partial x^2} - \frac{\partial P}{\partial x} \frac{\partial w}{\partial x} + \frac{\partial f_{nc}}{\partial x} \right) \delta w \Big\} dx dt \\ & + \int_{t_0}^{t_f} \left\{ (\bar{N} + P) \delta u + (\bar{V} + P \frac{\partial w}{\partial x} - f_{nc}) \delta w - (\bar{M}_c + \bar{M}_{nc}) \frac{\partial \delta w}{\partial x} \right\}_0^L dt, \end{aligned} \tag{27}$$

in which, f and q are the distributed axial and transverse loads per unit length along the x -axis; P is the applied external compressive axial; and f_{nc} is the y - component of the body couple per unit length along the x -axis. \bar{N} and \bar{V} are the applied axial force and transverse force at the two ends of the beam, respectively; and \bar{M}_c and \bar{M}_{nc} denote the classical

and non-classical bending moments due to, respectively, the normal stress component σ_{xx} and the couple stress component m_{xy} at the two ends of the microbeam.

To this end, the Hamilton’s principle states that

$$\delta \int_{t_0}^{t_f} [\Pi^k - (\Pi^t - \Pi^w)] dt = 0. \tag{28}$$

Substituting Eqs. (22), (24) and (27) into Eq. (28), applying the fundamental lemma of calculus of variation and invoking the condition of zero variation at times $t = t_0$ and $t = t_f$, the governing equations of the nonuniform BDFG nanobeam are obtained as the follows:

$$\delta u \Rightarrow -I_A(x) \frac{\partial^2 u}{\partial t^2} + I_B(x) \frac{\partial^3 w}{\partial x \partial t^2} + \frac{\partial \mathbb{N}(x)}{\partial x} + f - \frac{\partial P}{\partial x} = 0, \tag{29a}$$

$$\begin{aligned} \delta w \Rightarrow & -I_A(x) \frac{\partial^2 w}{\partial t^2} - I_B(x) \frac{\partial^3 u}{\partial x \partial t^2} - \frac{\partial I_B(x)}{\partial x} \frac{\partial^2 u}{\partial t^2} \\ & + I_D(x) \frac{\partial^4 w}{\partial x^2 \partial t^2} + \frac{\partial I_D(x)}{\partial x} \frac{\partial^3 w}{\partial x \partial t^2} + \frac{\partial^2 \mathbb{M}(x)}{\partial x^2} \\ & + (C_{n1}(x) - P) \frac{\partial^2 w}{\partial x^2} + \left(\frac{\partial C_{n1}(x)}{\partial x} - \frac{\partial P}{\partial x} \right) \frac{\partial w}{\partial x} \\ & + \frac{\partial f_{nc}}{\partial x} + q = 0, \end{aligned} \tag{29b}$$

with the following boundary conditions:

$$\delta u : \text{Either } u = \tilde{u} \text{ or } -\mathbb{N}(x) + (\bar{N} + P) = 0, \tag{30a}$$

$$\begin{aligned} \delta w : \text{Either } w = \tilde{w} \text{ or } & \frac{\partial \mathbb{M}(x)}{\partial x} + C_n^s(x) \frac{\partial w}{\partial x} - P \frac{\partial w}{\partial x} \\ & - I_B(x) \frac{\partial^2 u}{\partial t^2} + I_D(x) \frac{\partial^3 w}{\partial x \partial t^2} + f_{nc} - \bar{V} = 0 \text{ or } w = \tilde{w}, \end{aligned} \tag{30b}$$

$$\delta \frac{\partial w}{\partial x} : \text{Either } \frac{\partial w}{\partial x} = \tilde{\frac{\partial w}{\partial x}} \text{ or } \mathbb{M}(x) - (\bar{M}_c + \bar{M}_{nc}) = 0. \tag{30c}$$

2.5 The equations of motion of BDFG nanobeam in terms of the displacement field

Substitution of Eqs. (17a, 17b), (18) and (20) into Eq. (29a, 29b) gives the following size-dependent governing differential equations in terms of the displacement field:

$$\begin{aligned} \delta u \Rightarrow & -I_A(x) \frac{\partial^2 u}{\partial t^2} + I_B(x) \frac{\partial^3 w}{\partial x \partial t^2} \\ & + \mathcal{A}_{11}(x) \frac{\partial^2 u}{\partial x^2} + \frac{\partial \mathcal{A}_{11}(x)}{\partial x} \frac{\partial u}{\partial x} \\ & - \mathcal{B}_{11}(x) \frac{\partial^3 w}{\partial x^3} - \frac{\partial \mathcal{B}_{11}(x)}{\partial x} \frac{\partial^2 w}{\partial x^2} \\ & + \frac{1}{2} \frac{\partial C_0^s(x)}{\partial x} + f_u - \frac{\partial P}{\partial x} = 0, \end{aligned} \tag{31a}$$

$$\begin{aligned} \delta w \Rightarrow & -I_A(x) \frac{\partial^2 w}{\partial t^2} - I_B(x) \frac{\partial^3 u}{\partial x \partial t^2} - \frac{\partial I_B(x)}{\partial x} \frac{\partial^2 u}{\partial t^2} \\ & + I_D(x) \frac{\partial^4 w}{\partial x^2 \partial t^2} + \frac{\partial I_D(x)}{\partial x} \frac{\partial^3 w}{\partial x \partial t^2} + \mathcal{B}_{11}(x) \frac{\partial^3 u}{\partial x^3} \\ & + 2 \frac{\partial \mathcal{B}_{11}(x)}{\partial x} \frac{\partial^2 u}{\partial x^2} + \frac{\partial^2 \mathcal{B}_{11}(x)}{\partial x^2} \frac{\partial u}{\partial x} - \mathcal{D}_{11}(x) \frac{\partial^4 w}{\partial x^4} \\ & - 2 \frac{\partial \mathcal{D}_{11}(x)}{\partial x} \frac{\partial^3 w}{\partial x^3} + \left(C_n^s(x) - P - \frac{\partial^2 \mathcal{D}_{11}(x)}{\partial x^2} \right) \frac{\partial^2 w}{\partial x^2} \\ & + \left(\frac{\partial C_n^s(x)}{\partial x} - \frac{\partial P}{\partial x} \right) \frac{\partial w}{\partial x} + \frac{1}{2} \frac{\partial^2 C_1^s(x)}{\partial x^2} + \frac{\partial f_{nc}}{\partial x} + q = 0. \end{aligned} \tag{31b}$$

Moreover, the corresponding boundary conditions at $x = 0$ and $x = L$ are as follows:

$$\delta u : \text{Either } u = \tilde{u} \text{ or } \mathcal{A}_{11}(x) \frac{\partial u}{\partial x} - \mathcal{B}_{11}(x) \frac{\partial^2 w}{\partial x^2} + \frac{1}{2} C_0^s(x) - (\bar{N} + P) = 0, \tag{32a}$$

$$\begin{aligned} \delta w : \text{Either } w = \tilde{w} \text{ or } & -I_B(x) \frac{\partial^2 u}{\partial t^2} + I_D(x) \frac{\partial^3 w}{\partial x \partial t^2} \\ & + \left(C_n^s(x) - P \right) \frac{\partial w}{\partial x} + \mathcal{B}_{11}(x) \frac{\partial^2 u}{\partial x^2} + \frac{\partial \mathcal{B}_{11}(x)}{\partial x} \frac{\partial u}{\partial x} \\ & - \mathcal{D}_{11}(x) \frac{\partial^3 w}{\partial x^3} - \frac{\partial \mathcal{D}_{11}(x)}{\partial x} \frac{\partial^2 w}{\partial x^2} \\ & + \frac{1}{2} \frac{\partial C_1^s(x)}{\partial x} + f_{nc} - \bar{V} = 0, \end{aligned} \tag{32b}$$

$$\begin{aligned} \frac{\partial \delta w}{\partial x} : \text{Either } \frac{\partial w}{\partial x} = \frac{\partial \tilde{w}}{\partial x} \text{ or } & \mathcal{B}_{11}(x) \frac{\partial u}{\partial x} \\ & - \mathcal{D}_{11}(x) \frac{\partial^2 w}{\partial x^2} + \frac{1}{2} C_1^s(x) - (\bar{M}_c + \bar{M}_{nc}) = 0, \end{aligned} \tag{32c}$$

with

$$\left\{ \begin{matrix} \mathcal{A}_{11}(x) \\ \mathcal{B}_{11}(x) \\ \mathcal{D}_{11}(x) \end{matrix} \right\} = \left\{ \begin{matrix} A_{xx}(x) + A_{xx}^s(x) \\ B_{xx}(x) + B_{xx}^s(x) \\ D_{xx}(x) + D_{xx}^s(x) + A_{xz}(x) \end{matrix} \right\}. \tag{33}$$

When the material gradation is assumed in thickness direction only and by neglecting the axial displacement

component, the obtained equation of motion and boundary conditions for the transverse displacement are identical with those reported in [120, 121]. Moreover, without considering surface energy and the material gradation in the axial direction, the obtained governing equations and associated boundary conditions of a uniform transverse functionally graded (TFG) microbeam are the same as those presented in [46].

3 Solution procedure

In general, deriving an analytical solution of the equations of motion (Eqs. 31a, 31b) is quite difficult because of their variable coefficients attributed to the nature of bi-directional material nonhomogeneity and the nonuniform cross section. In addition, accounting for the physical neutral axis as a function of axial direction of the beam and considering the gradation of all the material properties of both the bulk and surface continua makes the problem more complex. However, obtaining closed form formulas for the governing equations coefficients is quite difficult. To solve this issue, these coefficients are numerically calculated in an accurate way using quadrature method at each point of coordinate x . In this circumstance, the generalized differential quadrature method (GDQM) is employed to translate Eqs. (31a, 31b) into a set of coupled fourth-order ordinary differential equations. Besides, with the help of GDQM, the derivative of the discretized calculated coefficients with respect to coordinate x is easily obtained. First, the procedure of GDQM is briefly reviewed.

3.1 Generalized differential quadrature method

The generalized differential quadrature method (GDQM), as an efficient and effective method in differentiating smooth functions, is employed to obtain the derivatives of the coefficients with respect to coordinate x arise in the governing equations, i.e., $\partial \mathcal{B}_{11}(x) / \partial x, \partial^2 \mathcal{B}_{11}(x) / \partial x^2, \dots$ etc. For this purpose, let the nanobeam length ($0 \leq x \leq L$) is discretized to N sampling points along the axial direction according to the Chebyshev–Gauss–Lobatto formula as

$$x_i = \frac{1}{2} \left[1 - \cos \left(\frac{i-1}{N-1} \pi \right) \right], \quad i = 1, 2, \dots, N, \tag{34}$$

where the inner sampling points x_i are not equally spread in the domain.

In the framework of the GDQM, the r th-order derivative vector of any continuously function (coefficient) can be expressed as follows:

$$F^{(r)} = \mathcal{D}^r F, \tag{35a}$$

with

$$F^{(r)} = \left[f_1^{(r)}, f_2^{(r)}, \dots, f_n^{(r)} \right]^T \text{ and } f_i^{(r)} = \left. \frac{d^r f}{dx^r} \right|_{x_i}, \tag{35b}$$

where \mathcal{D}^r is the r th-order derivative weighting coefficient matrix of dimension $N \times N$. If $r = 1$, the first-order derivative weighting coefficient matrix (\mathcal{D}^1) is computed as follows [133, 134]:

$$\mathcal{D}_{ij}^1 = \begin{cases} \frac{1}{x_i - x_j} \prod_{m=1, m \neq i, m \neq j}^N \frac{x_i - x_m}{x_j - x_m} & i \neq j \\ \sum_{m \neq i, m=1}^N \frac{1}{x_m - x_i} & i = j \end{cases}, \tag{36}$$

and $\mathcal{D}^r = \mathcal{D}^1 \mathcal{D}^{r-1}$ for $r \geq 2$.

For simplicity, in the following subsections, the notation of the discretized calculated coefficients at each node will be unchangeable, just dropping (x) . The corresponding vector of the first and second derivates of any coefficient will be noted by subscripts d and dd , respectively.

3.2 Semi-analytical solutions

After evaluating the nodal values of the coefficients as well as their derivatives accurately, the Navier-type solution is developed for nonuniform BDFG simply supported nanobeam in the form of power series with M terms. Equations (31a, b) are analytically solved to obtain the static bending, buckling, and free vibration of BDFG nanobeam. The displacement field is assumed as follows:

$$u(x, t) = \sum_{n=1}^M U_n \cos(\alpha_n x) e^{i\omega t} \text{ and } w(x, t) = \sum_{n=1}^M W_n \sin(\alpha_n x) e^{i\omega t}, \tag{37}$$

where $i = \sqrt{-1}$, $\alpha_n = n\pi/L$, ω is the fundamental linear frequency, and U_n and W_n are the unknown Fourier coefficients to be determined.

Substituting Eqs. (37) into Eqs. (31a, 31b) yields

$$\begin{aligned} e^{i\omega t} \sum_{n=1}^M & - [A_{11} \alpha_n^2 \cos(\alpha_n x) + A_{11d} \alpha_n \sin(\alpha_n x) - \omega^2 I_A \cos(\alpha_n x)] U_n \\ & + [B_{11} \alpha_n^3 \cos(\alpha_n x) + B_{11d} \alpha_n^2 \sin(\alpha_n x) - \omega^2 [I_B \alpha_n \cos(\alpha_n x)]] W_n \\ & + C_{0d}^s + f_u - \frac{\partial P}{\partial x} = 0, \end{aligned} \tag{38a}$$

$$\begin{aligned} e^{i\omega t} \sum_{n=1}^M & [-D_{11} \alpha_n^4 \sin(\alpha_n x) + 2D_{11d} \alpha_n^3 \cos(\alpha_n x) \\ & - (C_n^s - D_{11dd}) \alpha_n^2 \sin(\alpha_n x) + C_{nd}^s \alpha_n \cos(\alpha_n x) + P \alpha_n^2 \sin(\alpha_n x) \\ & + \omega^2 [I_D \alpha_n^2 \sin(\alpha_n x) + I_A \sin(\alpha_n x) - I_{Dd} \alpha_n \cos(\alpha_n x)]] W_n \\ & + [B_{11} \alpha_n^3 \sin(\alpha_n x) - 2B_{11d} \alpha_n^2 \cos(\alpha_n x) \\ & - B_{11dd} \alpha_n \sin(\alpha_n x) + \omega^2 [I_{Bd} \cos(\alpha_n x) - I_B \alpha_n \sin(\alpha_n x)]] U_n \\ & + C_{1dd}^s + q + \frac{\partial f_{nc}}{\partial x} = 0. \end{aligned} \tag{38b}$$

For simplicity, the terms C_{0d}^s and $C_{1dd}^s(x)$ are dropped from Eqs. (38a) and (38b), respectively.

3.2.1 Semi-analytical solution for static bending

The static bending problem of simply supported nanobeam is obtained from Eqs. (38a) and (38b) by setting ω to zero and the external forces P and f body couple f_{nc} are also set to zero. The applied transverse load q is expanded in Fourier series as follows:

$$q(x) = \sum_{n=1}^{\infty} Q_n \sin(\alpha_n x), \tag{39a}$$

$$Q_n = 2 \int_0^L q(x) \sin(\alpha_n x) dx, \tag{39b}$$

where the coefficient Q_n is determined according to the applied load, i.e., for a uniform load with load intensity q_0 , $Q_n = 4q_0/n\pi$, ($n = 1, 3, 5, \dots$).

Multiplying Eq. (38a) and (38b) by $\cos(\alpha_m x)$ and $\sin(\alpha_m x)$, respectively, $m = 1, 2, 3, \dots, M$, and integrating the resulting equations with respect to x from 0 to L , the following system of linear algebraic equations of the unknown vectors of coefficients W_n and U_n is obtained:

$$\begin{bmatrix} [K_{11}] & [K_{12}] \\ [K_{21}] & [K_{22}] \end{bmatrix} \begin{Bmatrix} W_n \\ U_n \end{Bmatrix} = \begin{Bmatrix} 0 \\ [Q_2] \end{Bmatrix}. \tag{40}$$

Then, by solving the above algebraic system, the displacement field amplitudes can be obtained as

$$\begin{Bmatrix} W_n \\ U_n \end{Bmatrix} = [K]^{-1} Q, \tag{41}$$

in which,

$$\begin{Bmatrix} \mathbb{K}_{11}(n, m) \\ \mathbb{K}_{12}(n, m) \\ \mathbb{K}_{21}(n, m) \\ \mathbb{K}_{22}(n, m) \end{Bmatrix} = \int_0^L \left\{ \begin{array}{l} [\mathcal{B}_{11}\alpha_n^3 \cos(\alpha_n x) + \mathcal{B}_{11d}\alpha_n^2 \sin(\alpha_n x)] \cos(\alpha_m x) \\ [-\mathcal{A}_{11}\alpha_n^2 \cos(\alpha_n x) - \mathcal{A}_{11d}\alpha_n \sin(\alpha_n x)] \cos(\alpha_m x) \\ \{(\mathcal{D}_{11dd} - \mathcal{C}_n^s)\alpha_n^2 - \mathcal{D}_{11}\alpha_n^4\} \sin(\alpha_n x) + \{2\mathcal{D}_{11d}\alpha_n^3 + \mathcal{C}_{nd}^s\alpha_n\} \cos(\alpha_n x) \\ [\mathcal{B}_{11}\alpha_n^3 - \mathcal{B}_{11d}\alpha_n] \sin(\alpha_n x) - 2\mathcal{B}_{11d}\alpha_n^2 \cos(\alpha_n x) \end{array} \right\} \sin(\alpha_m x) dx, \tag{42}$$

$$\mathbb{Q}_2(n, m) = \int_0^L [\mathcal{Q}_n \sin(\alpha_n x)] \sin(\alpha_m x) dx. \tag{43}$$

3.2.2 Semi-analytical solution for buckling

The critical buckling load can be obtained from Eqs. (38a) and (38b) after setting all the external loads except P to zero and ω is also set to zero. With some mathematical operations, one gets the following matrix form of coupled system of equations

$$\left[\begin{bmatrix} \mathbb{K}_{11} & \mathbb{K}_{12} \\ \mathbb{K}_{21} & \mathbb{K}_{22} \end{bmatrix} - \begin{bmatrix} 0 & 0 \\ \mathbb{P}_{21} & 0 \end{bmatrix} \right] \begin{Bmatrix} W_n \\ U_n \end{Bmatrix} = \begin{Bmatrix} 0 \\ 0 \end{Bmatrix}, \tag{44}$$

with

$$\mathbb{P}_{21}(n, m) = P \int_0^L \alpha_n^2 \sin(\alpha_n x) \sin(\alpha_m x) dx, \tag{45}$$

where the elements of $[\mathbb{K}]$ are pre-defined in Eqs. (42). Equation (44) represents a standard eigenvalue problem and has nontrivial solution only for a critical axial load $P_{cr}(n)$, by setting the determinant of its coefficient matrix to zero.

3.2.3 Semi-analytical solution for free vibration

For free vibration analysis, setting all the external forces in Eqs. (38a) and (38b) to zero leads to

$$\left(\left[\begin{bmatrix} \mathbb{K}_{11} & \mathbb{K}_{12} \\ \mathbb{K}_{21} & \mathbb{K}_{22} \end{bmatrix} + \begin{bmatrix} \mathbb{M}_{11} & \mathbb{M}_{12} \\ \mathbb{M}_{21} & \mathbb{M}_{22} \end{bmatrix} \omega^2 \right) \begin{Bmatrix} W_n \\ U_n \end{Bmatrix} = \begin{Bmatrix} 0 \\ 0 \end{Bmatrix}, \tag{46}$$

where

$$\begin{Bmatrix} \mathbb{M}_{11}(n, m) \\ \mathbb{M}_{12}(n, m) \\ \mathbb{M}_{21}(n, m) \\ \mathbb{M}_{22}(n, m) \end{Bmatrix} = \int_0^L \left\{ \begin{array}{l} -I_B \alpha_n \cos(\alpha_n x) \cos(\alpha_m x) \\ I_A \cos(\alpha_n x) \cos(\alpha_m x) \\ \{I_D \alpha_n^2 + I_A\} \sin(\alpha_n x) - I_{Dd} \alpha_n \cos(\alpha_n x) \\ [I_{Bd} \cos(\alpha_n x) - I_B \alpha_n \sin(\alpha_n x)] \sin(\alpha_m x) \end{array} \right\} dx. \tag{47}$$

Equation (47) represents a polynomial eigenvalue problem in the form

$$([\mathbb{K}] + [\mathbb{M}]\omega^2)X = 0, \tag{48}$$

which is numerically solved to obtain the fundamental frequency ω .

To this end, the integrals in Eqs. (42, 43, 45, 47) are implemented via numerical differential integral quadrature method (DIQM) [133, 134].

4 Model verification

Before performing the parametric study, this section is devoted to the validation and accuracy assessment of the developed nonclassical model and the proposed solution procedure. Since there are no published data for BDFG micro/nanobeams including the simultaneous effects of surface energy and modified couple stress, we compared the present Euler–Bernoulli model results for bending, buckling, and free vibration behaviors with those available in the literature for simply supported micro/nanobeams.

The dimensionless center deflection of a simply supported homogeneous microbeam under a uniformly distributed load is presented in Table 1, based on MCST and compared with references [38, 45]. Table 2 shows the validation of the present model by comparing the dimensionless center deflection based on the classical and integrated modified couple stress–surface energy formulations with the reported results in [114, 125].

To check the accuracy of the present buckling analysis, different numerical examples are solved and compared with the available literatures [60, 135, 136]. A comparison of the critical buckling load of a homogeneous microbeam based on surface energy formulation is provided in Table 3, whereas Table 4 validates the predicted critical buckling load of a BDFG uniform beam based on the classical elasticity theory at various gradient indices. Table 5 compares the present classical dimensionless critical buckling load of AFG tapered beam and that reported by Shahba et al. [135].

Tables 6, 7, 8 are devoted to comparing the fundamental frequency obtained via the current model and those reported in the previous studies. The fundamental frequency are presented and compared in Tables 6, 7, 8 for, respectively, a homogeneous uniform nanobeam including both effects of the modified couple stress and surface energy, a BDFG uniform microbeam based on modified couple stress theory, and

Table 1 Comparison of the dimensionless center deflection $\bar{w} = 100(wEI/(qL^4))$ of a homogeneous microbeam under uniform load based on the MCST analysis ($E = 1.44$ GPa, $\nu = 0.38$, $h = 88$ μm , $L = 20h$ and $b = 2h$)

	Dimensionless material length parameter (l/h)					
	0.0	0.2	0.4	0.6	0.8	1.0
Present	1.3021	1.1092	0.7679	0.5076	0.3442	0.2435
Reddy [45]	1.3021	1.1092	0.7679	0.5076	0.3442	0.2435
Arbind and Reddy [38]	1.3021	–	–	0.5076	–	0.2435

Table 2 Comparison of dimensionless center deflection ($\bar{w} = w/h$) of homogeneous nanobeam under midpoint load based on classical and integrated couple stress–surface energy analyses ($E = 90$ GPa, $\rho = 2700$, $\nu = 0.23$, $l = 6.58$ μm , $\lambda^s = 3.4939$ N/m, $\mu^s = -5.4251$ N/m, $\tau^s = 0.5689$ N/m, $L = 20h$ and $b = 2h$)

	Classical elasticity theory				Integrated couple stress–surface energy			
	Thickness-to-material length-scale parameter ratio, h/l							
	1	2	4	6	1	2	4	6
Present	0.0221	0.0055	0.0014	0.0006	0.0043	0.0027	0.0011	0.0006
Gao [114]	0.0223	0.0056	0.0014	0.0006	0.0043	0.0027	0.0011	0.0006
Shanab et al. [125]	0.0223	0.0056	0.0014	–	0.0043	0.0027	0.0011	–

Table 3 Comparison of the dimensionless critical buckling load $\bar{P}_{cr} = 10^5 \times P_{cr}/(EL^2)$ of homogeneous nanobeam based on surface energy formulation ($E = 210$ GPa, $\nu = 0.24$, $h = 5$ nm, $L = 10h$ and $b = h$)

	Surface modulus of elasticity, E_s			Dimensionless surface residual stress, $\bar{\tau}_s = (\tau_s/EL)$		
	– 7.262	0.0	7.262	– 0.626	0.0	0.626
	Present	7.7696	8.2247	8.6797	8.2246	8.2247
Hashemian et al. [136]	7.8834	8.2247	8.5660	8.2224	8.2247	8.2269

Table 4 Comparison of the dimensionless critical buckling load $\bar{P}_{cr} = P_{cr}(L^2/E_0I)$ for BDFG beam based on classical analysis ($E_r/E_L = 2$ and $L/h = 50$)

k_x	Present (EBT)					Simsek [60] (TBT)				
	$k_z=0.0$	$k_z=0.5$	$k_z=1$	$k_z=2$	$k_z=5$	$k_z=0.0$	$k_z=0.5$	$k_z=1$	$k_z=2$	$k_z=5$
0	19.7392	15.7575	14.2561	13.2006	12.3298	19.7099	15.7385	14.2383	13.1845	12.3149
0.5	16.5678	13.9372	12.9591	12.2591	11.6279	16.5451	13.9210	12.9437	12.2448	11.6145
1	14.5113	12.7473	12.0898	11.6090	11.1483	14.4924	12.7328	12.0758	11.5957	11.1357
2	12.3414	11.4478	11.1106	10.8563	10.5954	12.3271	11.4355	11.0985	10.8445	10.5839
5	10.5264	10.2993	10.2131	10.1460	10.0728	10.5157	10.2889	10.2026	10.1356	10.0623

Table 5 Comparison of the dimensionless critical buckling load $\bar{P}_{cr} = P_{cr}(L^2/E_0I)$ for AFG tapered beam based on classical analysis, with $E(x) = E_0(1 + x/L)$

β_h	Present				Shahba et al. [135]			
	$\beta_b = 0$	0.2	0.4	0.6	$\beta_h = 0$	0.2	0.4	0.6
0	14.5113	13.1398	11.6969	10.1451	14.5113	13.1398	11.6969	10.1451
0.2	10.6860	9.5971	8.4543	7.2285	10.6860	9.5971	8.4543	7.2285
0.4	7.2831	6.4715	5.6228	4.7165	7.2831	6.4715	5.6228	4.7164
0.6	4.3289	3.7894	3.2286	2.6343	4.3287	3.7892	3.2284	2.6338

Table 6 Comparison of fundamental frequency (MHz) for homogeneous nanobeam based on classical and integrated couple stress–surface energy analyses ($E = 90 \text{ GPa}, \rho = 2700, \nu = 0.23, l = 6.58 \text{ }\mu\text{m}, \lambda^s = 3.4939 \text{ N/m}, \mu^s = -5.4251 \text{ N/m}, \tau^s = 0.5689 \text{ N/m}, L = 20h \text{ and } b = 2h$)

	Classical elasticity theory				Integrated couple stress–surface energy			
	Thickness-to-material length-scale parameter ratio, h/l							
	1	6	11	16	1	6	11	16
Present	6.7222	1.1204	0.6111	0.4201	15.3416	1.1841	0.6217	0.4236
Gao [114]	6.7222	1.1204	0.6111	0.4201	15.3416	1.1841	0.6217	0.4236
Attia et al. [128]	6.7222	1.1204	0.6111	0.4201	15.3425	1.1842	0.6217	0.4236

Table 7 Comparison of the dimensionless fundamental frequency $\bar{\omega} = \omega(L^2 \sqrt{\rho_r/E_r}/h)$ for BDFG uniform microbeam based on the classical and couple stress analysis ($l_L = 15 \text{ }\mu\text{m}, l_r = 22.5 \text{ }\mu\text{m}, h = l_r, L = 100h, b = h$)

Analysis	k_z	Present (Euler beam theory)					Chen et al. [92] (Reddy beam theory)				
		$k_x=0.5$	$k_x=1.0$	$k_x=2$	$k_x=5$	$k_x=10$	$k_x=0.5$	$k_x=1.0$	$k_x=2$	$k_x=5$	$k_x=10$
		CL	0.5	2.0602	1.8499	1.5872	1.3349	1.2610	2.0488	1.8373	1.5753
	1	1.8523	1.7021	1.5103	1.3157	1.2562	1.8408	1.6900	1.4989	1.3059	1.2471
	2	1.6840	1.5853	1.4499	1.3004	1.2524	1.6728	1.5737	1.4388	1.2907	1.2433
	5	1.5809	1.5069	1.4024	1.2859	1.2486	1.5687	1.4948	1.3912	1.2762	1.2394
	10	1.5169	1.4512	1.3645	1.2735	1.2452	1.5041	1.4390	1.3535	1.2638	1.2361
CS	0.5	4.4628	3.7381	2.9819	2.3739	2.2124	4.5013	3.7688	2.9936	2.3659	2.1989
	1	3.9697	3.4061	2.8176	2.3331	2.2020	3.9999	3.4289	2.8247	2.3240	2.1882
	2	3.4684	3.0679	2.6471	2.2900	2.1912	3.4873	3.0807	2.6484	2.2792	2.1769
	5	2.9427	2.7089	2.4597	2.2406	2.1787	2.9462	2.7088	2.4533	2.2277	2.1639
	10	2.6631	2.5132	2.3533	2.2115	2.1714	2.6579	2.5061	2.3429	2.1975	2.1563

Table 8 Convergence of the dimensionless frequency $(\bar{\omega} = \omega L^2 \sqrt{\rho_L A/E_L I})$ for AFG tapered beam based on classical analysis, with $E(x) = E_0(1 + (x/L))$ and $\rho(x) = \rho_0(1 + (x/L) + (x/L)^2)$

β_h	Present				Shahba et al. [134]			
	$\beta_b = 0$	0.2	0.4	0.6	$\beta_h = 0$	0.2	0.4	0.6
0	9.0239	9.0553	9.0822	9.0951	9.0286	9.0599	9.0867	9.0994
0.2	8.1309	8.1430	8.1466	8.1305	8.1341	8.1462	8.1498	8.1336
0.4	7.1509	7.1434	7.1232	7.0772	7.1531	7.1455	7.1254	7.0794
0.6	6.0343	6.0068	5.9623	5.8853	6.0357	6.0082	5.9638	5.8868

an AFG tapered beam based on the classical model. It can be noticed from the comparisons in Tables 1, 2, 3, 4, 5, 6, 7, 8 that the obtained results from the newly developed model and solution procedure are in a good accordance with those in the literature.

5 Parametric study

The newly developed nonclassical modified couple stress–surface energy BDFG model incorporating the effects of physical neutral axis and Poisson’s ratio to investigate the mechanical response of simply supported graded non-uniform micro/nanobeams. The effects of various material properties, i.e., gradient indices in thickness and length directions, dimensionless material length-scale parameter, surface residual stress, surface modulus of elasticity, and geometrical parameters, i.e., aspect ratio and taperness

ratios, on the mechanics of BDFG tapered simply supported nanobeams are investigated in detail.

In the forthcoming parametric studies, the BDFG beam shown in Fig. 1, is made from aluminum (Al) and silicon (Si) as metallic and ceramic constituent materials, respectively, with the material properties given in Table 9 [105, 109, 114]. The values of geometrical parameters are as follows: thickness $h(x) = h_0(1 - \beta_h x/L)$, width $b(x) = b_0(1 - \beta_b x/L)$, in which $h_0 = h(0)$ and $b_0 = b(0)$ with $b_0 = h_0$, taperness parameters are $-1 \leq \beta_h, \beta_b < 1$, and aspect ratio $L/h_0=25$, unless specifying other material or geometrical parameters. However, due to the lack of experimental data for the material length-scale parameter for silicon (l_{Si}) or bi-directionally functionally graded materials $l(x, z)$ in the open literature, a range of h/l can be supposed to investigate the effect of the material length-scale parameter on the response of micro-scale structures [37]. In this study, we avoided the problem of the unknown material length-scale parameter of silicon

l_{Si} by assuming l_{Si} as a ratio of that of aluminum l_{AL} , [47, 91, 92, 129]. The material length-scale parameter-to-thickness ratio is taken as $l_l = 0.5h$ and $l_r = (4/3)l_l$, unless other values are mentioned.

The size-dependent static and dynamic responses of the BDFG nanobeam are explored using different formulations; “CL” which is based on the classical elasticity theory, “SE” incorporating effect of surface energy only ($l = 0$), “CS” which is based on the modified couple stress theory, and fully integrated model “CSSER” which is based on the modified couple stress and surface elasticity theories. The predicted results are presented as figures and tables to serve as benchmarks for future analyses of nonuniform BDFG micro/nanobeams. For convenience, the results are presented in terms of the following dimensionless deflection, critical buckling load, and fundamental frequency, respectively:

$$\bar{w}(x) = 100 \frac{E_r I}{qL^4} w(x), \quad \bar{P}_{cr} = \frac{E_r L^2}{I} P_{cr} \quad \text{and} \quad \bar{\omega} = \omega \sqrt{\frac{\rho_r A}{E_r I}} L^2 \tag{49}$$

where E_r and ρ_r are, respectively, the Young’s modulus and mass density of the bulk material at the upper right corner of the beam (metallic phase) and I is the second moment of area about the y -axis.

5.1 Effect of the taperness parameters

The effect of the rates of cross-section changes along thickness and width directions, β_h and β_b , respectively, on the bending, buckling, and vibration responses of BDFG is investigated using classical (CL) and nonclassical (CSSER) analyses. The dimensionless deflection throughout the beam length shows asymmetric curve as shown in Fig. 2, which is attributed to the tapering effect as well as the material gradation in the axial direction. The predicted deflection with positive values of β_h and β_b is much higher than that with negative values, which can be explained in view of Fig. 3. It

is depicted from Fig. 3 that the equivalent stiffness $\mathcal{D}_{11}(x)$, defined in Eq. (33), of the nanobeam becomes higher when β_h and β_b are negative. Such asymmetric distribution of the equivalent stiffness through beam length leads to asymmetric deflection.

Figures 4, 5, 6 demonstrate the simultaneous effects of varying the taperness parameters β_b and β_h on the dimensionless maximum deflection, critical buckling load, and fundamental frequency, respectively, for BDFG nanobeams at $k_x = k_z = 1$. Some numerical values of the dimensionless maximum deflection, critical buckling load, and fundamental frequency are tabulated in Tables 10, 11, 12 at different values of β_b and β_h and different gradation schemes; AFG, TFG, and BDFG. Generally, it is notable that increasing the taperness parameter β_h and/or β_b from negative to positive values significantly increases the dimensionless maximum deflection and decreases the dimensionless critical buckling load and the dimensionless fundamental frequency. For both the static and vibration responses, the influence of varying the thickness parameter β_h is significantly greater than that of the width parameter β_b , especially with the classical formulation. As β_h changes from negative to positive values, the influence of β_b rises and vice versa. Generally, the influence of changing the rates of cross section in classical analysis is higher than that for the nonclassical one for all gradation distributions. The mutual contribution of the nonclassical parameters, i.e., material length-scale parameter and surface properties, on the static and vibration responses is greatly increased by increasing β_h and slightly affected by increasing β_b . In addition, it is important to emphasize that the maximum impact of the taperness parameters is associated with the deflection response, followed with the buckling, and vibration responses. For both the classical and nonclassical formulations, the highest and lowest effects of the taperness parameters are associated with AFG and homogeneous nanobeams, respectively. The taperness parameters β_h and β_b have the same effect on the classical response of homogeneous and TFG nanobeams. Furthermore, for the

Table 9 Material properties of the constituents of BDFG nanobeam

Property	Silicon “l”	Aluminum “r”
Bulk properties		
Young’s modulus (GPa)	$E_l^B = 210$	$E_r^B = 90$
Poisson’s ratio	$\nu_l = 0.24$	$\nu_r = 0.23$
Bulk density (kg/m ³)	$\rho_l^B = 2331$	$\rho_r^B = 2700$
Material length-scale parameter (μm)	–	$l_r = 6.58$
Surface properties		
Surface density (kg/m ²)	$\rho_l^s = 3.1688 \times 10^{-7}$	$\rho_r^s = 5.46 \times 10^{-7}$
Surface residual stress (N/m)	$\tau_l^s = 0.6056$	$\tau_r^s = 0.5689$
Surface Lamé modulus (N/m)	$\mu_l^s = -2.7779$	$\mu_r^s = -5.4251$
Surface Lamé modulus (N/m)	$\lambda_l^s = -4.4939$	$\lambda_r^s = 3.4939$
Surface elastic modulus (N/m)	$E_l^s = -10.0497$	$E_r^s = -7.3563$

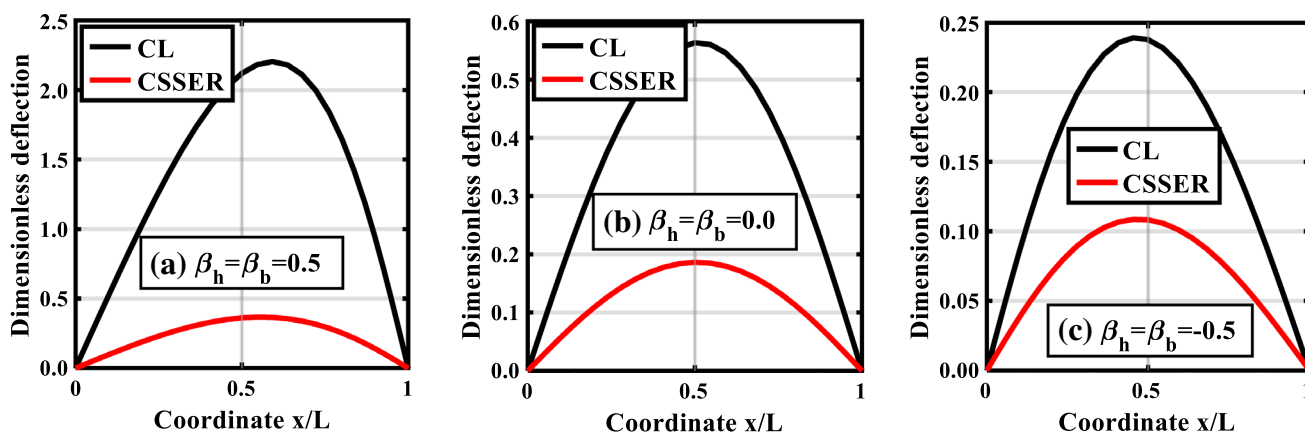


Fig. 2 The effect of the taperness parameters β_h and β_b on the dimensionless deflection along the length of BDFG nanobeam at $k_x = k_z = 1$

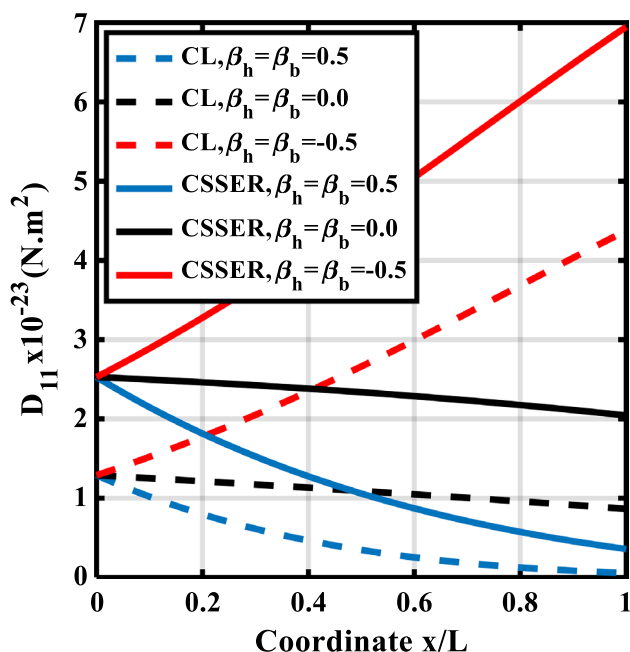


Fig. 3 Variation of the equivalent stiffness $D_{11}(x)$ (Eq. (33)) along the length of BDFG nanobeam at different taperness parameters and $k_x = k_z = 1$

same taperness ratio and material gradation, the predicted deflection based on the nonclassical formulation is lower than that predicted using classical elasticity theory, whereas the predicted nonclassical critical load and fundamental frequency are distinctly higher than their corresponding classical values.

5.2 Effect of the material gradation

The effect of bi-directional gradient indices along thickness and length directions, k_z and k_x , respectively, on the

response of BDFG nanobeams is investigated, considering both uniform and tapered cross sections. The dimensionless deflection versus the beam length is shown in Fig. 7 at different gradient indices. It is seen that the axial gradient index k_x as well as the nonuniform cross section can tend the deflection of BDFG nanobeam to asymmetric curves for both classical and nonclassical analyses. Uniform and nonclassical nanobeams give lower dimensionless deflection along the beam length compared with tapered and classical nanobeams, respectively. It is important to emphasize that a homogeneous nanobeam with $k_x = k_z = 0$ is made from pure metal constituent and therefore has the smallest stiffness. The variations of the dimensionless maximum deflection, dimensionless critical buckling load, and dimensionless fundamental frequency are plotted in Figs. 8, 9, 10, respectively, and are recorded in Tables 13, 14, 15 versus the gradation indices k_x and k_z at different taperness parameters ($\beta_b = \beta_h = \beta$). For the considered material properties, it is noticed that inclusion of the microstructure and surface energy effects leads to increasing the beam rigidity. Therefore, the predicted dimensionless deflection using CSSER formulation is always lower than that predicted using CL one, whereas the obtained dimensionless critical buckling load and the dimensionless fundamental frequency based on CSSER are larger than those obtained using CL analysis. Such behavior is observed for all values of the gradient indices and taperness parameters.

Also, the obtained results reveal that due to the increase in the stiffness of the nanobeam, increasing k_z and/or k_x decreases the maximum deflection and increases the dimensionless critical buckling load, and the dimensionless natural frequencies. Further increasing of the gradient indices (almost more than 5), the response converges towards the pure ceramic behavior. The influence of the gradation indices is reduced by incorporating the nonclassical effect and/or nonuniform cross section. Considering BDFG nanobeams,

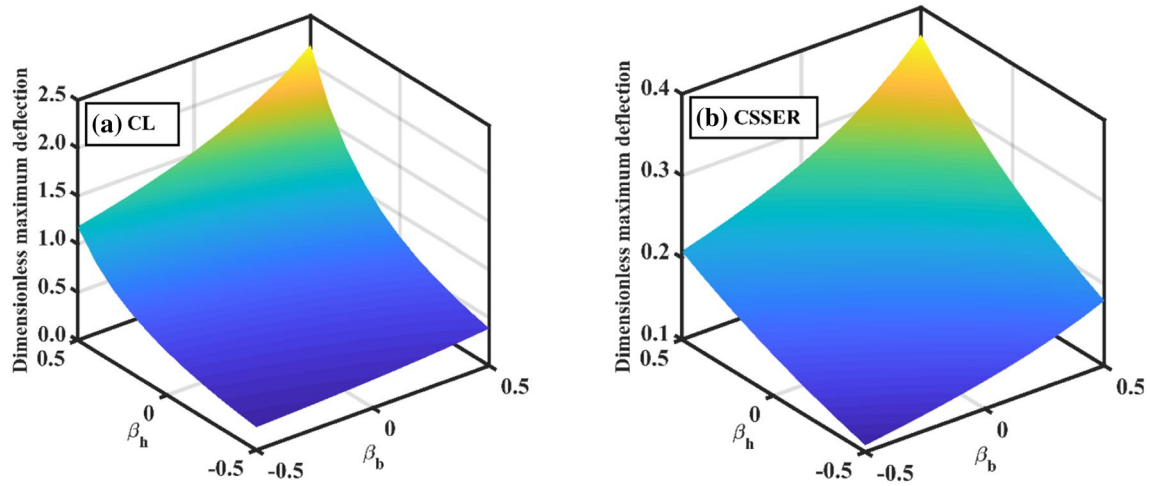


Fig. 4 The effect of the taperness parameters on the dimensionless maximum deflection of BDFG nanobeam at $k_x = k_z = 1$

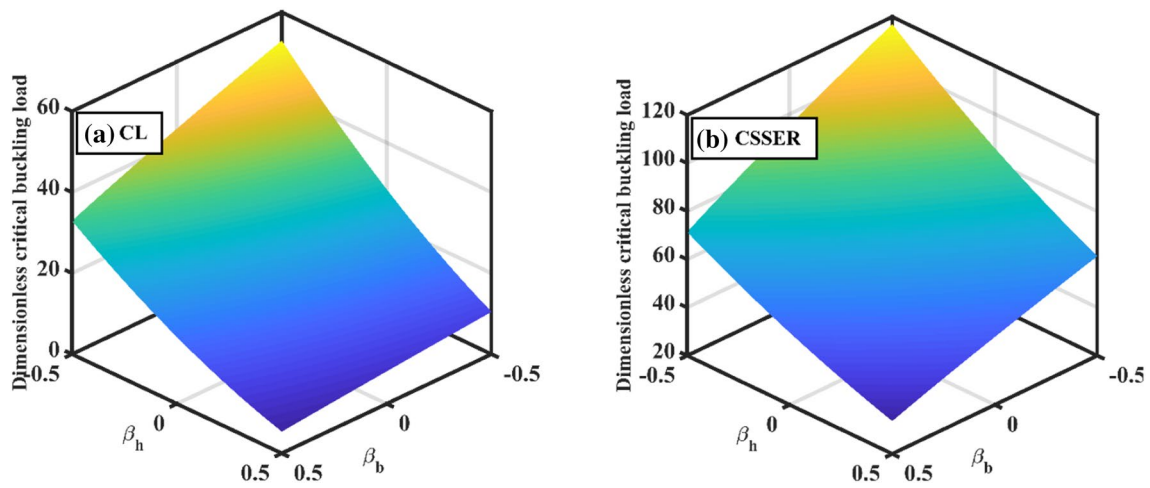


Fig. 5 The effect of the taperness parameters on the dimensionless critical buckling load of BDFG nanobeam at $k_x = k_z = 1$

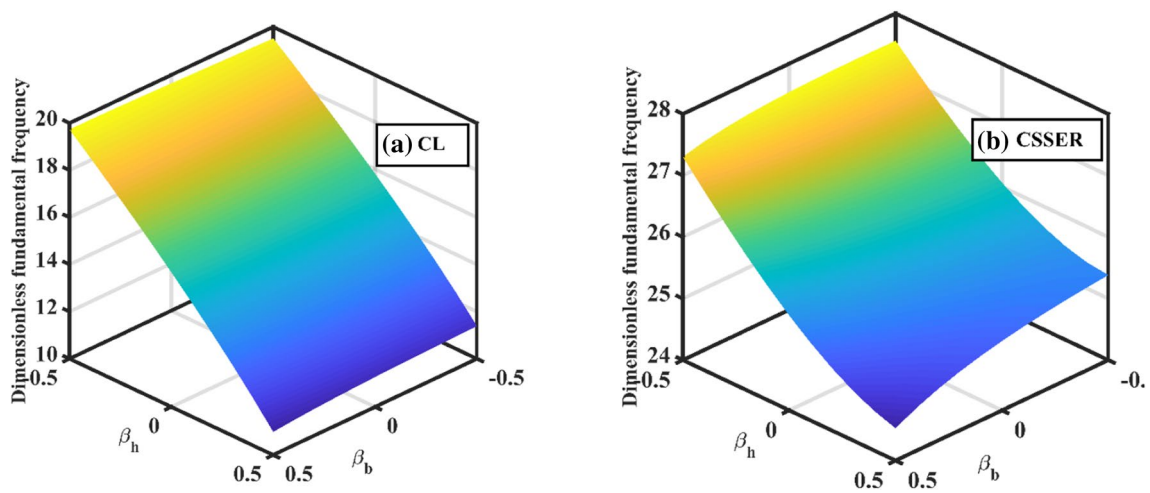


Fig. 6 The effect of the taperness parameters on the dimensionless fundamental frequency of BDFG nanobeam at $k_x = k_z = 1$

Table 10 Dimensionless maximum deflection of FG nanobeam at different values of taperness parameters and gradient indices

(k_x, k_z)	β_h	Classical analysis					Nonclassical CSSER analysis				
		Width taperness parameter β_b					Width taperness parameter β_b				
		- 0.5	- 0.25	0.0	0.25	0.5	- 0.5	- 0.25	0.0	0.25	0.5
(0,0)	- 0.5	0.4875	0.5345	0.5931	0.6714	0.7811	0.1587	0.1750	0.1959	0.2235	0.2622
	- 0.25	0.6451	0.7117	0.7959	0.9067	1.0614	0.1797	0.1988	0.2229	0.2550	0.3002
	0.0	0.9029	0.9999	1.1232	1.2868	1.5183	0.2039	0.2259	0.2539	0.2912	0.3441
	0.25	1.3538	1.5061	1.7016	1.9650	2.3596	0.2313	0.2567	0.2893	0.3327	0.3956
	0.5	2.2931	2.5755	2.9448	3.4528	4.2079	0.2622	0.2916	0.3293	0.3804	0.4577
(1,0)	- 0.5	0.2819	0.3115	0.3490	0.3985	0.4682	0.1183	0.1309	0.1468	0.1680	0.1980
	- 0.25	0.3815	0.4228	0.4754	0.5455	0.6450	0.1376	0.1525	0.1715	0.1968	0.2328
	0.0	0.5429	0.6040	0.6822	0.7874	0.9455	0.1606	0.1783	0.2009	0.2312	0.2752
	0.25	0.8350	0.9362	1.0679	1.2483	1.5146	0.1876	0.2086	0.2356	0.2723	0.3274
	0.5	1.4774	1.6666	1.9162	2.2634	2.7997	0.2191	0.2442	0.2773	0.3230	0.3902
(0,1)	- 0.5	0.3065	0.3360	0.3729	0.4221	0.4911	0.1228	0.1353	0.1513	0.1725	0.2021
	- 0.25	0.4056	0.4475	0.5004	0.5700	0.6673	0.1418	0.1568	0.1758	0.2010	0.2365
	0.0	0.5677	0.6286	0.7062	0.8090	0.9546	0.1646	0.1823	0.2050	0.2350	0.2777
	0.25	0.8512	0.9469	1.0698	1.2354	1.4835	0.1913	0.2124	0.2394	0.2754	0.3277
	0.5	1.4417	1.6193	1.8515	2.1708	2.6456	0.2225	0.2476	0.2798	0.3239	0.3899
(1,1)	- 0.5	0.2383	0.2621	0.2928	0.3331	0.3893	0.1082	0.1196	0.1339	0.1528	0.1794
	- 0.25	0.3195	0.3532	0.3961	0.4527	0.5324	0.1269	0.1404	0.1576	0.1804	0.2127
	0.0	0.4507	0.5001	0.5633	0.6475	0.7676	0.1493	0.1655	0.1863	0.2139	0.2532
	0.25	0.6827	0.7611	0.8643	1.0063	1.2142	0.1761	0.1956	0.2207	0.2543	0.3042
	0.5	1.1819	1.3302	1.5249	1.7940	2.1971	0.2078	0.2314	0.2618	0.3044	0.3671

Table 11 Dimensionless critical buckling load of FG nanobeam at different values of taperness parameters and gradient indices

(k_x, k_z)	β_h	Classical analysis					Nonclassical CSSER analysis				
		Width taperness parameter β_b					Width taperness parameter β_b				
		- 0.5	- 0.25	0.0	0.25	0.5	- 0.5	- 0.25	0.0	0.25	0.5
(0,0)	- 0.5	25.7440	23.5647	21.3027	18.9256	16.3725	79.5045	72.4374	65.0797	57.3124	48.9086
	- 0.25	19.6372	17.8777	16.0553	14.1445	12.0979	70.7177	64.2160	57.4515	50.3156	42.6008
	0.0	14.2018	12.8442	11.4417	9.9758	8.4114	62.6900	56.7196	50.5118	43.9682	36.8995
	0.25	9.4628	8.4867	7.4819	6.4360	5.3257	55.4008	49.9238	44.2326	38.2374	31.7659
	0.5	5.4576	4.8392	4.2058	3.5506	2.8606	48.7890	43.7633	38.5428	33.0455	27.1139
(1,0)	- 0.5	45.1491	40.9989	36.6988	32.1879	27.3505	107.6622	97.6468	87.2382	76.2729	64.4368
	- 0.25	33.6195	30.3600	26.9916	23.4692	19.7071	92.9605	84.0187	74.7377	64.9757	54.4591
	0.0	23.5870	21.1586	18.6571	16.0517	13.2830	79.8197	71.8719	63.6338	54.9827	45.6825
	0.25	15.0973	13.4310	11.7216	9.9502	8.0805	68.1928	61.1531	53.8658	46.2257	38.0295
	0.5	8.2199	7.2333	6.2265	5.1904	4.1069	57.9622	51.7389	45.3043	38.5679	31.3546
(0,1)	- 0.5	40.9464	37.4801	33.8824	30.1016	26.0408	102.7439	93.6503	84.1933	74.2250	63.4640
	- 0.25	31.2333	28.4349	25.5363	22.4972	19.2419	89.6289	81.3986	72.8472	63.8425	54.1325
	0.0	22.5882	20.4290	18.1983	15.8667	13.3785	77.7246	70.3065	62.6065	54.5074	45.7851
	0.25	15.0508	13.4983	11.9001	10.2366	8.4706	67.0230	60.3601	53.4508	46.1919	38.3851
	0.5	8.6804	7.6969	6.6894	5.6472	4.5499	57.4656	51.4940	45.3072	38.8142	31.8398
(1,1)	- 0.5	52.9768	48.3136	43.4773	38.3987	32.9474	116.9352	106.3910	95.4315	83.8867	71.4317
	- 0.25	39.9618	36.2446	32.3983	28.3704	24.0611	100.5506	91.1436	81.3778	71.1046	60.0398
	0.0	28.4975	25.6753	22.7637	19.7252	16.4888	85.8493	77.5033	68.8499	59.7608	49.9892
	0.25	18.6383	16.6526	14.6116	12.4917	10.2470	72.8191	65.4491	57.8176	49.8144	41.2272
	0.5	10.4667	9.2474	8.0007	6.7142	5.3640	61.3840	54.8962	48.1864	41.1602	33.6350

Table 12 Dimensionless fundamental frequency of FG nanobeam at different values of taperness parameters and gradient indices

(k_x, k_z)	β_h	Classical analysis					Nonclassical CSSER analysis				
		Width taperness parameter β_b					Width taperness parameter β_b				
		- 0.5	- 0.25	0.0	0.25	0.5	- 0.5	- 0.25	0.0	0.25	0.5
(0,0)	- 0.5	12.9861	13.0385	13.0917	13.1409	13.1735	21.2947	21.2822	21.2471	21.1712	21.0138
	- 0.25	11.8347	11.8668	11.8959	11.9163	11.9131	21.0006	20.9709	20.9153	20.8141	20.6244
	0.0	10.6028	10.6145	10.6196	10.6111	10.5719	20.8251	20.7772	20.6995	20.5708	20.3457
	0.25	9.2577	9.2491	9.2304	9.1929	9.1174	20.8106	20.7423	20.6399	20.4803	20.2144
	0.5	7.7354	7.7071	7.6648	7.5987	7.4871	21.0159	20.9237	20.7920	20.5951	20.2796
(1,0)	- 0.5	17.5435	17.5925	17.6376	17.6696	17.6656	25.6800	25.6649	25.6218	25.5270	25.3276
	- 0.25	15.8732	15.8966	15.9116	15.9076	15.8594	25.0119	24.9765	24.9094	24.7856	24.5501
	0.0	14.0937	14.0921	14.0776	14.0384	13.9467	24.4837	24.4271	24.3347	24.1801	23.9058
	0.25	12.1617	12.1360	12.0931	12.0197	11.8858	24.1487	24.0691	23.9490	23.7602	23.4421
	0.5	9.9925	9.9442	9.8747	9.7694	9.5961	24.0811	23.9748	23.8221	23.5923	23.2205
(0,1)	- 0.5	16.9661	17.0346	17.1041	17.1685	17.2110	25.3191	25.3196	25.2970	25.2310	25.0764
	- 0.25	15.4621	15.5040	15.5421	15.5688	15.5646	24.7241	24.7022	24.6528	24.5540	24.3578
	0.0	13.8528	13.8681	13.8748	13.8637	13.8124	24.2538	24.2083	24.1306	23.9969	23.7558
	0.25	12.0955	12.0844	12.0599	12.0109	11.9123	23.9599	23.8887	23.7800	23.6076	23.3162
	0.5	10.1067	10.0697	10.0145	9.9280	9.7822	23.9150	23.8144	23.6697	23.4519	23.1005
(1,1)	- 0.5	19.5128	19.5806	19.6470	19.7038	19.7288	27.5566	27.5600	27.5386	27.4700	27.3035
	- 0.25	17.7231	17.7611	17.7926	17.8074	17.7806	26.7442	26.7232	26.6727	26.5688	26.3581
	0.0	15.8119	15.8206	15.8174	15.7905	15.7120	26.0674	26.0210	25.9403	25.7993	25.5414
	0.25	13.7306	13.7104	13.6732	13.6052	13.4755	25.5853	25.5117	25.3982	25.2167	24.9067
	0.5	11.3837	11.3359	11.2659	11.1582	10.9789	25.3815	25.2771	25.1259	24.8972	24.5253

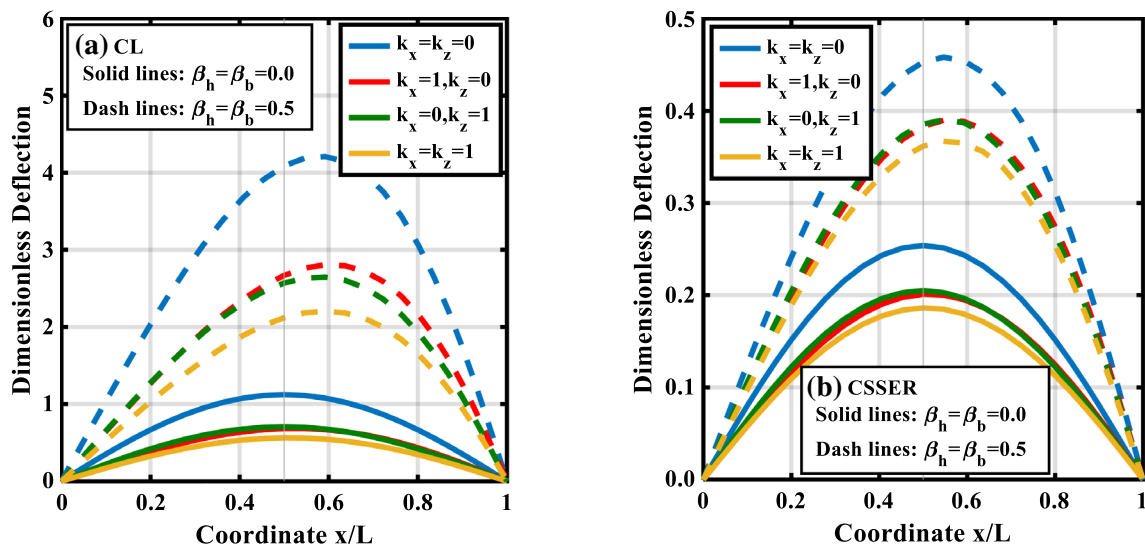


Fig. 7 The effect of the gradient indices k_x and k_z on the dimensionless deflection along the length of FG nanobeams with uniform and tapered cross-sections

it is notable that the effect of varying k_z decreases as k_x increases and being very small as k_x approach 10. Also, the influence of k_x is decreased with increasing k_z . Using classical analysis, varying (k_x, k_z) from (0,0) to (2,2) decreases

the dimensionless maximum deflection by 54.6% ($\beta=0$) and 53.2% ($\beta=0.5$), increases the dimensionless critical buckling load by 119.9% ($\beta=0$) and 109.6% ($\beta=0.5$), and increases the dimensionless frequency by 58.5% ($\beta=0$) and 27.2% ($\beta=0.5$). Introducing the nonclassical microstructure and

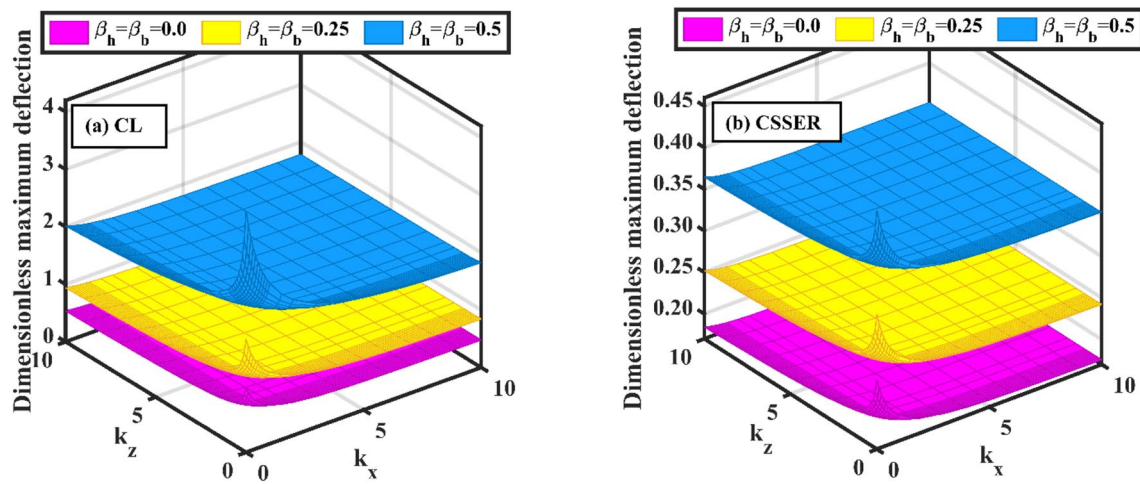


Fig. 8 The effect of the gradient indices k_x and k_z on the dimensionless maximum deflection of BDFG nanobeam at different taperness parameters

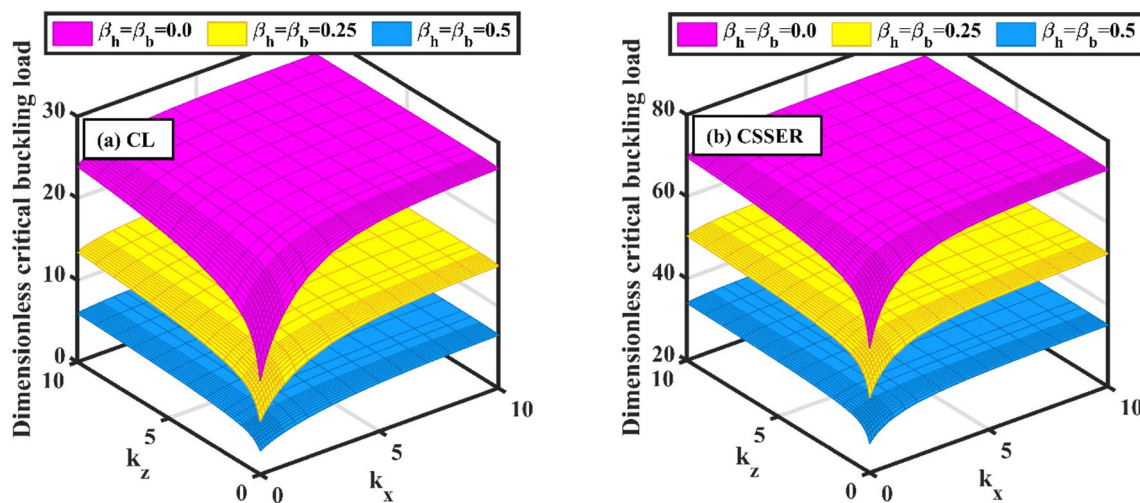


Fig. 9 The effect of the gradient indices k_x and k_z on the dimensionless critical buckling load of BDFG nanobeam at different taperness parameters

surface energy effects reduces the impact of the gradient indices, i.e., based on CSSER formulation, varying (k_x, k_z) from $(0,0)$ to $(2,2)$ decreases the dimensionless maximum deflection by 29.3% ($\beta=0$) and 21.7% ($\beta=0.5$), increases the dimensionless critical buckling load by 41.4% ($\beta=0$) and 27.2% ($\beta=0.5$), and increases the dimensionless frequency by 29.6% ($\beta=0$) and 24.3% ($\beta=0.5$). Therefore, ignoring the nonclassical effects leads to a significant error in the predicted static and vibration responses of BDFG micro/nanobeams.

For AFG nanobeams ($k_z = 0$), increasing k_x has a more significant influence on the static and dynamic responses for classical and uniform nanobeams compared with non-classical and tapered nanobeams, respectively. As k_x

increases from 0 to 2, the dimensionless maximum deflection decreases by 48.7% ($\beta=0$) and 43.9% ($\beta=0.5$) using CL analysis and by 26% ($\beta=0$) and 18.8% ($\beta=0.5$) using CSSER analysis. Whereas, increasing k_x from 0 to 2, shows an increase in the dimensionless critical buckling load by 93% ($\beta=0$) and 69% ($\beta=0.5$) for CL formulation and by 34.7% ($\beta=0$) and 21.6% ($\beta=0.5$) for CSSER formulation. Rising k_x of AFG nanobeam from 0 to 2 leads to an increase in the dimensionless fundamental frequency by about 47% ($\beta=0$) and 42% ($\beta=0.5$) based on CL analysis and by 24.4% ($\beta=0$) and 19.9% ($\beta=0.5$) based on CSSER analysis. Again, the highest impact of k_x is associated with the buckling response. Regarding TFG nanobeams ($k_x = 0$), it is depicted that the impact of varying k_z on the bending, buckling, and vibration

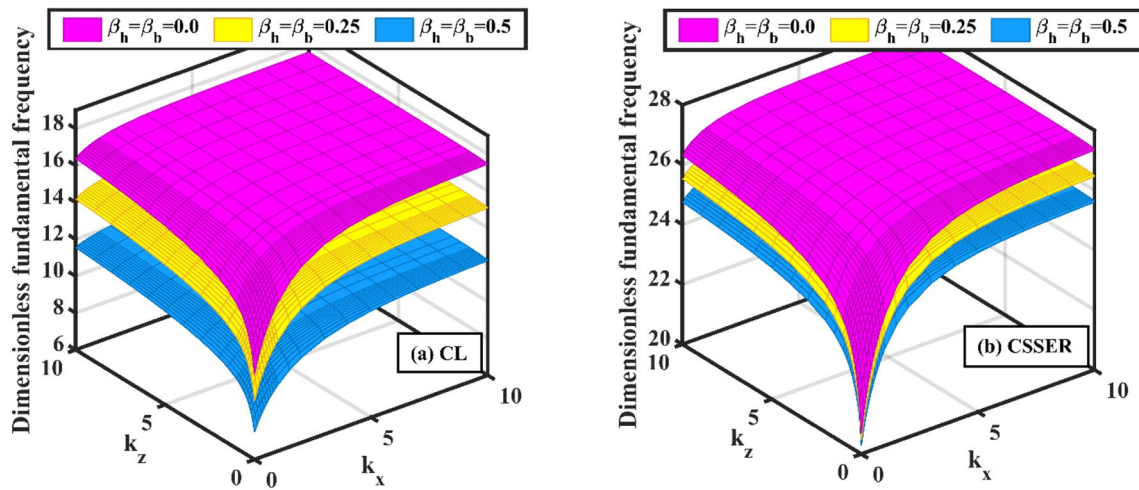


Fig. 10 The effect of the gradient indices k_x and k_z on the dimensionless fundamental frequency of BDFG nanobeam at different taperness parameters

Table 13 Dimensionless maximum deflection of BDFG nanobeam at different gradient indices and taperness parameters β_b and β_h

(β_b, β_h)	k_z	Classical analysis						Nonclassical CSSER analysis					
		Axial gradient index k_x						Axial gradient index k_x					
		0.0	0.5	1.0	2.0	5.0	10.0	0.0	0.5	1.0	2.0	5.0	10.0
(0.0,0.0)	0.0	1.1232	0.8066	0.6822	0.5761	0.4979	0.4790	0.2539	0.2162	0.2009	0.1878	0.1783	0.1759
	0.50	0.7810	0.6493	0.5888	0.5326	0.4880	0.4768	0.2144	0.1972	0.1893	0.1822	0.1768	0.1754
	1.0	0.7062	0.6093	0.5633	0.5198	0.4850	0.4761	0.2050	0.1922	0.1863	0.1808	0.1765	0.1753
	2.0	0.6460	0.5775	0.5431	0.5098	0.4826	0.4756	0.1974	0.1883	0.1839	0.1796	0.1762	0.1753
	5.0	0.5789	0.5407	0.5197	0.4982	0.4798	0.4749	0.1893	0.1840	0.1811	0.1783	0.1759	0.1752
	10.0	0.5381	0.5162	0.5034	0.4897	0.4777	0.4744	0.1844	0.1810	0.1792	0.1773	0.1757	0.1752
(0.25, 0.25)	0.0	1.9650	1.4637	1.2483	1.0512	0.8895	0.8438	0.3327	0.2899	0.2723	0.2567	0.2455	0.2425
	0.50	1.3663	1.1599	1.0573	0.9552	0.8646	0.8376	0.2864	0.2669	0.2579	0.2497	0.2435	0.2419
	1.0	1.2354	1.0839	1.0063	0.9277	0.8569	0.8357	0.2754	0.2611	0.2543	0.2480	0.2431	0.2418
	2.0	1.1301	1.0234	0.9658	0.9060	0.8509	0.8341	0.2668	0.2566	0.2515	0.2467	0.2428	0.2417
	5.0	1.0127	0.9536	0.9188	0.8807	0.8439	0.8324	0.2578	0.2516	0.2484	0.2453	0.2425	0.2416
	10.0	0.9415	0.9077	0.8866	0.8627	0.8387	0.8310	0.2523	0.2484	0.2463	0.2441	0.2422	0.2416
(0.5,0.5)	0.0	4.2079	3.2405	2.7997	2.3613	1.9550	1.8262	0.4577	0.4110	0.3902	0.3716	0.3575	0.3537
	0.50	2.9258	2.5301	2.3198	2.0977	1.8803	1.8052	0.4026	0.3817	0.3716	0.3621	0.3546	0.3526
	1.0	2.6456	2.3558	2.1971	2.0267	1.8576	1.7986	0.3899	0.3746	0.3671	0.3600	0.3542	0.3525
	2.0	2.4201	2.2166	2.0997	1.9708	1.8398	1.7934	0.3802	0.3693	0.3637	0.3584	0.3538	0.3524
	5.0	2.1687	2.0567	1.9869	1.9058	1.8191	1.7874	0.3704	0.3637	0.3602	0.3567	0.3535	0.3524
	10.0	2.0161	1.9523	1.9104	1.8599	1.8039	1.7829	0.3648	0.3602	0.3578	0.3554	0.3532	0.3523

responses is independent of the taperness parameters when the classical formulation is employed, i.e. With the rise of k_z from 0 to 2 based on CL analysis, the dimensionless maximum deflection is reduced by 42.5% and the dimensionless buckling load and dimensionless fundamental frequency are increased by 73.9% and 38.3%, respectively. On the contrary, the effect of k_z on the nonclassical responses of TFG nanobeam becomes more pronounced with uniform cross section,

i.e., as k_z changes from 0 to 2 based on CSSER analysis, the dimensionless maximum deflection is decreased by 22.3% ($\beta=0$) and 16.9% ($\beta=0.5$) and the dimensionless buckling load and dimensionless fundamental frequency are raised by, respectively, 28.7% and 20.4% ($\beta=0$) and 17% ($\beta=0.5$).

In addition, it is observed that the taperness parameters have a significant influence on the role of k_x in AFG and have no influence on the role of k_z in TFG nanobeams.

Table 14 Dimensionless critical buckling load of BDFG tapered nanobeam at different gradient indices and taperness parameters β_b and β_h

(β_b, β_h)	k_z	Classical analysis						Nonclassical CSSER analysis					
		Axial gradient index k_x						Axial gradient index k_x					
		0.0	0.5	1.0	2.0	5.0	10.0	0.0	0.5	1.0	2.0	5.0	10.0
(0.0,0.0)	0.0	11.4417	15.8437	18.6571	22.0828	25.6923	26.7950	50.5118	59.1929	63.6338	68.0743	71.8618	72.9334
	0.50	16.4553	19.7598	21.7520	24.0311	26.2711	26.9329	59.8323	65.0393	67.6965	70.3174	72.5285	73.1507
	1.0	18.1983	21.0706	22.7637	24.6515	26.4535	26.9771	62.6065	66.7377	68.8499	70.9279	72.6842	73.1869
	2.0	19.8940	22.2425	23.6287	25.1582	26.5968	27.0115	65.0083	68.1378	69.7712	71.3988	72.8002	73.2136
	5.0	22.1999	23.7650	24.7149	25.7699	26.7637	27.0513	67.7831	69.7700	70.8463	71.9490	72.9364	73.2451
	10.0	23.8806	24.8955	25.5238	26.2259	26.8889	27.0814	69.6094	70.9161	71.6300	72.3684	73.0461	73.2711
(0.25, 0.25)	0.0	6.4360	8.5387	9.9502	11.7921	14.0566	14.9267	38.2374	43.4716	46.2257	49.0481	51.5701	52.3456
	0.50	9.2561	10.8459	11.8632	13.1148	14.5402	15.0626	44.4233	47.4536	49.0474	50.6616	52.0919	52.5305
	1.0	10.2366	11.6214	12.4917	13.5373	14.6917	15.1058	46.1919	48.5652	49.8144	51.0778	52.2037	52.5577
	2.0	11.1904	12.3228	13.0368	13.8872	14.8115	15.1395	47.6865	49.4654	50.4175	51.3931	52.2845	52.5769
	5.0	12.4874	13.2407	13.7289	14.3145	14.9518	15.1785	49.3458	50.4763	51.0982	51.7523	52.3785	52.5996
	10.0	13.4329	13.9207	14.2429	14.6322	15.0566	15.2080	50.4065	51.1655	51.5821	52.0224	52.4554	52.6193
(0.5,0.5)	0.0	2.8606	3.5883	4.1069	4.8393	5.9234	6.4837	27.1139	29.8467	31.3546	32.9590	34.4704	34.9681
	0.50	4.1141	4.6688	5.0511	5.5642	6.2650	6.6043	30.8382	32.3449	33.1729	34.0411	34.8485	35.1129
	1.0	4.5499	5.0343	5.3640	5.7979	6.3720	6.6424	31.8398	33.0005	33.6350	34.2976	34.9185	35.1296
	2.0	4.9738	5.3698	5.6410	5.9956	6.4577	6.6723	32.6541	33.5141	33.9867	34.4848	34.9655	35.1398
	5.0	5.5503	5.8129	5.9976	6.2413	6.5594	6.7071	33.4978	34.0505	34.3562	34.6839	35.0176	35.1517
	10.0	5.9705	6.1402	6.2618	6.4235	6.6350	6.7333	34.0079	34.3949	34.6044	34.8276	35.0610	35.1632

Table 15 Dimensionless fundamental frequency of BDFG tapered nanobeam at different gradient indices and taperness parameters β_b and β_h

(β_b, β_h)	k_z	Classical analysis						Nonclassical CSSER analysis					
		Axial gradient index k_x						Axial gradient index k_x					
		0.0	0.5	1.0	2.0	5.0	10.0	0.0	0.5	1.0	2.0	5.0	10.0
(0.0,0.0)	0.0	10.6196	12.7854	14.0776	15.5600	17.0280	17.4646	20.6995	23.0455	24.3347	25.7084	26.9738	27.3464
	0.50	13.0354	14.5045	15.3680	16.3301	17.2492	17.5177	23.2799	24.7329	25.5430	26.4006	27.1806	27.4077
	1.0	13.8748	15.1049	15.8174	16.5969	17.3261	17.5365	24.1306	25.2921	25.9403	26.6232	27.2415	27.4223
	2.0	14.6876	15.6541	16.2162	16.8264	17.3905	17.5521	24.9260	25.8046	26.2995	26.8216	27.2951	27.4353
	5.0	15.7138	16.3242	16.6901	17.0908	17.4626	17.5695	25.8114	26.3712	26.6931	27.0365	27.3526	27.4491
	10.0	16.3941	16.7760	17.0103	17.2695	17.5114	17.5813	26.3274	26.7084	26.9293	27.1665	27.3878	27.4577
(0.25, 0.25)	0.0	9.1929	10.9434	12.0197	13.2954	14.6427	15.0836	20.4803	22.5950	23.7602	24.9975	26.1283	26.4601
	0.50	11.2842	12.4754	13.1976	14.0290	14.8733	15.1434	22.8421	24.1377	24.8626	25.6280	26.3188	26.5189
	1.0	12.0109	13.0084	13.6052	14.2804	14.9519	15.1639	23.6076	24.6391	25.2167	25.8242	26.3714	26.5313
	2.0	12.7144	13.4971	13.9676	14.4965	15.0172	15.1809	24.3207	25.0987	25.5374	25.9996	26.4177	26.5422
	5.0	13.6028	14.0956	14.4008	14.7475	15.0911	15.1998	25.0962	25.5958	25.8821	26.1866	26.4669	26.5539
	10.0	14.1916	14.4994	14.6944	14.9182	15.1418	15.2131	25.5343	25.8823	26.0825	26.2965	26.4964	26.5609
(0.5,0.5)	0.0	7.4871	8.7743	9.5961	10.6125	11.7851	12.2273	20.2796	22.1734	23.2205	24.3266	25.3205	25.6055
	0.50	9.1904	10.0705	10.6256	11.2923	12.0291	12.2989	22.4225	23.5715	24.2160	24.8924	25.4915	25.6603
	1.0	9.7822	10.5193	10.9789	11.5222	12.1104	12.3228	23.1005	24.0134	24.5253	25.0605	25.5344	25.6699
	2.0	10.3552	10.9323	11.2942	11.7201	12.1775	12.3422	23.7302	24.4187	24.8060	25.2112	25.5722	25.6783
	5.0	11.0787	11.4406	11.6741	11.9524	12.2542	12.3643	24.3960	24.8450	25.0997	25.3678	25.6115	25.6871
	10.0	11.5582	11.7837	11.9324	12.1115	12.3078	12.3800	24.7564	25.0796	25.2626	25.4558	25.6342	25.6923

Furthermore, as the gradation indices rise for all the gradation distributions, the impact of the taperness parameters greatly decreases for the classical analysis and slightly increases for the nonclassical analysis.

5.3 Effect of the surface energy

This study is the first attempt to model and investigate the response of BDFG nanobeams in the presence of surface energy. In this section, the effect of the surface residual stress $\tau^s(x, z)$ and surface elasticity modulus $E^s(x, z)$, on the static and vibration responses of simply supported nanobeams is explored, considering different gradation schemes. For this purpose, the material properties of bulk continuum and surface layers provided in Table 9 are used, while the microstructure effect is ignored, i.e., $l_f=l_r=0$. The nanobeam dimensions are $b_0 = h_0 = 5\text{nm}$ with equal thickness and width taperness parameters, i.e., $\beta=\beta_h=\beta_b$. The effect of the surface residual stress τ_r^s (metallic phase) and τ_l^s (ceramic phase) of the surface layers on the dimensionless maximum deflection, dimensionless critical buckling load, and dimensionless fundamental frequency is depicted in Figs. 11, 12, 13, respectively, for both uniform and tapered BDFG nanobeams and $L/h_0=25$ and 50. The reference values are those given in Table 9 ($\tau_{r0}^s=0.5689\text{N/m}$, $\tau_{l0}^s=0.6056\text{N/m}$). Tables 16, 17, 18 provide, respectively, the dimensionless maximum deflection, dimensionless critical buckling load, and dimensionless fundamental frequency at different values of the residual surface stress, length-to-thickness ratio, and taperness parameters for AFG, TFG, and BDFG nanobeams.

For the material properties under consideration, it is noticeable that increasing the surface residual stress of the metallic (τ_r^s) and/or ceramic (τ_l^s) constituent materials

significantly decreases the dimensionless deflection and increases both the dimensionless critical buckling load and dimensionless fundamental frequency for all the gradation distributions. Accounting for the residual surface effect induces tension stress in the surface layers, and hence, stiffer surface results in lower deflections. The influence of the surface residual stresses τ_r^s and τ_l^s becomes more prominent with the increase of the aspect ratio (L/h) and may lead to an increase or a decrease in the equivalent stiffness of nanobeam depending on its material properties. For AFG, TFG, and BDFG nanobeams, rising the residual surface stress τ_l^s reduces the contribution of τ_r^s , and vice versa. It is also depicted that the highest effects of τ_l^s and τ_r^s correspond to BDFG and TFG distributions, respectively. On the other hand, the lowest effects of τ_l^s and τ_r^s are associated with, respectively, AFG and BDFG distributions. In other words, the effect of varying the surface residual stress is mainly controlled with the directions of gradation and the geometrical parameters of the beam. Increasing the aspect ratio noticeably rises the effect of surface residual stress on the static and vibration responses, which is attributed to the increase of the surface area-to-bulk volume ratio, and therefore, an increase in surface energy. It is also worth noting that, the impact of the surface residual stress and aspect ratio on the response of tapered nanobeams is much greater than that of uniform nanobeams.

The effect of surface elasticity moduli E_r^s and E_l^s of the metallic and ceramic phases, respectively, of the surface layers is illustrated in Figs. 14, 15, 16 and Tables 19, 20, 21 at different aspect ratios, taperness parameters, and material gradations. The reference values E_{r0}^s and E_{l0}^s are taken -7.3563N/m and -10.0497N/m , respectively, as given in Table 9. It is found that the dimensionless maximum

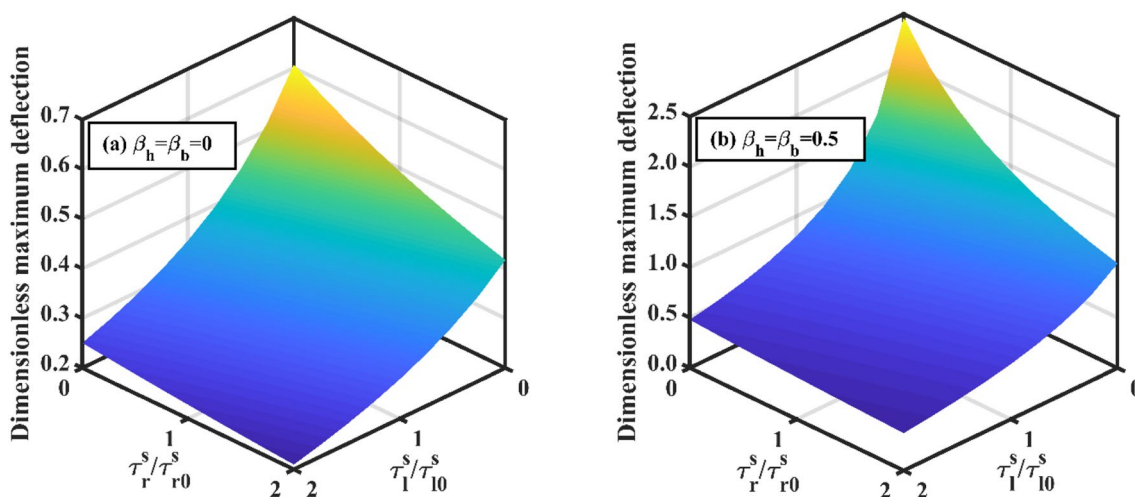


Fig. 11 The effect of the surface residual stress ratios τ_l^s/τ_{l0}^s and τ_r^s/τ_{r0}^s on the dimensionless maximum deflection of BDFG nanobeam with $k_x=k_z=1$

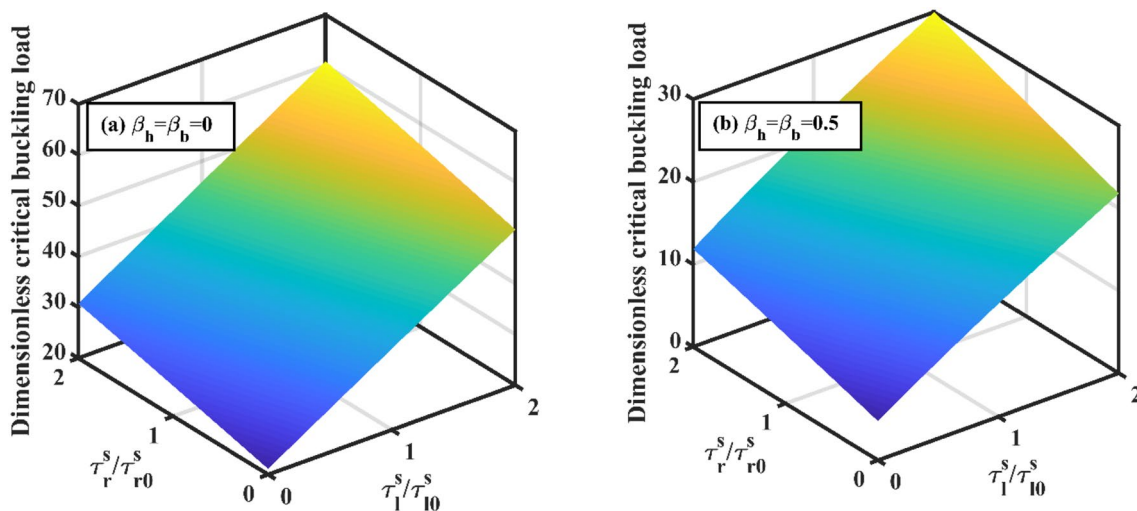


Fig. 12 The effect of the surface residual stress ratios τ_1^s/τ_{10}^s and τ_r^s/τ_{r0}^s on the dimensionless critical buckling load of BDFG nanobeam with $k_x=k_z=1$

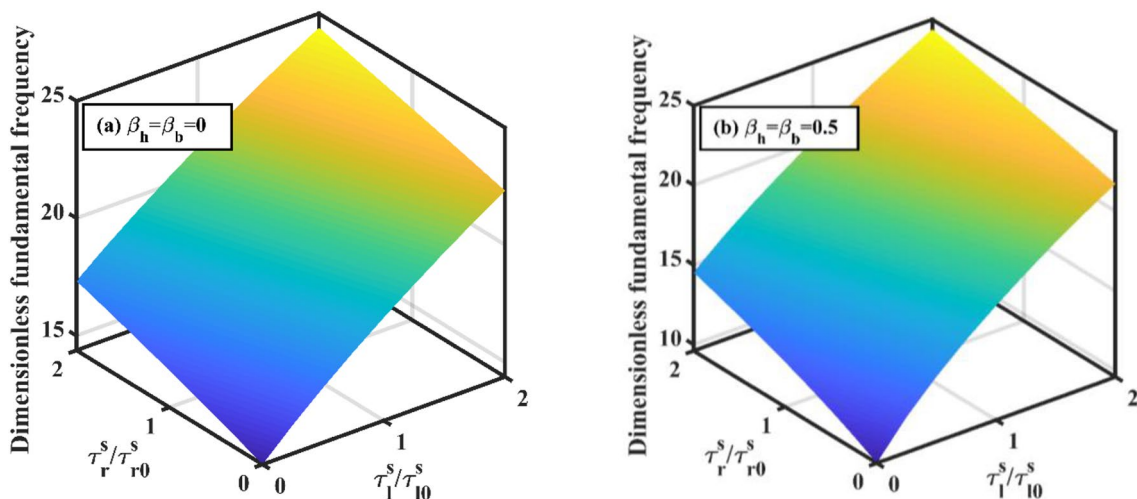


Fig. 13 The effect of the surface residual stress ratios τ_1^s/τ_{10}^s and τ_r^s/τ_{r0}^s on the dimensionless fundamental frequency of BDFG nanobeam with $k_x=k_z=1$

deflection for both uniform and tapered nanobeams is slightly increased by increasing E_r^s and E_l^s individually or simultaneously, whereas the both dimensionless critical buckling load and dimensionless fundamental frequency are decreased. It is observed that the effect of the surface elasticity moduli on the static and vibration responses is reduced with increasing the aspect ratio and taperness parameters. Unlike the surface residual stress, the contribution of E_r^s or E_l^s is almost unaffected by varying E_l^s or E_r^s , respectively. Compared with surface residual stress, the bending, buckling, and vibration responses have less sensitivity to surface elasticity modulus.

5.4 Effect of the material length-scale parameter

Effect of microstructure effect via MCST on the mechanics of tapered BDFG micro/nanobeams is explored by considering different values of the dimensionless material length-scale parameter (l_r/h) and material length-scale parameter ratio (l_l/l_r) for various width and thickness taperness ratios and material gradations. When a constant material length-scale parameter is considered, the ratio l_l/l_r is set to unity. To extract a clear investigation of the effect of the material length-scale parameter, the present results are based on the MCST formulation using the material properties in Table 9 with $l_r = 6.58 \mu\text{m}$. In Figs. 17, 18, 19, the dimensionless

Table 16 Dimensionless maximum deflection of uniform and tapered FG nanobeams at different surface residual stresses, aspect ratios, and gradation indices ($\beta_h = \beta_b = \beta$)

β	$\frac{l}{h}$	$\frac{\tau_1^s}{\tau_0^s}$	AFG, $(k_x, k_z) = (1, 0)$					TFG, $(k_x, k_z) = (0, 1)$					BDFG, $(k_x, k_z) = (1, 1)$				
			τ_1^s / τ_0^s					τ_1^s / τ_0^s					τ_1^s / τ_0^s				
			0	0.5	1.0	1.5	2.0	0	0.5	1.0	1.5	2.0	0	0.5	1.0	1.5	2.0
Uniform ($\beta=0.0$)	25	0	0.743	0.585	0.485	0.416	0.365	0.770	0.591	0.479	0.403	0.347	0.607	0.448	0.355	0.294	0.250
		0.5	0.575	0.473	0.402	0.352	0.314	0.599	0.484	0.407	0.350	0.307	0.544	0.412	0.332	0.278	0.239
		1.0	0.472	0.399	0.347	0.307	0.276	0.490	0.411	0.353	0.310	0.276	0.494	0.382	0.312	0.264	0.228
		1.5	0.402	0.346	0.305	0.273	0.248	0.415	0.356	0.312	0.278	0.250	0.452	0.357	0.294	0.251	0.218
		2.0	0.350	0.307	0.274	0.247	0.226	0.359	0.314	0.280	0.252	0.229	0.417	0.334	0.279	0.239	0.210
	50	0	0.743	0.365	0.247	0.188	0.153	0.770	0.347	0.224	0.165	0.131	0.607	0.250	0.158	0.115	0.091
		0.5	0.350	0.226	0.170	0.138	0.117	0.359	0.229	0.168	0.132	0.109	0.417	0.210	0.140	0.105	0.084
		1.0	0.235	0.168	0.133	0.111	0.096	0.234	0.170	0.134	0.110	0.094	0.321	0.181	0.126	0.097	0.079
		1.5	0.181	0.135	0.111	0.094	0.082	0.173	0.136	0.111	0.095	0.082	0.262	0.160	0.115	0.090	0.074
		2.0	0.148	0.115	0.095	0.082	0.073	0.137	0.113	0.095	0.083	0.073	0.223	0.143	0.106	0.085	0.070
Tapered ($\beta=0.5$)	25	0	3.227	1.820	1.285	1.000	0.826	3.007	1.613	1.101	0.835	0.673	2.465	1.211	0.803	0.600	0.479
		0.5	1.649	1.143	0.891	0.735	0.628	1.660	1.123	0.848	0.681	0.569	1.816	1.027	0.716	0.549	0.445
		1.0	1.136	0.859	0.696	0.590	0.516	1.145	0.861	0.689	0.574	0.492	1.447	0.895	0.648	0.508	0.417
		1.5	0.875	0.694	0.580	0.500	0.441	0.874	0.697	0.580	0.496	0.434	1.208	0.795	0.593	0.473	0.393
		2.0	0.718	0.586	0.500	0.437	0.390	0.706	0.586	0.501	0.437	0.388	1.040	0.717	0.547	0.443	0.372
	50	0	3.227	0.826	0.498	0.361	0.285	3.007	0.673	0.378	0.262	0.201	2.465	0.479	0.265	0.183	0.140
		0.5	0.718	0.390	0.279	0.222	0.185	0.706	0.388	0.267	0.204	0.164	1.040	0.372	0.227	0.164	0.128
		1.0	0.430	0.272	0.207	0.169	0.146	0.399	0.272	0.207	0.166	0.139	0.679	0.308	0.201	0.149	0.119
		1.5	0.310	0.214	0.168	0.141	0.122	0.278	0.210	0.168	0.141	0.121	0.513	0.264	0.180	0.137	0.111
		2.0	0.246	0.178	0.143	0.122	0.107	0.213	0.170	0.142	0.122	0.107	0.415	0.233	0.164	0.127	0.104

values of the maximum deflection, critical buckling load, and the fundamental frequency are plotted versus l_r/h and l_l/l_r for uniform and tapered BDFG microbeams with $k_x = k_z = 1$. The mutual effects of l_r/h and l_l/l_r on the microbeam response are recorded in Tables 22, 23, 24, for different gradient indices k_x and k_z and taperness ratios ($\beta = \beta_h = \beta_b$). Based on the obtained results, it is noticeable that introducing the microstructure effect enhances the microbeam rigidity, and consequently, decreases the dimensionless deflection and increases the dimensionless critical buckling load and dimensionless frequency.

It is noticeable that as the dimensionless material length-scale parameter (l_r/h) increases, the impact of microstructure on the static and vibration responses is distinctly enhanced for all material gradations. For a homogeneous microbeam, there is no effect of the material length-scale parameter by varying l_r/h and l_l/l_r on the dimensionless values of deflection, critical buckling load, and frequency. It is revealed that the impact of l_r/h rises as l_l/l_r increases and the maximum effect of l_r/h for different gradation distributions depends mainly on the value of l_l/l_r , i.e., the maximum effect of l_r/h corresponds to AFG when $l_l/l_r < 1$ and to

BDFG when $l_l/l_r \geq 1$. Also, the predicted responses using a spatially constant material length-scale parameter ($l_l = l_r$) are significantly different from those by the spatial-dependent material length-scale parameter ($l_l \neq l_r$). For a uniform microbeam with $l_r/h = 0.5$, altering the material length-scale parameter ratio l_l/l_r from 0.5 to 2, the dimensionless maximum deflection decreases by 49.5, 58.0, and 66.9%, the dimensionless critical buckling load increases by 93.0, 138.2, and 200.9%, and dimensionless frequency increases by 40.5, 54.3, and 73.7% for AFG, TFG, and BDFG distributions, respectively. Therefore, assumption of a constant material length-scale parameter for graded microbeams is unacceptable and leads to distinct error in the predicted response. Also, it is depicted that response of BDFG microbeam is the most sensitive to l_l/l_r , followed with TFG and AFG. The effect of l_l/l_r is enhanced by increasing l_r/h or taperness parameters towards positive values. The obtained results agree well with those in the previous sections, as rising the taperness parameters, while holding l_l/l_r and l_r/h fixed, leads to a noticeable decrease in the microbeam deflection and an increase in the dimensionless critical buckling load and dimensionless frequency.

Table 17 Dimensionless critical buckling load of uniform and tapered FG nanobeams at different surface residual stresses, aspect ratios, and gradation indices ($\beta_h = \beta_p = \beta$)

β	$\frac{L}{h}$	$\frac{\tau_1^s}{\tau_0^s}$	AFG, $(k_x, k_z) = (1, 0)$					TFG, $(k_x, k_z) = (0, 1)$					BDFG, $(k_x, k_z) = (1, 1)$				
			τ_1^s / τ_0^s					τ_1^s / τ_0^s					τ_1^s / τ_0^s				
			0	0.5	1.0	1.5	2.0	0	0.5	1.0	1.5	2.0	0	0.5	1.0	1.5	2.0
Uniform ($\beta=0.0$)																	
	25	0	17.115	21.569	25.823	29.884	33.762	16.693	21.740	26.786	31.833	36.880	21.122	28.559	35.954	43.309	50.623
		0.5	22.227	26.872	31.314	35.556	39.606	21.434	26.481	31.527	36.574	41.621	23.580	31.056	38.490	45.883	53.235
		1.0	27.160	31.996	36.629	41.058	45.289	26.175	31.221	36.268	41.315	46.361	26.002	33.516	40.989	48.421	55.811
		1.5	31.913	36.940	41.765	46.385	50.802	30.916	35.962	41.009	46.056	51.102	28.388	35.940	43.452	50.922	58.351
		2.0	36.492	41.705	46.720	51.532	56.140	35.656	40.703	45.750	50.796	55.843	30.737	38.328	45.878	53.387	60.855
	50	0	17.115	33.762	47.656	59.523	69.974	16.693	36.880	57.066	77.253	97.440	21.122	50.623	79.486	107.751	135.472
		0.5	36.492	56.140	72.602	86.353	98.118	35.656	55.843	76.030	96.216	116.403	30.737	60.855	90.317	119.142	147.372
		1.0	53.205	75.700	95.153	111.432	125.042	54.620	74.806	94.993	115.180	135.366	39.778	70.508	100.586	130.008	158.796
		1.5	67.786	92.571	114.897	134.154	150.252	73.583	93.770	113.956	134.143	154.330	48.269	79.585	110.276	140.314	169.697
		2.0	80.793	107.272	131.928	154.082	173.143	92.546	112.733	132.920	153.106	173.293	56.250	88.110	119.390	150.042	180.040
Tapered ($\beta=0.5$)																	
	25	0	3.528	5.805	7.608	9.089	10.355	3.984	7.364	10.701	13.996	17.251	4.749	9.355	13.698	17.823	21.775
		0.5	7.237	9.771	11.762	13.367	14.715	7.161	10.500	13.797	17.055	20.277	6.573	11.262	15.676	19.859	23.856
		1.0	10.817	13.632	15.841	17.596	19.042	10.299	13.598	16.859	20.083	23.273	8.370	13.146	17.635	21.880	25.926
		1.5	14.263	17.374	19.833	21.766	23.331	13.400	16.662	19.888	23.081	26.242	10.141	15.006	19.574	23.884	27.982
		2.0	17.577	20.987	23.722	25.865	27.573	16.466	19.694	22.888	26.051	29.187	11.884	16.840	21.490	25.870	30.024
	50	0	3.528	10.355	14.312	17.431	20.147	3.984	17.251	29.943	42.230	54.243	4.749	21.775	36.469	50.189	63.409
		0.5	17.577	27.573	32.282	35.654	38.498	16.466	29.187	41.494	53.521	65.352	11.884	30.024	45.178	59.095	72.419
		1.0	29.666	43.860	50.035	53.791	56.803	28.429	40.757	52.798	64.639	76.336	18.582	38.030	53.793	67.957	81.405
		1.5	40.336	58.432	67.400	71.806	75.049	40.019	52.075	63.926	75.631	87.224	24.853	45.721	62.286	76.765	90.362
		2.0	50.045	70.933	83.983	89.626	93.215	51.351	63.213	74.925	86.524	98.035	30.738	53.025	70.615	85.507	99.285

Table 18 Dimensionless fundamental frequency of uniform and tapered FG nanobeams at different surface residual stresses τ_x^s and τ_y^s and aspect ratios L/h ($\beta_h = \beta_b = \beta$)

β	$\frac{L}{h}$	$\frac{\tau_x^s}{\tau_{x0}^s}$	AFG, $(k_x, k_y) = (1, 0)$					TFG, $(k_x, k_y) = (0, 1)$					BDFG, $(k_x, k_y) = (1, 1)$				
			τ_x^s / τ_{x0}^s					τ_x^s / τ_{x0}^s					τ_x^s / τ_{x0}^s				
			0	0.5	1.0	1.5	2.0	0	0.5	1.0	1.5	2.0	0	0.5	1.0	1.5	2.0
Uniform ($\beta=0.0$)																	
	25	0	12.642	14.229	15.623	16.874	18.018	12.460	14.220	15.784	17.207	18.521	14.373	16.720	18.771	20.615	22.304
		0.5	14.383	15.840	17.140	18.322	19.410	14.119	15.694	17.124	18.444	19.675	15.182	17.428	19.410	21.204	22.853
		1.0	15.891	17.257	18.491	19.622	20.669	15.603	17.041	18.366	19.603	20.765	15.941	18.100	20.022	21.770	23.384
		1.5	17.233	18.533	19.717	20.807	21.822	16.957	18.289	19.530	20.697	21.801	16.657	18.741	20.609	22.316	23.898
		2.0	18.450	19.699	20.843	21.902	22.890	18.211	19.457	20.628	21.736	22.790	17.336	19.354	21.174	22.844	24.396
	50	0	12.649	18.028	21.874	24.993	27.671	12.468	18.532	23.052	26.821	30.122	14.381	22.317	28.060	32.798	36.924
		0.5	18.461	22.903	26.341	29.216	31.725	18.222	22.804	26.608	29.933	32.923	17.346	24.409	29.795	34.321	38.302
		1.0	22.515	26.569	29.814	32.568	34.990	22.552	26.393	29.742	32.750	35.504	19.775	26.268	31.381	35.737	39.597
		1.5	25.772	29.597	32.720	35.399	37.769	26.176	29.549	32.575	35.343	37.909	21.867	27.950	32.849	37.064	40.822
		2.0	28.557	32.221	35.258	37.883	40.215	29.356	32.400	35.181	37.759	40.171	23.724	29.495	34.218	38.315	41.984
Tapered ($\beta=0.5$)																	
	25	0	8.211	11.017	13.176	14.984	16.565	8.435	11.480	13.859	15.880	17.666	9.594	13.676	16.793	19.416	21.724
		0.5	11.347	13.678	15.599	17.261	18.741	11.319	13.727	15.765	17.563	19.191	11.130	14.796	17.719	20.223	22.449
		1.0	13.561	15.674	17.470	19.051	20.473	13.594	15.649	17.460	19.096	20.601	12.415	15.794	18.566	20.973	23.130
		1.5	15.341	17.319	19.033	20.558	21.940	15.532	17.355	19.001	20.513	21.919	13.533	16.700	19.350	21.676	23.774
		2.0	16.861	18.744	20.396	21.878	23.230	17.250	18.906	20.425	21.837	23.162	14.531	17.532	20.082	22.339	24.386
	50	0	8.214	16.570	21.614	25.548	28.878	8.438	17.673	23.481	28.102	32.058	9.597	21.732	29.195	35.105	40.153
		0.5	16.867	23.238	27.771	31.436	34.584	17.257	23.171	27.844	31.832	35.371	14.536	24.394	31.255	36.850	41.696
		1.0	21.584	27.377	31.724	35.303	38.400	22.857	27.583	31.605	35.167	38.398	17.786	26.591	33.058	38.423	43.113
		1.5	25.179	30.623	34.841	38.361	41.426	27.320	31.376	34.961	38.210	41.203	20.345	28.496	34.677	39.865	44.429
		2.0	28.186	33.379	37.495	40.965	44.003	31.145	34.754	38.021	41.027	43.827	22.512	30.200	36.158	41.204	45.664

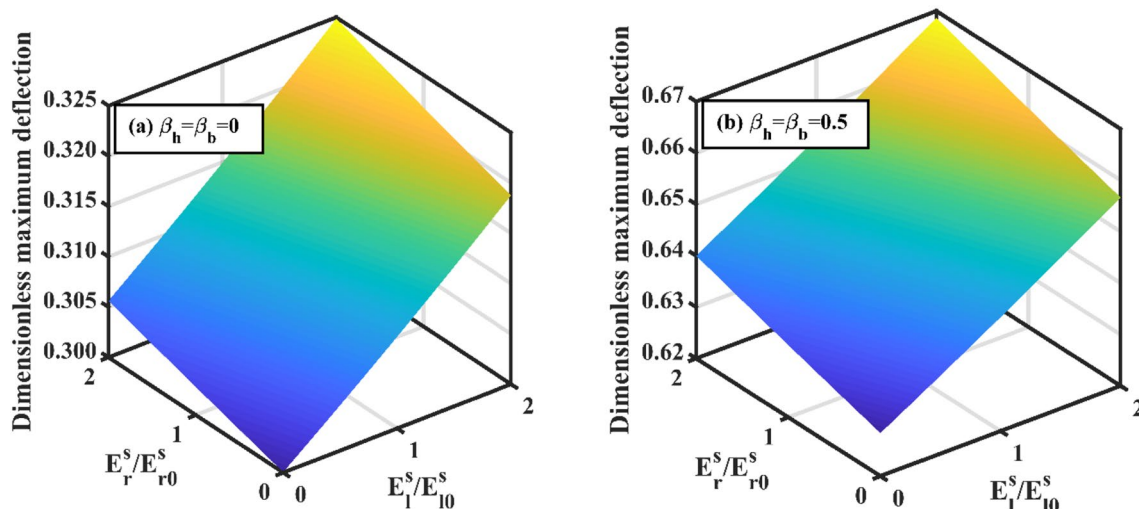


Fig. 14 The effect of the surface elasticity moduli E_r^s/E_{r0}^s and E_1^s/E_{10}^s on the dimensionless maximum deflection of BDFG nanobeam with $k_x=k_z=1$

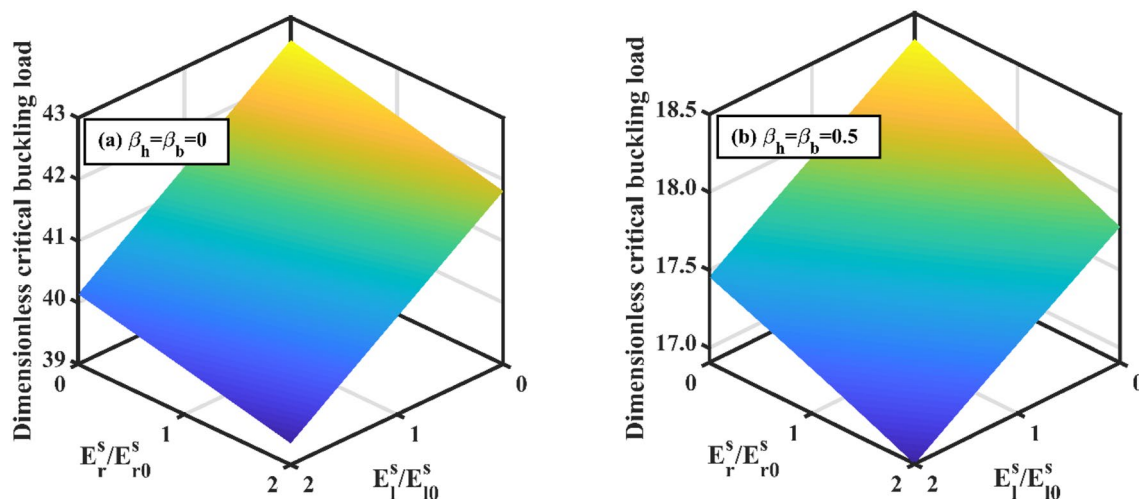


Fig. 15 The effect of the surface elasticity moduli E_r^s/E_{r0}^s and E_1^s/E_{10}^s on the dimensionless critical buckling load of BDFG nanobeam with $k_x=k_z=1$

5.5 Influence of the slenderness ratio

The effect of the slenderness ratio (L/h) on the dimensionless deflection, buckling and frequency of BDFG nanobeam with $h=15$ nm is illustrated in Figs. 20, 21, 22, employing classical “CL” and nonclassical “NC”, i.e., CS, SE, and CSSER, theories. In this section, the results are obtained for FG nanobeams with the material properties provided in Table 9 and the material length-scale parameters are $l_1=10$ nm and $l_r/l_1=3/4$. For convenience and better understanding of the effect of slenderness ratio and thickness on the role of nonclassical parameters, the predicted dimensionless maximum deflection, critical

buckling load, and free vibration frequency using non-classical theories are normalized with their corresponding values using the classical theory, i.e., $\bar{w}^N = \bar{w}^{NC}/\bar{w}^{CL}$, $\bar{P}_{cr}^N = \bar{P}_{cr}^{NC}/\bar{P}_{cr}^{CL}$, and $\bar{\omega}^N = \bar{\omega}^{NC}/\bar{\omega}^{CL}$, respectively. Based on the three different nonclassical theories, Tables 25, 26, 27 record the dimensionless maximum deflection, critical buckling load, and fundamental frequency ratios (\bar{w}^N , \bar{P}_{cr}^N , and $\bar{\omega}^N$), at various values of the slenderness ratio and thickness, considering different material gradations of both uniform and tapered nanobeams. From these results, it is revealed that for a fixed value of the beam thickness, the ratios \bar{w}^N , \bar{P}_{cr}^N , and $\bar{\omega}^N$ predicted using the MCST theory are unchanged by varying the slenderness ratio. Employing the

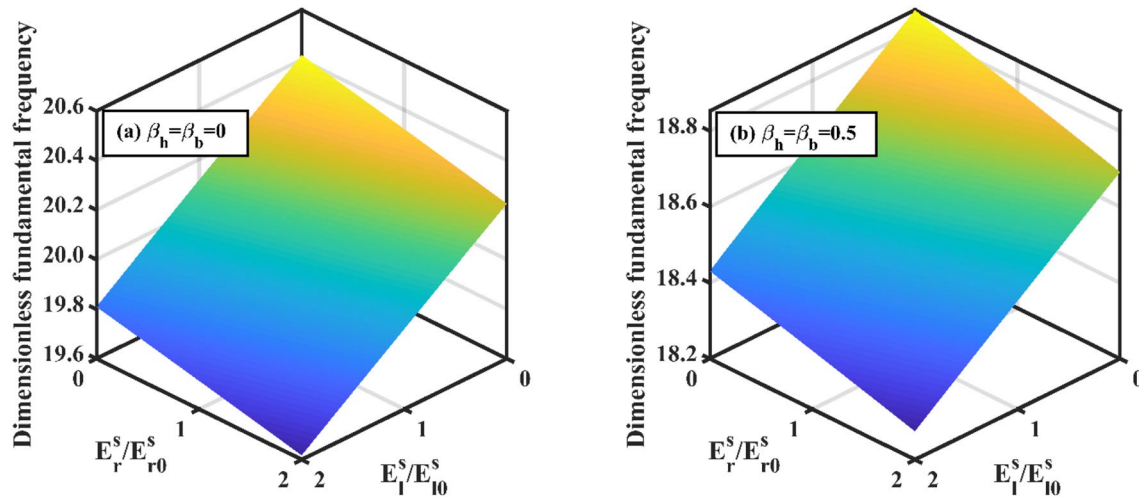


Fig. 16 The effect of the surface elasticity moduli E_l^s/E_{l0}^s and E_r^s/E_{r0}^s on the dimensionless fundamental frequency of BDFG nanobeam with $k_x=k_z=1$

Table 19 Dimensionless maximum deflection of uniform and tapered FG nanobeams at different surface elasticity moduli, aspect ratios, and gradation indices ($\beta_h=\beta_b=\beta$)

β	$\frac{L}{h}$	$\frac{E_r^s}{E_{r0}^s}$	AFG, $(k_x, k_z)=(1,0)$					TFG, $(k_x, k_z)=(0,1)$					BDFG, $(k_x, k_z)=(1,1)$				
			E_l^s/E_{l0}^s					E_l^s/E_{l0}^s					E_l^s/E_{l0}^s				
			0	0.5	1.0	1.5	2.0	0	0.5	1.0	1.5	2.0	0	0.5	1.0	1.5	2.0
Uniform ($\beta=0.0$)	25	0	0.333	0.336	0.340	0.344	0.348	0.339	0.342	0.345	0.348	0.352	0.300	0.305	0.309	0.314	0.319
		0.5	0.336	0.340	0.343	0.347	0.351	0.343	0.346	0.349	0.352	0.356	0.301	0.306	0.311	0.315	0.320
		1.0	0.339	0.343	0.347	0.350	0.354	0.347	0.350	0.353	0.356	0.360	0.303	0.307	0.312	0.317	0.322
		1.5	0.342	0.346	0.350	0.354	0.358	0.351	0.354	0.357	0.361	0.364	0.304	0.309	0.313	0.318	0.323
		2.0	0.346	0.349	0.353	0.357	0.361	0.355	0.358	0.362	0.365	0.368	0.306	0.310	0.315	0.320	0.325
	50	0	0.131	0.131	0.132	0.132	0.133	0.132	0.132	0.133	0.133	0.134	0.124	0.125	0.126	0.127	0.128
		0.5	0.131	0.132	0.132	0.133	0.133	0.132	0.133	0.133	0.134	0.134	0.125	0.125	0.126	0.127	0.128
		1.0	0.132	0.132	0.133	0.133	0.134	0.133	0.133	0.134	0.134	0.135	0.125	0.126	0.126	0.127	0.128
		1.5	0.132	0.133	0.133	0.134	0.134	0.134	0.134	0.134	0.135	0.135	0.125	0.126	0.127	0.127	0.128
		2.0	0.133	0.133	0.134	0.134	0.135	0.134	0.135	0.135	0.136	0.136	0.125	0.126	0.127	0.128	0.128
Tapered ($\beta=0.5$)	25	0	0.675	0.680	0.684	0.689	0.693	0.669	0.673	0.678	0.682	0.687	0.628	0.635	0.642	0.649	0.657
		0.5	0.681	0.685	0.690	0.694	0.699	0.674	0.679	0.683	0.688	0.693	0.631	0.638	0.645	0.652	0.660
		1.0	0.687	0.691	0.696	0.700	0.705	0.680	0.684	0.689	0.694	0.699	0.634	0.641	0.648	0.655	0.663
		1.5	0.692	0.697	0.702	0.707	0.711	0.686	0.690	0.695	0.700	0.704	0.637	0.644	0.651	0.658	0.666
		2.0	0.698	0.703	0.708	0.713	0.718	0.692	0.697	0.701	0.706	0.711	0.640	0.647	0.654	0.661	0.669
	50	0	0.206	0.206	0.206	0.207	0.207	0.205	0.205	0.206	0.206	0.206	0.199	0.200	0.200	0.201	0.202
		0.5	0.206	0.206	0.207	0.207	0.208	0.205	0.206	0.206	0.206	0.207	0.199	0.200	0.201	0.201	0.202
		1.0	0.206	0.207	0.207	0.208	0.208	0.206	0.206	0.207	0.207	0.207	0.199	0.200	0.201	0.201	0.202
		1.5	0.207	0.207	0.208	0.208	0.209	0.206	0.207	0.207	0.207	0.208	0.200	0.200	0.201	0.202	0.202
		2.0	0.207	0.208	0.208	0.209	0.209	0.207	0.207	0.208	0.208	0.208	0.200	0.201	0.201	0.202	0.203

SE and CSSE theories and with the increase of L/h , the predicted dimensionless maximum deflection ratio decreases, whereas the predicted dimensionless critical buckling load and dimensionless frequency ratios increase. This effect of

L/h is observed for different taperness parameters, thicknesses, and material gradations. For the studied ranges of L/h and h , the CSSER theory provides the maximum stiffening effect in comparison with CS and SE theories. For low

Table 20 Dimensionless critical buckling load of uniform and tapered FG nanobeams at different surface elasticity moduli, aspect ratios, and gradation indices ($\beta_h = \beta_\beta = \beta$)

β	$\frac{L}{h}$	$\frac{E_s^*}{E_0^*}$	AFG, $(k_x, k_y) = (1, 0)$					TFG, $(k_x, k_y) = (0, 1)$					BDFG, $(k_x, k_y) = (1, 1)$				
			0	0.5	1.0	1.5	2.0	0	0.5	1.0	1.5	2.0	0	0.5	1.0	1.5	2.0
Uniform ($\beta=0.0$)																	
	25	0	38.174	37.788	37.400	37.010	36.619	37.773	37.438	37.098	36.754	36.405	42.631	42.010	41.388	40.763	40.138
		0.5	37.786	37.402	37.017	36.630	36.242	37.351	37.021	36.686	36.346	36.002	42.430	41.810	41.189	40.567	39.943
		1.0	37.392	37.011	36.629	36.245	35.859	36.924	36.598	36.268	35.934	35.595	42.225	41.608	40.989	40.369	39.747
		1.5	36.993	36.615	36.235	35.854	35.472	36.491	36.170	35.845	35.515	35.181	42.019	41.403	40.786	40.168	39.548
		2.0	36.588	36.212	35.836	35.458	35.078	36.053	35.736	35.416	35.092	34.763	41.810	41.196	40.581	39.964	39.346
	50	0	96.710	96.329	95.947	95.564	95.179	96.498	96.163	95.823	95.479	95.130	102.230	101.610	100.989	100.366	99.742
		0.5	96.310	95.932	95.553	95.172	94.790	96.076	95.746	95.411	95.071	94.727	102.026	101.408	100.789	100.168	99.545
		1.0	95.905	95.529	95.153	94.775	94.396	95.649	95.323	94.993	94.659	94.320	101.820	101.204	100.586	99.967	99.346
		1.5	95.493	95.120	94.747	94.372	93.995	95.216	94.895	94.570	94.240	93.906	101.611	100.997	100.381	99.763	99.145
		2.0	95.074	94.704	94.334	93.961	93.588	94.778	94.461	94.141	93.817	93.488	101.400	100.787	100.173	99.557	98.940
Tapered ($\beta=0.5$)																	
	25	0	16.550	16.460	16.371	16.281	16.191	17.505	17.363	17.216	17.064	16.908	18.334	18.119	17.902	17.681	17.457
		0.5	16.290	16.201	16.112	16.023	15.933	17.326	17.185	17.040	16.891	16.736	18.202	17.988	17.771	17.551	17.327
		1.0	16.018	15.930	15.841	15.752	15.663	17.140	17.002	16.859	16.711	16.559	18.066	17.852	17.635	17.415	17.192
		1.5	15.731	15.643	15.554	15.466	15.377	16.949	16.812	16.671	16.525	16.375	17.924	17.711	17.495	17.275	17.052
		2.0	15.425	15.337	15.249	15.160	15.071	16.751	16.616	16.477	16.333	16.184	17.778	17.565	17.349	17.129	16.906
	50	0	51.240	51.135	51.029	50.922	50.815	53.837	53.611	53.377	53.132	52.876	54.877	54.575	54.265	53.946	53.616
		0.5	50.762	50.655	50.547	50.439	50.330	53.553	53.328	53.094	52.850	52.594	54.648	54.346	54.035	53.714	53.382
		1.0	50.254	50.145	50.035	49.925	49.814	53.256	53.032	52.798	52.554	52.298	54.410	54.106	53.793	53.471	53.137
		1.5	49.712	49.600	49.488	49.375	49.261	52.945	52.721	52.487	52.243	51.987	54.161	53.856	53.541	53.216	52.880
		2.0	49.128	49.013	48.898	48.781	48.664	52.617	52.393	52.159	51.915	51.658	53.901	53.593	53.276	52.948	52.609

Table 21 Dimensionless fundamental frequency of uniform and tapered FG nanobeams at different surface elasticity moduli, aspect ratios, and gradation indices ($\beta_l = \beta_p = \beta$)

β	$\frac{L}{h}$	AFG, $(k_x, k_z) = (1, 0)$					TFG, $(k_x, k_z) = (0, 1)$					BDFG, $(k_x, k_z) = (1, 1)$					
		E_s^*/E_0^*					E_s^*/E_0^*					E_s^*/E_0^*					
		0	0.5	1.0	1.5	2.0	0	0.5	1.0	1.5	2.0	0	0.5	1.0	1.5	2.0	
Uniform ($\beta=0.0$)																	
	25	0	18.873	18.774	18.675	18.574	18.473	18.744	18.660	18.575	18.489	18.401	20.418	20.268	20.117	19.964	19.810
		0.5	18.782	18.683	18.584	18.483	18.382	18.638	18.556	18.472	18.386	18.299	20.371	20.221	20.070	19.917	19.763
		1.0	18.690	18.591	18.491	18.391	18.290	18.531	18.450	18.366	18.281	18.195	20.323	20.173	20.022	19.869	19.715
		1.5	18.596	18.497	18.398	18.297	18.196	18.422	18.341	18.259	18.175	18.089	20.274	20.125	19.973	19.821	19.666
		2.0	18.501	18.403	18.303	18.203	18.101	18.311	18.231	18.149	18.066	17.981	20.225	20.076	19.924	19.772	19.617
	50	0	30.051	29.988	29.925	29.862	29.798	29.976	29.924	29.871	29.818	29.763	31.636	31.539	31.442	31.344	31.245
		0.5	29.995	29.933	29.870	29.806	29.743	29.911	29.859	29.807	29.754	29.700	31.605	31.509	31.412	31.314	31.216
		1.0	29.939	29.877	29.814	29.751	29.687	29.844	29.793	29.742	29.689	29.636	31.575	31.478	31.381	31.284	31.186
		1.5	29.883	29.820	29.757	29.694	29.631	29.776	29.726	29.675	29.624	29.571	31.544	31.448	31.351	31.253	31.155
		2.0	29.826	29.763	29.701	29.638	29.574	29.708	29.658	29.608	29.557	29.505	31.513	31.417	31.320	31.223	31.125
Tapered ($\beta=0.5$)																	
	25	0	17.737	17.675	17.612	17.549	17.485	17.727	17.667	17.607	17.545	17.481	18.853	18.749	18.644	18.538	18.431
		0.5	17.667	17.604	17.542	17.478	17.415	17.652	17.594	17.534	17.473	17.411	18.814	18.710	18.605	18.500	18.393
		1.0	17.595	17.533	17.470	17.407	17.344	17.576	17.518	17.460	17.400	17.338	18.774	18.670	18.566	18.461	18.354
		1.5	17.523	17.461	17.398	17.335	17.272	17.497	17.441	17.383	17.324	17.264	18.733	18.630	18.526	18.421	18.315
		2.0	17.450	17.388	17.325	17.262	17.199	17.417	17.362	17.305	17.247	17.188	18.692	18.589	18.485	18.381	18.275
	50	0	31.872	31.833	31.795	31.756	31.717	31.755	31.722	31.687	31.653	31.617	33.220	33.159	33.097	33.035	32.973
		0.5	31.837	31.798	31.759	31.721	31.682	31.713	31.680	31.647	31.612	31.577	33.200	33.139	33.078	33.016	32.954
		1.0	31.801	31.763	31.724	31.685	31.646	31.670	31.638	31.605	31.571	31.537	33.179	33.119	33.058	32.996	32.934
		1.5	31.766	31.727	31.689	31.650	31.611	31.626	31.594	31.562	31.529	31.496	33.159	33.098	33.037	32.976	32.914
		2.0	31.730	31.691	31.653	31.614	31.575	31.581	31.550	31.519	31.486	31.454	33.138	33.078	33.017	32.956	32.894

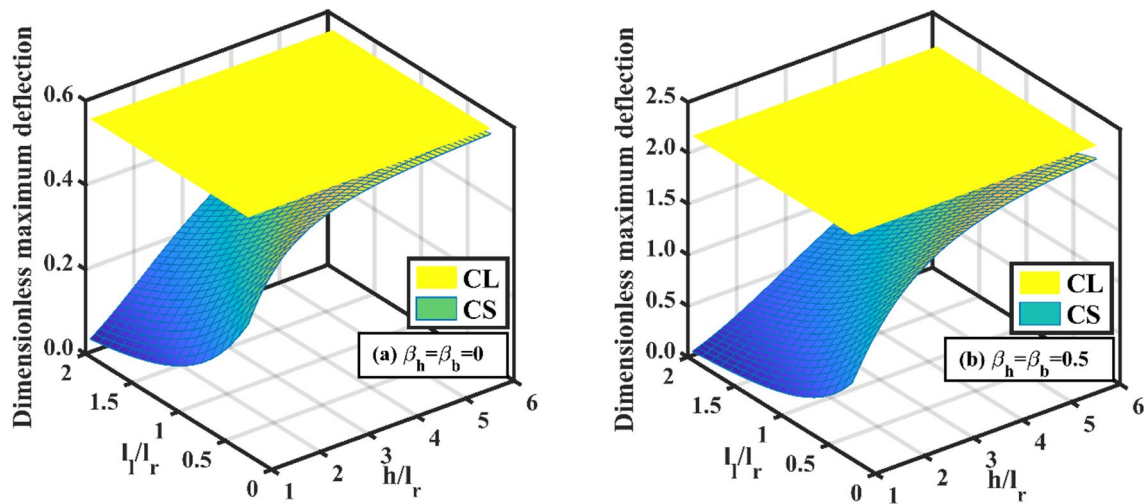


Fig. 17 The mutual effect of the dimensionless material length scale parameter (l/h) and material length scale parameter ratio (l/l_r) on the dimensionless maximum deflection of BDFG microbeam with $k_x = k_z = 1$

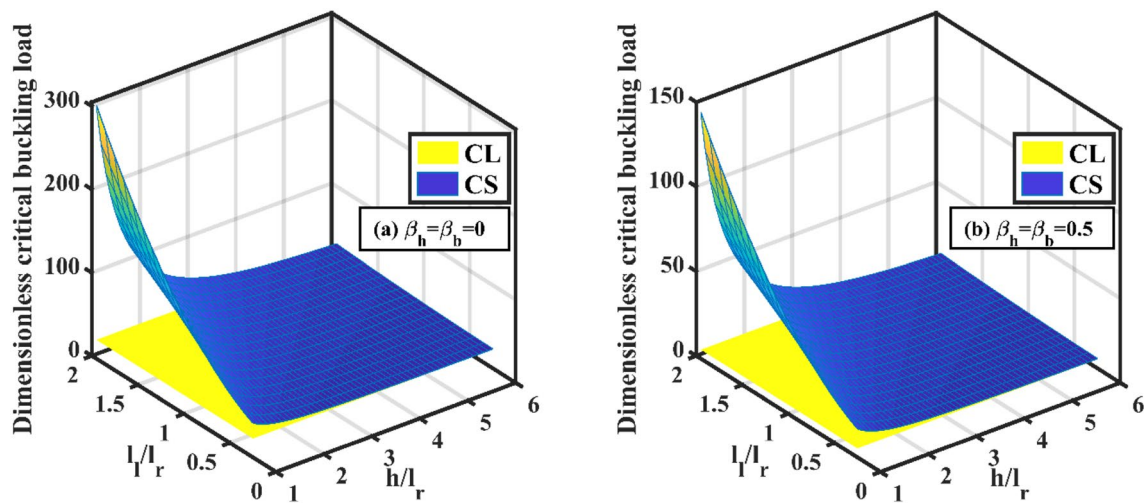


Fig. 18 The mutual effect of the dimensionless material length scale parameter (l/h) and material length scale parameter ratio (l/l_r) on the dimensionless critical buckling load of BDFG microbeam with $k_x = k_z = 1$

values of L/h , the microstructure effect is greater than the surface energy effect. With the increase of L/h , the contribution of surface energy rises and the predicted results from SE theory become greater than those from CS theory. For different material gradations, with increasing the beam thickness or varying the taperness from positive to negative values,

the effect of the slenderness ratio reduces. Increasing the beam thickness decreases the influence of both the material length-scale parameter and surface energy on the static and vibration behaviors of nanobeams. The effect of the beam thickness on the beam response becomes more pronounced

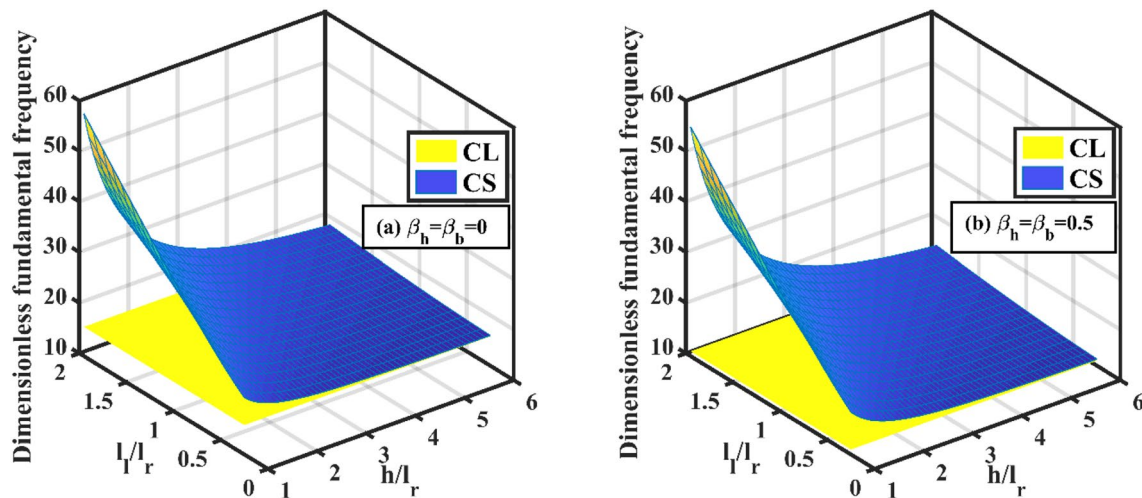


Fig. 19 The mutual effect of the dimensionless material length scale parameter (l/h) and material length scale parameter ratio (l/l_r) on the dimensionless fundamental frequency of BDFG microbeam with $k_x = k_z = 1$

with increasing the slenderness ratio. Amongst the gradation distributions, AFG nanobeam shows the highest sensitivity to the slenderness ratio and thickness.

6 Conclusion

In this study, a nonclassical integrated modified couple stress–surface elasticity model is developed to explore the size-dependent static bending, buckling, and free vibration responses of BDFG tapered micro/nanobeams, for the first time. All the material properties describing the bulk and surface continua, including the material length-scale parameter and surface parameters, are assumed to vary along the thickness and length directions according to power-law distribution. The governing equations and boundary conditions of the proposed Euler–Bernoulli nanobeam are exactly derived using Hamilton principle on the basis of the modified couple stress theory and Gurtin–Murdoch surface elasticity theory. Accounting for the physical neutral surface concept, a semi-analytical solution for the static deflection, critical buckling load, and natural frequency of simply supported BDFG tapered nanobeam are derived using the Navier’s method combined with the GDQM. An extensive detailed study on the effect of different characteristic material and geometrical parameters on the static and vibration

responses is presented. The main results of this study are summarized as follows:

- Both the microstructure via the MCST and surface residual stress have distinct influences in stiffness-hardening of FG nanobeams, and thus, the static deflection decreases and both the critical buckling load and fundamental frequency increase. In contrast, the surface elastic modulus has a softening effect leading to higher deflection and lower critical buckling load and vibration frequency.
- As the cross section of the nanobeam along the length direction decreases, i.e. (β_b, β_h) changes from $(0, 0)$ to $(0.5, 0.5)$, the predicted deflection increases; whereas, both the critical buckling load and vibration frequency decrease, for all gradation distributions. On the contrary, changing (β_b, β_h) from $(0, 0)$ to $(-0.5, -0.5)$ has an opposite effect. The effect of β_b and β_h becomes more pronounced for AFG nanobeams. Employing the CSSE formulation significantly reduces the influence effect of β_h , while that of β_b may increase or decrease depending on the gradation distribution. As β_b increases towards positive values, the impact of β_h increases and vice versa.
- Increasing the surface residual stress of the ceramic (τ_r^s) and/or metallic (τ_r^m) phases shows a distinct reduction in the dimensionless bending deflection and a noticeable

Table 22 Dimensionless maximum deflection of FG nanobeam at different dimensionless material length-scale parameters (l_r/h), material length-scale parameter ratios (l_x/l_r), gradation indices, and taperness parameters ($\beta_h = \beta_l = \beta$)

β	$\frac{h}{l_r}$	Homogeneous, $(k_x, k_y) = (0, 0)$					AFG, $(k_x, k_y) = (1, 0)$					TFG, $(k_x, k_y) = (0, 1)$					BDFG, $(k_x, k_y) = (1, 1)$				
		l_r/l_r					l_r/l_r					l_x/l_r					l_x/l_r				
		0.5	1.0	1.5	2.0	2.0	0.5	1.0	1.5	2.0	2.0	0.5	1.0	1.5	2.0	2.0	0.5	1.0	1.5	2.0	
0.5	1	0.4420	0.4420	0.4420	0.4420	0.4321	0.2861	0.2065	0.1583	0.4590	0.2676	0.1678	0.1130	0.4815	0.2278	0.1282	0.0813				
	2	1.3331	1.3331	1.3331	1.3331	1.1427	0.8675	0.6748	0.5414	1.1971	0.8145	0.5600	0.3985	1.1393	0.6887	0.4344	0.2918				
	4	2.7159	2.7159	2.7159	2.7159	2.0165	1.7822	1.5612	1.3705	2.0227	1.6822	1.3585	1.0882	1.7703	1.4093	1.0841	0.8308				
	8	3.6938	3.6938	3.6938	3.6938	2.5379	2.4421	2.3349	2.2208	2.4548	2.3103	2.1321	1.9390	2.0701	1.9242	1.7440	1.5524				
	16	4.0657	4.0657	4.0657	4.0657	2.7285	2.7004	2.6668	2.6284	2.5950	2.5525	2.4942	2.4226	2.1637	2.1214	2.0623	1.9892				
0.0	CL	4.2079	4.2079	4.2079	4.2079	2.7997	2.7997	2.7997	2.7997	2.6456	2.6456	2.6456	2.6456	2.1971	2.1971	2.1971	2.1971				
	1	0.2157	0.2157	0.2157	0.2157	0.2030	0.1322	0.0942	0.0713	0.2112	0.1310	0.0850	0.0583	0.2151	0.1087	0.0627	0.0402				
	2	0.5474	0.5474	0.5474	0.5474	0.4261	0.3345	0.2653	0.2152	0.4453	0.3367	0.2497	0.1869	0.4003	0.2754	0.1880	0.1323				
	4	0.8893	0.8893	0.8893	0.8893	0.5921	0.5415	0.4881	0.4384	0.6160	0.5542	0.4847	0.4168	0.5111	0.4466	0.3757	0.3103				
	8	1.0539	1.0539	1.0539	1.0539	0.6571	0.6406	0.6204	0.5973	0.6812	0.6608	0.6338	0.6017	0.5492	0.5288	0.5008	0.4678				
-0.5	16	1.1050	1.1050	1.1050	1.1050	0.6758	0.6713	0.6656	0.6587	0.6998	0.6943	0.6866	0.6768	0.5597	0.5542	0.5462	0.5359				
	CL	1.1232	1.1232	1.1232	1.1232	0.6822	0.6822	0.6822	0.6822	0.7062	0.7062	0.7062	0.7062	0.5633	0.5633	0.5633	0.5633				
	1	0.1271	0.1271	0.1271	0.1271	0.1146	0.0759	0.0540	0.0406	0.1185	0.0775	0.0518	0.0363	0.1172	0.0634	0.0378	0.0246				
	2	0.2842	0.2842	0.2842	0.2842	0.2063	0.1676	0.1357	0.1110	0.2190	0.1755	0.1369	0.1065	0.1894	0.1405	0.1018	0.0746				
	4	0.4132	0.4132	0.4132	0.4132	0.2582	0.2406	0.2210	0.2011	0.2786	0.2581	0.2336	0.2081	0.2238	0.2026	0.1778	0.1529				
0.085	8	0.4665	0.4665	0.4665	0.4665	0.2756	0.2703	0.2635	0.2556	0.2990	0.2927	0.2843	0.2740	0.2345	0.2282	0.2193	0.2085				
	16	0.4821	0.4821	0.4821	0.4821	0.2803	0.2789	0.2770	0.2747	0.3046	0.3029	0.3006	0.2976	0.2373	0.2357	0.2332	0.2300				
	CL	0.4875	0.4875	0.4875	0.4875	0.2819	0.2819	0.2819	0.2819	0.3065	0.3065	0.3065	0.3065	0.2383	0.2383	0.2383	0.2383				

Table 23 Dimensionless critical buckling load of FG nanobeams at different dimensionless material length-scale parameters (l_r/h), material length-scale parameter ratios (l_r/l_r), gradation indices, and taperness parameters ($\beta_h = \beta_b = \beta$)

β	$\frac{h}{l_r}$	Homogeneous, $(k_x, k_y) = (0,0)$					AFG, $(k_x, k_y) = (1,0)$					TFG, $(k_x, k_y) = (0,1)$					BDFG, $(k_x, k_y) = (1,1)$				
		l_r/l_r					l_r/l_r					l_r/l_r					l_r/l_r				
		0.5	1.0	1.5	2.0	2.0	0.5	1.0	1.5	2.0	2.0	0.5	1.0	1.5	2.0	2.0	0.5	1.0	1.5	2.0	
0.5	1	28.437	28.437	28.437	28.437	28.437	29.126	42.830	57.401	72.706	72.706	27.327	46.969	74.996	111.415	111.415	26.118	54.735	96.672	151.902	
	2	9.365	9.365	9.365	9.365	9.365	10.824	13.948	17.463	21.257	21.257	10.373	15.333	22.375	31.503	31.503	10.849	17.934	28.370	42.148	
	4	4.530	4.530	4.530	4.530	4.530	5.922	6.630	7.461	8.394	8.394	6.042	7.317	9.115	11.431	11.431	6.807	8.596	11.211	14.657	
	8	3.286	3.286	3.286	3.286	3.286	4.581	4.749	4.949	5.179	5.179	4.928	5.255	5.718	6.315	6.315	5.733	6.188	6.851	7.720	
	16	2.968	2.968	2.968	2.968	2.968	4.227	4.269	4.318	4.375	4.375	4.645	4.727	4.845	4.998	4.998	5.457	5.572	5.739	5.958	
0.0	CL	2.861	2.861	2.861	2.861	2.861	4.107	4.107	4.107	4.107	4.107	4.550	4.550	4.550	4.550	4.550	5.364	5.364	5.364	5.364	
	1	59.586	59.586	59.586	59.586	59.586	63.218	96.297	133.390	173.648	173.648	60.835	98.071	151.256	220.388	220.388	59.703	118.000	203.962	317.509	
	2	23.478	23.478	23.478	23.478	23.478	30.094	38.067	47.538	58.087	58.087	28.857	38.167	51.463	68.746	68.746	32.086	46.574	68.089	96.534	
	4	14.451	14.451	14.451	14.451	14.451	21.570	23.510	25.942	28.777	28.777	20.863	23.190	26.514	30.835	30.835	25.107	28.717	34.105	41.247	
	8	12.194	12.194	12.194	12.194	12.194	19.391	19.870	20.488	21.234	21.234	18.865	19.446	20.277	21.358	21.358	23.351	24.252	25.601	27.394	
-0.5	16	11.630	11.630	11.630	11.630	11.630	18.841	18.960	19.116	19.306	19.306	18.365	18.510	18.718	18.988	18.988	22.911	23.136	23.473	23.922	
	CL	11.442	11.442	11.442	11.442	11.442	18.657	18.657	18.657	18.657	18.657	18.198	18.198	18.198	18.198	18.198	22.764	22.764	22.764	22.764	
	1	99.807	99.807	99.807	99.807	99.807	110.137	168.924	236.795	311.725	311.725	106.771	163.792	245.105	350.731	350.731	107.670	201.507	339.648	521.972	
	2	44.429	44.429	44.429	44.429	44.429	61.479	76.372	94.643	115.332	115.332	57.555	71.936	92.389	118.898	118.898	66.650	90.413	125.600	171.845	
	4	30.450	30.450	30.450	30.450	30.450	49.243	53.012	57.942	63.820	63.820	45.121	48.753	53.921	60.617	60.617	56.395	62.398	71.423	83.340	
8	26.924	26.924	26.924	26.924	26.924	46.174	47.121	48.401	49.992	49.992	41.992	42.904	44.205	45.894	45.894	53.831	55.339	57.629	60.686		
	26.039	26.039	26.039	26.039	26.039	45.405	45.642	45.967	46.376	46.376	41.208	41.436	41.762	42.186	42.186	53.191	53.568	54.143	54.916		
	CL	25.744	25.744	25.744	25.744	25.744	45.149	45.149	45.149	45.149	40.946	40.946	40.946	40.946	40.946	52.977	52.977	52.977	52.977		

Table 24 Dimensionless fundamental frequency of FG nanobeams at different dimensionless material length-scale parameters (l_r/h), material length-scale parameter ratios (l_r/l_r), gradation indices, and taperness parameters ($\beta_h = \beta_b = \beta$)

β	$\frac{h}{l_r}$	Homogeneous, $(k_x, k_y) = (0,0)$						AFG, $(k_x, k_y) = (1,0)$						TFG, $(k_x, k_y) = (0,1)$						BDFG, $(k_x, k_y) = (1,1)$					
		l_r/l_r						l_r/l_r						l_r/l_r						l_r/l_r					
		0.5	1.0	1.5	2.0	2.0	2.0	0.5	1.0	1.5	2.0	2.0	2.0	0.5	1.0	1.5	2.0	2.0	2.0	0.5	1.0	1.5	2.0	2.0	2.0
0.5	1	22.744	22.744	22.744	22.744	22.744	23.819	29.637	35.123	40.341	40.341	23.156	30.278	38.208	46.537	46.537	23.016	33.630	44.953	56.553	56.553				
	2	13.155	13.155	13.155	13.155	13.155	14.800	17.076	19.444	21.816	21.816	14.420	17.433	20.983	24.841	24.841	15.101	19.421	24.470	29.876	29.876				
0.0	4	9.271	9.271	9.271	9.271	9.271	11.233	11.962	12.801	13.713	13.713	11.151	12.203	13.550	15.112	15.112	12.191	13.648	15.549	17.755	17.755				
	8	7.978	7.978	7.978	7.978	7.978	10.048	10.249	10.493	10.774	10.774	10.146	10.450	10.868	11.384	11.384	11.301	11.715	12.300	13.030	13.030				
0.0	16	7.614	7.614	7.614	7.614	7.614	9.713	9.764	9.828	9.904	9.904	9.875	9.954	10.067	10.211	10.211	11.061	11.169	11.326	11.530	11.530				
	CL	7.487	7.487	7.487	7.487	7.487	9.596	9.596	9.596	9.596	9.596	9.782	9.782	9.782	9.782	9.782	10.979	10.979	10.979	10.979	10.979				
-0.5	1	24.235	24.235	24.235	24.235	24.235	25.867	31.979	37.875	43.549	43.549	25.368	32.210	40.001	48.284	48.284	25.609	36.008	47.384	59.169	59.169				
	2	15.212	15.212	15.212	15.212	15.212	17.844	20.107	22.560	25.073	25.073	17.472	20.093	23.332	26.967	26.967	18.771	22.623	27.371	32.614	32.614				
-0.5	4	11.935	11.935	11.935	11.935	11.935	15.123	15.802	16.626	17.552	17.552	14.856	15.663	16.748	18.061	18.061	16.609	17.765	19.366	21.305	21.305				
	8	10.963	10.963	10.963	10.963	10.963	14.348	14.528	14.759	15.035	15.035	14.127	14.343	14.646	15.031	15.031	16.019	16.326	16.775	17.355	17.355				
-0.5	16	10.707	10.707	10.707	10.707	10.707	14.146	14.192	14.251	14.324	14.324	13.938	13.993	14.072	14.173	14.173	15.868	15.946	16.062	16.216	16.216				
	CL	10.620	10.620	10.620	10.620	10.620	14.078	14.078	14.078	14.078	14.078	13.875	13.875	13.875	13.875	13.875	15.817	15.817	15.817	15.817	15.817				
-0.5	1	25.290	25.290	25.290	25.290	25.290	27.565	33.682	39.681	45.497	45.497	27.143	33.559	41.008	49.024	49.024	27.821	37.717	48.767	60.335	60.335				
	2	16.949	16.949	16.949	16.949	16.949	20.524	22.714	25.156	27.695	27.695	20.023	22.338	25.270	28.628	28.628	21.888	25.356	29.756	34.709	34.709				
-0.5	4	14.088	14.088	14.088	14.088	14.088	18.336	18.977	19.780	20.700	20.700	17.783	18.465	19.395	20.538	20.538	20.133	21.134	22.551	24.297	24.297				
	8	13.271	13.271	13.271	13.271	13.271	17.745	17.913	18.136	18.408	18.408	17.174	17.354	17.607	17.930	17.930	19.670	19.931	20.320	20.828	20.828				
-0.5	16	13.058	13.058	13.058	13.058	13.058	17.594	17.637	17.694	17.766	17.766	17.018	17.064	17.129	17.213	17.213	19.552	19.618	19.718	19.851	19.851				
	CL	12.986	12.986	12.986	12.986	12.986	17.544	17.544	17.544	17.544	17.544	16.966	16.966	16.966	16.966	16.966	19.513	19.513	19.513	19.513	19.513				

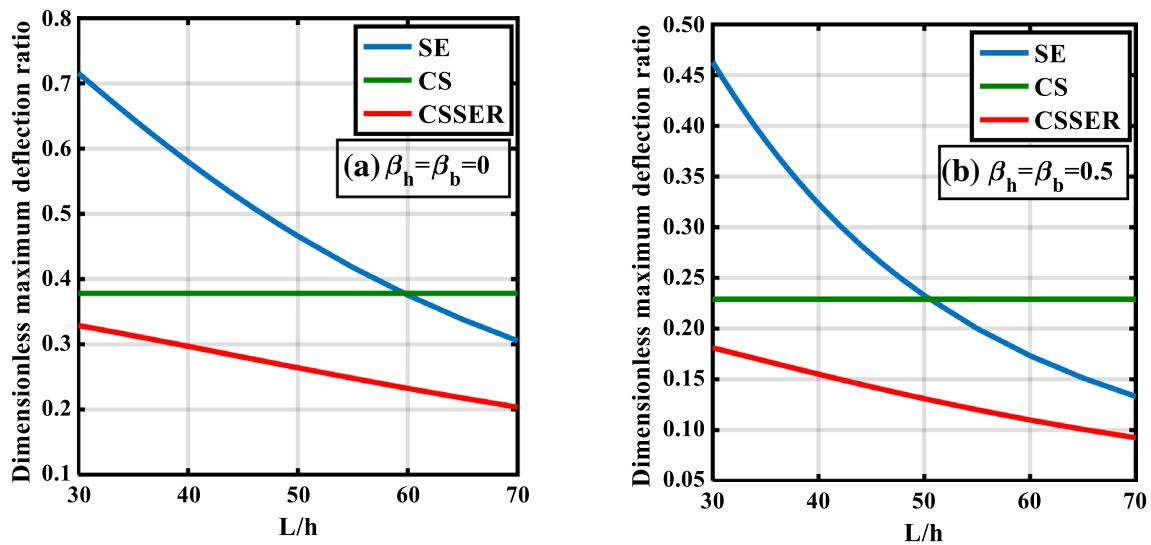


Fig. 20 Variation of the dimensionless maximum deflection ratio (\bar{w}/N) with the slenderness ratio (L/h) of BDFG nanobeam using SE, CS, and CSSER theories ($h = 15 \text{ nm}$ and $k_x = k_z = 1.0$)

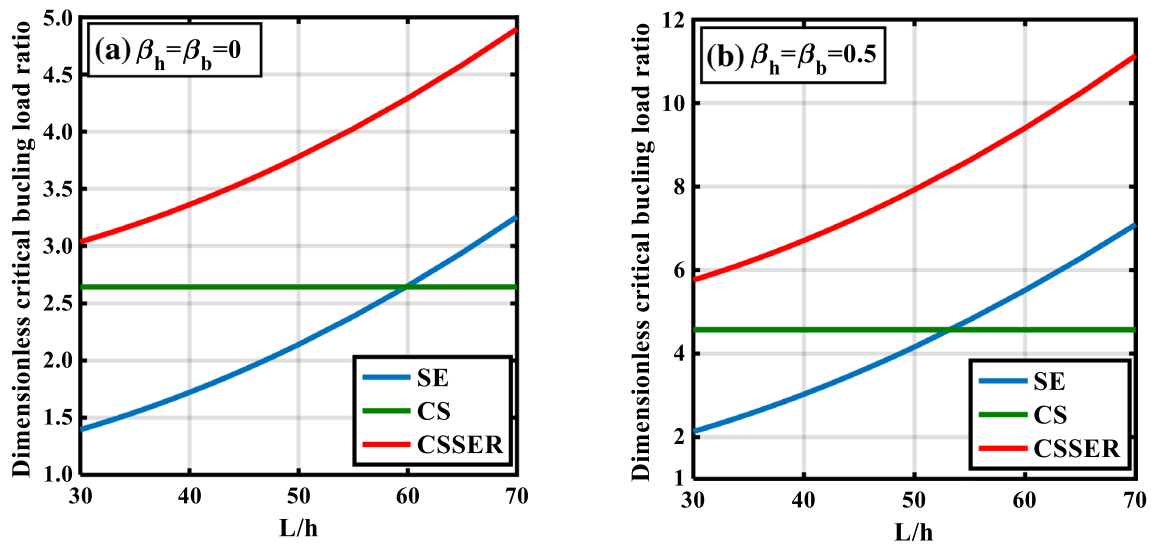


Fig. 21 Variation of the dimensionless critical buckling load ratio (\bar{P}_{cr}^N) with the slenderness ratio (L/h) of BDFG nanobeam using SE, CS, and CSSER theories ($h = 15 \text{ nm}$ and $k_x = k_z = 1.0$)

increase in the dimensionless critical buckling load and vibration frequency, for all gradation distributions. The buckling response is more sensitive to the surface residual stress than the vibration and bending responses. The highest impact of τ_l^s and τ_r^s are, respectively, correspond-

ing to BDFG and TFG nanobeams. Also, the impact of τ_l^s is reduced as τ_r^s increases and the opposite is true.

- The surface elasticity moduli E_l^s and E_r^s with negative values slightly enhances the stiffness-softening behavior of FG nanobeams, and accordingly, the dimension-

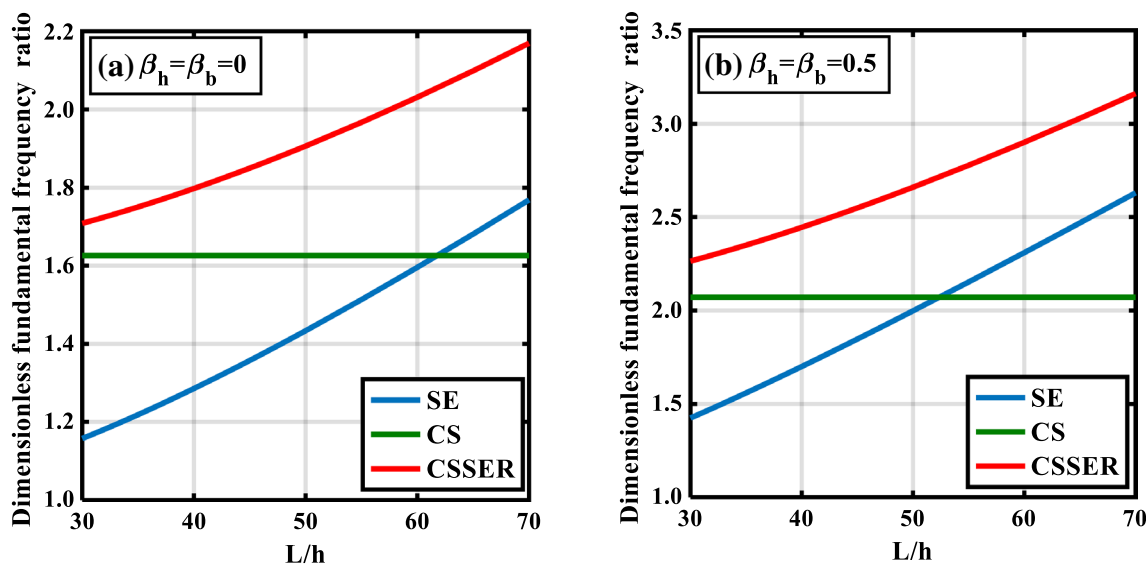


Fig. 22 Variation of the dimensionless natural frequency ratio ($\bar{\omega}N$) with the slenderness ratio (L/h) of BDFG nanobeam using SE, CS, and CSSER theories ($h = 15$ nm and $k_x = k_z = 1.0$)

less bending deflection increases and the dimensionless critical buckling load and vibration frequency decrease. BDFG and TFG nanobeams give the highest effect of the surface elasticity moduli E_l^s and E_r^s , respectively. It can be concluded that the effect of surface elasticity moduli is very small compared with that of the surface residual stress.

- Increasing the material length-scale parameter-to-thickness ratio (l_r/h) and/or the material length-scale parameter ratio (l_r/l_l) improves the stiffness-hardening effect of the microbeam compared with the classical beam model. Compared to the uniform microbeam, the effects of both l_r/h and l_r/l_l increase with positive taperness parameters. The roles of l_r/h and l_r/l_l are significantly influenced by the gradation distribution as the maximum effect of l_r/l_l is obtained for BDFG microbeams, followed by TFG and AFG.
- The gradation indices k_z and k_x have a significant effect on the response of BDFG tapered micro/nanobeams. Increasing k_z and/or k_x increases the stiffness-hardening of the beam and accordingly, the deflection decreases, whereas the critical buckling load and free vibration

frequency increase. Both the nonclassical formulation and positive taperness parameters noticeably reduces the effect of k_z and k_x . Also, the influence of the gradient indices on the bending response is much greater than that on the buckling and vibration responses.

- Increasing the aspect ratio enhances the influence surface energy, whereas the microstructure effect is unchanged. With the increase of aspect ratio, the influences of the surface residual stress increases; whereas, the influence of E_l^s and E_r^s significantly decreases. The impact of the aspect ratio is reduced by increasing the beam thickness or varying the taperness parameters from positive to negative values.

The present results could be helpful in reaching the desired static and free vibration responses of micro/nano-beam. As the beam response can be controlled by appropriate engaging of the gradient indices in thickness and/or length directions and proper selection of the cross section.

Table 25 Dimensionless maximum deflection ratio (\bar{w}^N) of uniform and tapered FG nanobeams at different values of the slenderness ratio and thickness employing various nonclassical theories

L/h	$h(\text{nm})$	AFG, $(k_x, k_z) = (1, 0)$			TFG, $(k_x, k_z) = (0, 1)$			BDFG, $(k_x, k_z) = (1, 1)$		
		SE	CS	CSSER	SE	CS	CSSER	SE	CS	CSSER
Nonuniform nanobeam, $(\beta_b, \beta_h) = (0.5, 0.5)$										
20	15	0.6138	0.2613	0.2247	0.6295	0.2390	0.2096	0.6687	0.2289	0.2057
	30	0.7609	0.5831	0.4933	0.7728	0.5524	0.4753	0.8015	0.5394	0.4761
	60	0.8643	0.8471	0.7477	0.8719	0.8293	0.7393	0.8898	0.8222	0.7464
30	15	0.4048	0.2613	0.1893	0.4208	0.2390	0.1799	0.4628	0.2289	0.1811
	30	0.5763	0.5831	0.4092	0.5927	0.5524	0.4007	0.6329	0.5394	0.4114
	60	0.7314	0.8471	0.6462	0.7444	0.8293	0.6458	0.7753	0.8222	0.6643
40	15	0.2744	0.2613	0.1551	0.2871	0.2390	0.1502	0.3232	0.2289	0.1551
	30	0.4303	0.5831	0.3303	0.4467	0.5524	0.3284	0.4889	0.5394	0.3455
	60	0.6017	0.8471	0.5431	0.6179	0.8293	0.5485	0.6568	0.8222	0.5756
60	15	0.1427	0.2613	0.1022	0.1502	0.2390	0.1019	0.1733	0.2289	0.1099
	30	0.2499	0.5831	0.2128	0.2619	0.5524	0.2165	0.2960	0.5394	0.2370
	60	0.3997	0.8471	0.3734	0.4156	0.8293	0.3832	0.4571	0.8222	0.4165
Uniform nanobeam, $(\beta_b, \beta_h) = (0.0, 0.0)$										
20	15	0.8358	0.4186	0.3867	0.8314	0.3906	0.3620	0.8599	0.3781	0.3562
	30	0.9106	0.7415	0.6911	0.9080	0.7194	0.6705	0.9247	0.7086	0.6699
	60	0.9532	0.9197	0.8800	0.9518	0.9112	0.8709	0.9609	0.9068	0.8745
30	15	0.6773	0.4186	0.3486	0.6706	0.3906	0.3278	0.7160	0.3781	0.3288
	30	0.8077	0.7415	0.6301	0.8029	0.7194	0.6115	0.8346	0.7086	0.6213
	60	0.8937	0.9197	0.8289	0.8907	0.9112	0.8196	0.9098	0.9068	0.8320
40	15	0.5352	0.4186	0.3066	0.5275	0.3906	0.2895	0.5799	0.3781	0.2969
	30	0.6974	0.7415	0.5608	0.6909	0.7194	0.5443	0.7343	0.7086	0.5640
	60	0.8218	0.9197	0.7667	0.8173	0.9112	0.7570	0.8468	0.9068	0.7790
60	15	0.3343	0.4186	0.2280	0.3273	0.3906	0.2169	0.3754	0.3781	0.2323
	30	0.5015	0.7415	0.4266	0.4938	0.7194	0.4142	0.5464	0.7086	0.4462
	60	0.6682	0.9197	0.6312	0.6614	0.9112	0.6214	0.7069	0.9068	0.6590
Nonuniform nanobeam, $(\beta_b, \beta_h) = (-0.5, -0.5)$										
20	15	0.9151	0.5159	0.4924	0.9082	0.4857	0.4629	0.9271	0.4756	0.4584
	30	0.9557	0.8075	0.7783	0.9519	0.7897	0.7594	0.9622	0.7814	0.7581
	60	0.9773	0.9433	0.9231	0.9754	0.9374	0.9157	0.9807	0.9338	0.9170
30	15	0.8093	0.5159	0.4600	0.7961	0.4857	0.4319	0.8324	0.4756	0.4340
	30	0.8946	0.8075	0.7374	0.8865	0.7897	0.7172	0.9086	0.7814	0.7244
	60	0.9444	0.9433	0.8937	0.9399	0.9374	0.8844	0.9521	0.9338	0.8919
40	15	0.6965	0.5159	0.4211	0.6787	0.4857	0.3948	0.7283	0.4756	0.4040
	30	0.8212	0.8075	0.6868	0.8088	0.7897	0.6654	0.8429	0.7814	0.6820
	60	0.9019	0.9433	0.8555	0.8943	0.9374	0.8439	0.9148	0.9338	0.8590
60	15	0.4979	0.5159	0.3393	0.4772	0.4857	0.3170	0.5362	0.4756	0.3371
	30	0.6651	0.8075	0.5741	0.6465	0.7897	0.5515	0.6984	0.7814	0.5843
	60	0.7990	0.9433	0.7624	0.7854	0.9374	0.7463	0.8225	0.9338	0.7772

Table 26 Dimensionless critical buckling load ratio (\bar{P}_{cr}^N) of uniform and tapered FG nanobeams at different values of the slenderness ratio and thickness, employing various nonclassical theories

L/h	$h(\text{nm})$	AFG, $(k_x, k_z)=(1,0)$			TFG, $(k_x, k_z)=(0,1)$			BDFG, $(k_x, k_z)=(1,1)$		
		SE	CS	CSSER	SE	CS	CSSER	SE	CS	CSSER
Nonuniform nanobeam, $(\beta_b, \beta_h)=(0.5, 0.5)$										
20	15	1.6112	3.9584	4.5919	1.5759	4.3510	4.9554	1.4851	4.5711	5.0795
	30	1.3070	1.7463	2.0591	1.2889	1.8589	2.1560	1.2433	1.9104	2.1604
	60	1.1539	1.1880	1.3428	1.1447	1.2195	1.3657	1.1219	1.2317	1.3549
30	15	2.4228	3.9584	5.4363	2.3389	4.3510	5.7596	2.1325	4.5711	5.7594
	30	1.7172	1.7463	2.4766	1.6738	1.8589	2.5513	1.5697	1.9104	2.4952
	60	1.3600	1.1880	1.5502	1.3380	1.2195	1.5609	1.2857	1.2317	1.5202
40	15	3.5401	3.9584	6.6130	3.3917	4.3510	6.8814	3.0271	4.5711	6.7082
	30	2.2865	1.7463	3.0582	2.2086	1.8589	3.1026	2.0235	1.9104	2.9621
	60	1.6475	1.1880	1.8394	1.6075	1.2195	1.8332	1.5142	1.2317	1.7510
60	15	6.6319	3.9584	9.9400	6.3142	4.3510	10.0608	5.5169	4.5711	9.4002
	30	3.8836	1.7463	4.7010	3.7127	1.8589	4.6633	3.3018	1.9104	4.2856
	60	2.4608	1.1880	2.6590	2.3715	1.2195	2.6060	2.1625	1.2317	2.4064
Uniform nanobeam, $(\beta_b, \beta_h)=(0.0, 0.0)$										
20	15	1.1956	2.3716	2.5664	1.2019	2.5600	2.7619	1.1622	2.6421	2.8042
	30	1.0978	1.3444	1.4420	1.1010	1.3900	1.4910	1.0811	1.4107	1.4918
	60	1.0489	1.0863	1.1352	1.0505	1.0975	1.1480	1.0405	1.1027	1.1432
30	15	1.4746	2.3716	2.8451	1.4887	2.5600	3.0487	1.3949	2.6421	3.0369
	30	1.2373	1.3444	1.5815	1.2444	1.3900	1.6344	1.1974	1.4107	1.6081
	60	1.1187	1.0863	1.2049	1.1222	1.0975	1.2197	1.0987	1.1027	1.2014
40	15	1.8651	2.3716	3.2352	1.8903	2.5600	3.4503	1.7207	2.6421	3.3627
	30	1.4326	1.3444	1.7766	1.4452	1.3900	1.8352	1.3604	1.4107	1.7710
	60	1.2163	1.0863	1.3025	1.2226	1.0975	1.3201	1.1802	1.1027	1.2829
60	15	2.9808	2.3716	4.3498	3.0377	2.5600	4.5977	2.6516	2.6421	4.2935
	30	1.9905	1.3444	2.3343	2.0188	1.3900	2.4088	1.8258	1.4107	2.2365
	60	1.4953	1.0863	1.5815	1.5094	1.0975	1.6069	1.4129	1.1027	1.5156
Nonuniform nanobeam, $(\beta_b, \beta_h)=(-0.5, -0.5)$										
20	15	1.0921	1.9546	2.0477	1.1000	2.0734	2.1747	1.0780	2.1261	2.2051
	30	1.0461	1.2444	1.2907	1.0500	1.2706	1.3209	1.0390	1.2852	1.3245
	60	1.0230	1.0618	1.0849	1.0250	1.0679	1.0930	1.0195	1.0718	1.0913
30	15	1.2339	1.9546	2.1913	1.2536	2.0734	2.3298	1.1996	2.1261	2.3281
	30	1.1170	1.2444	1.3620	1.1269	1.2706	1.3981	1.0999	1.2852	1.3856
	60	1.0585	1.0618	1.1204	1.0634	1.0679	1.1315	1.0499	1.0718	1.1218
40	15	1.4322	1.9546	2.3923	1.4684	2.0734	2.5469	1.3698	2.1261	2.5003
	30	1.2162	1.2444	1.4617	1.2344	1.2706	1.5060	1.1850	1.2852	1.4712
	60	1.1081	1.0618	1.1701	1.1172	1.0679	1.1853	1.0925	1.0718	1.1645
60	15	1.9980	1.9546	2.9662	2.0806	2.0734	3.1663	1.8553	2.1261	2.9919
	30	1.4996	1.2444	1.7466	1.5412	1.2706	1.8142	1.4282	1.2852	1.7155
	60	1.2499	1.0618	1.3121	1.2709	1.0679	1.3391	1.2142	1.0718	1.2863

Table 27 Dimensionless fundamental frequency ratio ($\bar{\omega}^N$) of uniform and tapered FG nanobeams at different values of the slenderness ratio and thickness, employing various nonclassical theories

L/h	$h(\text{nm})$	AFG, $(k_x, k_z) = (1, 0)$			TFG, $(k_x, k_z) = (0, 1)$			BDFG, $(k_x, k_z) = (1, 1)$		
		SE	CS	CSSER	SE	CS	CSSER	SE	CS	CSSER
Nonuniform nanobeam, $(\beta_b, \beta_h) = (0.5, 0.5)$										
20	15	1.2335	1.9437	2.0318	1.2204	2.0197	2.0932	1.1876	2.0708	2.1255
	30	1.1266	1.3038	1.3948	1.1190	1.3365	1.4183	1.1005	1.3549	1.4217
	60	1.0662	1.0845	1.1444	1.0621	1.0955	1.1509	1.0522	1.1010	1.1470
30	15	1.5139	1.9437	2.2119	1.4888	2.0197	2.2582	1.4244	2.0708	2.2644
	30	1.2915	1.3039	1.5302	1.2759	1.3365	1.5439	1.2369	1.3549	1.5286
	60	1.1576	1.0845	1.2297	1.1485	1.0955	1.2307	1.1265	1.1010	1.2152
40	15	1.8336	1.9437	2.4413	1.7972	2.0197	2.4707	1.7001	2.0708	2.4455
	30	1.4911	1.3039	1.7013	1.4670	1.3365	1.7039	1.4051	1.3549	1.6665
	60	1.2741	1.0845	1.3397	1.2594	1.0955	1.3343	1.2228	1.1010	1.3045
60	15	2.5288	1.9437	3.0000	2.4719	2.0197	2.9954	2.3098	2.0708	2.9009
	30	1.9487	1.3039	2.1134	1.9085	1.3365	2.0943	1.7993	1.3549	2.0083
	60	1.5583	1.0845	1.6120	1.5317	1.0955	1.5931	1.4625	1.1010	1.5308
Uniform nanobeam, $(\beta_b, \beta_h) = (0.0, 0.0)$										
20	15	1.0691	1.5437	1.5701	1.0720	1.6000	1.6251	1.0564	1.6260	1.6416
	30	1.0359	1.1606	1.1884	1.0374	1.1790	1.2073	1.0292	1.1879	1.2091
	60	1.0183	1.0425	1.0597	1.0191	1.0476	1.0654	1.0148	1.0501	1.0638
30	15	1.1873	1.5437	1.6531	1.1931	1.6000	1.7074	1.1574	1.6260	1.7083
	30	1.0998	1.1606	1.2445	1.1030	1.1790	1.2640	1.0832	1.1879	1.2554
	60	1.0516	1.0425	1.0917	1.0533	1.0476	1.0981	1.0428	1.0501	1.0905
40	15	1.3352	1.5437	1.7626	1.3445	1.6000	1.8164	1.2855	1.6260	1.7976
	30	1.1833	1.1606	1.3190	1.1886	1.1790	1.3394	1.1545	1.1879	1.3175
	60	1.0966	1.0425	1.1351	1.0994	1.0476	1.1424	1.0808	1.0501	1.1269
60	15	1.6878	1.5437	2.0434	1.7044	1.6000	2.0968	1.5958	1.6260	2.0312
	30	1.3947	1.1606	1.5117	1.4049	1.1790	1.5346	1.3375	1.1879	1.4805
	60	1.2158	1.0425	1.2507	1.2216	1.0476	1.2605	1.1826	1.0501	1.2248
Nonuniform nanobeam, $(\beta_b, \beta_h) = (-0.5, -0.5)$										
20	15	1.0265	1.3866	1.3939	1.0302	1.4286	1.4369	1.0216	1.4459	1.4488
	30	1.0136	1.1113	1.1216	1.0155	1.1234	1.1351	1.0111	1.1294	1.1372
	60	1.0069	1.0292	1.0356	1.0078	1.0323	1.0396	1.0056	1.0340	1.0392
30	15	1.0912	1.3866	1.4421	1.0999	1.4286	1.4875	1.0778	1.4459	1.4889
	30	1.0474	1.1113	1.1522	1.0520	1.1234	1.1678	1.0403	1.1294	1.1632
	60	1.0242	1.0292	1.0525	1.0266	1.0323	1.0578	1.0205	1.0340	1.0536
40	15	1.1758	1.3867	1.5070	1.1905	1.4286	1.5554	1.1519	1.4459	1.5431
	30	1.0930	1.1114	1.1938	1.1011	1.1234	1.2121	1.0799	1.1294	1.1986
	60	1.0480	1.0292	1.0756	1.0523	1.0323	1.0827	1.0410	1.0340	1.0735
60	15	1.3894	1.3867	1.6786	1.4176	1.4286	1.7348	1.3410	1.4459	1.6884
	30	1.2139	1.1114	1.3052	1.2306	1.1234	1.3306	1.1856	1.1294	1.2946
	60	1.1131	1.0292	1.1391	1.1223	1.0323	1.1509	1.0975	1.0340	1.1283

References

- Birman V, Byrd LW (2007) Modeling and analysis of functionally graded materials and structures. *Appl Mech Rev* 60:195–216
- Udupa G, Rao SS, Gangadharan K (2014) Functionally graded composite materials: an overview. *Procedia Mater Sci* 5:1291–1299
- Attia MA, El-Shafei AG (2019) Modeling and analysis of the nonlinear indentation problems of functionally graded elastic layered solids. *Proc Inst Mech Eng Part J: J Eng Tribol* 233(12):1903–1920
- Eltaher MA, Attia MA, Wagih A (2020) Predictive model for indentation of elasto-plastic functionally graded composites. *Compos B Eng* 197:108129. <https://doi.org/10.1016/j.compositesb.2020.108129>
- Wagih A, Attia MA, AbdelRahman AA, Bendine K, Sebaey TA (2019) On the indentation of elastoplastic functionally graded materials. *Mech Mater* 129:169–188
- Attia MA, El-Shafei AG (2020) investigation of multibody receding frictional indentation problems of unbonded elastic

- functionally graded layers. *Int J Mech Sci* 184:105838. <https://doi.org/10.1016/j.ijmecsci.2020.105838>
7. Zenkour AM (2014) On the magneto-thermo-elastic responses of FG annular sandwich disks. *Int J Eng Sci* 75:54–66
 8. Attia MA, Eltahir MA, Soliman AE, Abdelrahman AA, Alshorbagy AE (2018) Thermoelastic crack analysis in functionally graded pipelines conveying natural gas by an FEM. *Int J Appl Mech* 10(4):1850036. <https://doi.org/10.1142/S1758825118500369>
 9. Eltahir MA, Attia MA, Soliman AE, Alshorbagy AE (2018) Analysis of crack occurs under unsteady pressure and temperature in a natural gas facility by applying FGM. *Struct Eng Mech* 66(1):97–111
 10. Soliman AE, Eltahir MA, Attia MA, Alshorbagy AE (2018) Nonlinear transient analysis of FG pipe subjected to internal pressure and unsteady temperature in a natural gas facility. *Struct Eng Mech* 66(1):85–96
 11. Witvrouw A, Mehta A (2005) The use of functionally graded poly-SiGe layers for MEMS applications, Materials science forum. *Trans Tech Publ*, pp 255–260
 12. Lee Z, Ophus C, Fischer L, Nelson-Fitzpatrick N, Westra K, Evoy S, Radmilovic V, Dahmen U, Mitlin D (2006) Metallic NEMS components fabricated from nanocomposite Al–Mo films. *Nanotechnology* 17:3063
 13. Kahrobaiyan M, Asghari M, Rahaeifard M, Ahmadian M (2010) Investigation of the size-dependent dynamic characteristics of atomic force microscope microcantilevers based on the modified couple stress theory. *Int J Eng Sci* 48:1985–1994
 14. Fu Y, Du H, Huang W, Zhang S, Hu M (2004) TiNi-based thin films in MEMS applications: a review. *Sens Actuators A* 112:395–408
 15. Nix WD (1989) Mechanical properties of thin films. *Metall Trans A* 20:2217
 16. Fleck N, Muller G, Ashby MF, Hutchinson JW (1994) Strain gradient plasticity: theory and experiment. *Acta Metall Mater* 42:475–487
 17. Ma Q, Clarke DR (1995) Size dependent hardness of silver single crystals. *J Mater Res* 10:853–863
 18. Stölken JS, Evans A (1998) A microbend test method for measuring the plasticity length scale. *Acta Mater* 46:5109–5115
 19. Chong AC, Lam DC (1999) Strain gradient plasticity effect in indentation hardness of polymers. *J Mater Res* 14:4103–4110
 20. Lam DC, Yang F, Chong A, Wang J, Tong P (2003) Experiments and theory in strain gradient elasticity. *J Mech Phys Solids* 51:1477–1508
 21. Mindlin R, Tiersten H (1962) Effects of couple-stresses in linear elasticity. *Arch Ration Mech Anal* 11:415–448
 22. Mindlin RD (1964) Micro-structure in linear elasticity. *Arch Ration Mech Anal* 16:51–78
 23. Yang F, Chong A, Lam DCC, Tong P (2002) Couple stress based strain gradient theory for elasticity. *Int J Solids Struct* 39:2731–2743
 24. Eringen AC (2002) *Nonlocal continuum field theories*. Springer, Berlin
 25. Lim C, Zhang G, Reddy J (2015) A higher-order nonlocal elasticity and strain gradient theory and its applications in wave propagation. *J Mech Phys Solids* 78:298–313
 26. Wang K, Wang B, Kitamura T (2016) A review on the application of modified continuum models in modeling and simulation of nanostructures. *Acta Mech Sin* 32:83–100
 27. Thai H-T, Vo TP, Nguyen T-K, Kim S-E (2017) A review of continuum mechanics models for size-dependent analysis of beams and plates. *Compos Struct* 177:196–219
 28. Chandel VS, Wang G, Talha M (2020) Advances in modelling and analysis of nano structures: a review. *Nanotechnol Rev* 9:230–258
 29. Chong A, Yang F, Lam D, Tong P (2001) Torsion and bending of micron-scaled structures. *J Mater Res* 16:1052–1058
 30. Liu D, He Y, Tang X, Ding H, Hu P, Cao P (2012) Size effects in the torsion of microscale copper wires: Experiment and analysis. *Scripta Mater* 66:406–409
 31. Liu D, He Y, Dunstan DJ, Zhang B, Gan Z, Hu P, Ding H (2013) Toward a further understanding of size effects in the torsion of thin metal wires: an experimental and theoretical assessment. *Int J Plast* 41:30–52
 32. Park S, Gao X (2006) Bernoulli-Euler beam model based on a modified couple stress theory. *J Micromech Microeng* 16:2355
 33. Nix WD, Gao H (1998) Indentation size effects in crystalline materials: a law for strain gradient plasticity. *J Mech Phys Solids* 46:411–425
 34. Gurtin ME, Murdoch AI (1975) A continuum theory of elastic material surfaces. *Arch Ration Mech Anal* 57:291–323
 35. Gurtin ME, Murdoch AI (1978) Surface stress in solids. *Int J Solids Struct* 14:431–440
 36. Akgöz B, Civalek Ö (2014) Thermo-mechanical buckling behavior of functionally graded microbeams embedded in elastic medium. *Int J Eng Sci* 85:90–104
 37. Al-Basyouni K, Tounsi A, Mahmoud S (2015) Size dependent bending and vibration analysis of functionally graded micro beams based on modified couple stress theory and neutral surface position. *Compos Struct* 125:621–630
 38. Arbind A, Reddy J (2013) Nonlinear analysis of functionally graded microstructure-dependent beams. *Compos Struct* 98:272–281
 39. Babaei H, Eslami MR (2020) Size-dependent vibrations of thermally pre/post-buckled FG porous micro-tubes based on modified couple stress theory. *Int J Mech Sci*. <https://doi.org/10.1016/j.ijmecsci.2020.105694>
 40. Dehrouyeh-Semnani AM, Mostafaei H, Nikkiah-Bahrami M (2016) Free flexural vibration of geometrically imperfect functionally graded microbeams. *Int J Eng Sci* 105:56–79
 41. Ghayesh MH (2019) Viscoelastic mechanics of Timoshenko functionally graded imperfect microbeams. *Compos Struct* 225:110974
 42. Gholipour A, Ghayesh MH (2020) Nonlinear coupled mechanics of functionally graded nanobeams. *Int J Eng Sci* 150:103221
 43. Mollamahmutoğlu Ç, Mercan A (2019) A novel functional and mixed finite element analysis of functionally graded microbeams based on modified couple stress theory. *Compos Struct* 223:110950
 44. Nateghi A, Salamat-talab M, Rezapour J, Daneshian B (2012) Size dependent buckling analysis of functionally graded micro beams based on modified couple stress theory. *Appl Math Model* 36:4971–4987
 45. Reddy J (2011) Microstructure-dependent couple stress theories of functionally graded beams. *J Mech Phys Solids* 59:2382–2399
 46. Şimşek M, Reddy J (2013) Bending and vibration of functionally graded microbeams using a new higher order beam theory and the modified couple stress theory. *Int J Eng Sci* 64:37–53
 47. Thai H-T, Vo TP, Nguyen T-K, Lee J (2015) Size-dependent behavior of functionally graded sandwich microbeams based on the modified couple stress theory. *Compos Struct* 123:337–349
 48. Zhang Q, Liu H (2020) On the dynamic response of porous functionally graded microbeam under moving load. *Int J Eng Sci* 153:103317
 49. Akgöz B, Civalek Ö (2013) Free vibration analysis of axially functionally graded tapered Bernoulli-Euler microbeams based on the modified couple stress theory. *Compos Struct* 98:314–322
 50. Huang Y, Li X-F (2010) A new approach for free vibration of axially functionally graded beams with non-uniform cross-section. *J Sound Vib* 329:2291–2303

51. Huang Y, Yang L-E, Luo Q-Z (2013) Free vibration of axially functionally graded Timoshenko beams with non-uniform cross-section. *Compos B Eng* 45:1493–1498
52. Rajasekaran S (2013) Buckling and vibration of axially functionally graded nonuniform beams using differential transformation based dynamic stiffness approach. *Meccanica* 48:1053–1070
53. Shafiei N, Kazemi M, Ghadiri M (2016) Nonlinear vibration of axially functionally graded tapered microbeams. *Int J Eng Sci* 102:12–26
54. Şimşek M, Kocatürk T, Akbaş Ş (2012) Dynamic behavior of an axially functionally graded beam under action of a moving harmonic load. *Compos Struct* 94:2358–2364
55. Zheng S, Chen D, Wang H (2019) Size dependent nonlinear free vibration of axially functionally graded tapered microbeams using finite element method. *Thin-Walled Struct* 139:46–52
56. Nemat-Alla M (2003) Reduction of thermal stresses by developing two-dimensional functionally graded materials. *Int J Solids Struct* 40:7339–7356
57. Lü C, Chen W, Xu R, Lim CW (2008) Semi-analytical elasticity solutions for bi-directional functionally graded beams. *Int J Solids Struct* 45:258–275
58. Zhao L, Chen W, Lü C (2012) Symplectic elasticity for bi-directional functionally graded materials. *Mech Mater* 54:32–42
59. Şimşek M (2015) Bi-directional functionally graded materials (BDFGs) for free and forced vibration of Timoshenko beams with various boundary conditions. *Compos Struct* 133:968–978
60. Şimşek M (2016) Buckling of Timoshenko beams composed of two-dimensional functionally graded material (2D-FGM) having different boundary conditions. *Compos Struct* 149:304–314
61. Wang Z-H, Wang X-H, Xu G-D, Cheng S, Zeng T (2016) Free vibration of two-directional functionally graded beams. *Compos Struct* 135:191–198
62. Pydah A, Sabale A (2017) Static analysis of bi-directional functionally graded curved beams. *Compos Struct* 160:867–876
63. Pydah A, Batra R (2017) Shear deformation theory using logarithmic function for thick circular beams and analytical solution for bi-directional functionally graded circular beams. *Compos Struct* 172:45–60
64. Karamanlı A (2017a) Elastostatic analysis of two-directional functionally graded beams using various beam theories and Symmetric Smoothed Particle Hydrodynamics method. *Compos Struct* 160:653–669
65. Karamanlı A (2017b) Bending behaviour of two directional functionally graded sandwich beams by using a quasi-3d shear deformation theory. *Compos Struct* 174:70–86
66. Karamanlı A (2018) Free vibration analysis of two directional functionally graded beams using a third order shear deformation theory. *Compos Struct* 189:127–136
67. Nguyen DK, Nguyen QH, Tran TT (2017) Vibration of bi-dimensional functionally graded Timoshenko beams excited by a moving load. *Acta Mech* 228:141–155
68. Rajasekaran S, Khaniki HB (2018) Free vibration analysis of bi-directional functionally graded single/multi-cracked beams. *Int J Mech Sci* 144:341–356
69. Li J, Guan Y, Wang G, Zhao G, Lin J, Naceur H, Coutellier D (2018) Meshless modeling of bending behavior of bi-directional functionally graded beam structures. *Compos B Eng* 155:104–111
70. Tang Y, Lv X, Yang T (2019) Bi-directional functionally graded beams: asymmetric modes and nonlinear free vibration. *Compos B Eng* 156:319–331
71. Lei J, He Y, Li Z, Guo S, Liu D (2019) Postbuckling analysis of bi-directional functionally graded imperfect beams based on a novel third-order shear deformation theory. *Compos Struct* 209:811–829
72. Huang Y, Ouyang ZY (2020) Exact solution for bending analysis of two-directional functionally graded Timoshenko beams. *Arch Appl Mech* 90:1005–1023
73. Huang Y (2020) Bending and free vibrational analysis of bi-directional functionally graded beams with circular cross-section. *Appl Math Mech*. <https://doi.org/10.1007/s10483-020-2670-6>
74. Chen WR, Chang H (2020) Vibration analysis of bi-directional functionally graded Timoshenko beams using Chebyshev collocation method. *Int J Struct Stab Dyn*. <https://doi.org/10.1142/S0219455421500097>
75. Mohammadian M (2021) Nonlinear free vibration of damped and undamped bi-directional functionally graded beams using a cubic-quintic nonlinear model. *Compos Struct* 255:112866. <https://doi.org/10.1016/j.compstruct.2020.112866>
76. Nguyen DK, Vu ANT, Le NAT, Pham VN (2020) Dynamic behavior of a bidirectional functionally graded sandwich beam under nonuniform motion of a moving load. *Shock Vib* vol 2020, Article ID 8854076, 15 pages <https://doi.org/10.1155/2020/8854076>
77. Ghatage PS, Kar VR, Sudhagar PE (2020) On the numerical modelling and analysis of multi-directional functionally graded composite structures: a review. *Compos Struct* 236:111837. <https://doi.org/10.1016/j.compstruct.2019.111837>
78. Nejad MZ, Hadi A, Rastgoo A (2016) Buckling analysis of arbitrary two-directional functionally graded Euler-Bernoulli nano-beams based on nonlocal elasticity theory. *Int J Eng Sci* 103:1–10
79. Nejad MZ, Hadi A (2016) Non-local analysis of free vibration of bi-directional functionally graded Euler-Bernoulli nano-beams. *Int J Eng Sci* 105:1–11
80. Karamanlı A, Vo TP (2018) Size dependent bending analysis of two directional functionally graded microbeams via a quasi-3D theory and finite element method. *Compos B Eng* 144:171–183
81. Karamanlı A, Vo TP (2020) Bending, vibration, buckling analysis of bi-directional FG porous microbeams with a variable material length scale parameter. *Appl Math Model*. <https://doi.org/10.1016/j.apm.2020.09.058>
82. Shafiei N, Kazemi M (2017) Buckling analysis on the bi-dimensional functionally graded porous tapered nano-/micro-scale beams. *Aerosp Sci Technol* 66:1–11
83. Shafiei N, Mirjavadi SS, MohaselAfshari B, Rabby S, Kazemi M (2017) Vibration of two-dimensional imperfect functionally graded (2D-FG) porous nano-/micro-beams. *Comput Methods Appl Mech Eng* 322:615–632
84. Trinh LC, Vo TP, Thai H-T, Nguyen T-K (2018) Size-dependent vibration of bi-directional functionally graded microbeams with arbitrary boundary conditions. *Compos B Eng* 134:225–245
85. Li L, Li X, Hu Y (2018) Nonlinear bending of a two-dimensionally functionally graded beam. *Compos Struct* 184:1049–1061
86. Yang T, Tang Y, Li Q, Yang X-D (2018) Nonlinear bending, buckling and vibration of bi-directional functionally graded nanobeams. *Compos Struct* 204:313–319
87. Yu T, Hu H, Zhang J, Bui TQ (2019) Isogeometric analysis of size-dependent effects for functionally graded microbeams by a non-classical quasi-3D theory. *Thin-Walled Struct* 138:1–14
88. Yu T, Zhang J, Hu H, Bui TQ (2019) A novel size-dependent quasi-3D isogeometric beam model for two-directional FG microbeams analysis. *Compos Struct* 211:76–88
89. Khaniki HB, Rajasekaran S (2018) Mechanical analysis of non-uniform bi-directional functionally graded intelligent microbeams using modified couple stress theory. *Mater Res Exp* 5:055703
90. Rajasekaran S, Khaniki HB (2019) Size-dependent forced vibration of non-uniform bi-directional functionally graded beams embedded in variable elastic environment carrying a moving harmonic mass. *Appl Math Model* 72:129–154

91. Chen X, Zhang X, Lu Y, Li Y (2019) Static and dynamic analysis of the postbuckling of bi-directional functionally graded material microbeams. *Int J Mech Sci* 151:424–443
92. Chen X, Lu Y, Li Y (2019) Free vibration, buckling and dynamic stability of bi-directional FG microbeam with a variable length scale parameter embedded in elastic medium. *Appl Math Model* 67:430–448
93. Sahmani S, Safaei B (2019a) Nonlinear free vibrations of bi-directional functionally graded micro/nano-beams including nonlocal stress and microstructural strain gradient size effects. *Thin-Walled Struct* 140:342–356
94. Sahmani S, Safaei B (2019b) Nonlocal strain gradient nonlinear resonance of bi-directional functionally graded composite micro/nano-beams under periodic soft excitation. *Thin-Walled Struct* 143:106226
95. Sahmani S, Safaei B (2020) Influence of homogenization models on size-dependent nonlinear bending and postbuckling of bi-directional functionally graded micro/nano-beams. *Appl Math Model* 82:336–358
96. Rahmani A, Faroughi S, Friswell M (2020) The vibration of two-dimensional imperfect functionally graded (2D-FG) porous rotating nanobeams based on general nonlocal theory. *Mech Syst Signal Process* 144:106854
97. Attia MA, Mohamed SA (2020a) Nonlinear thermal buckling and postbuckling analysis of bidirectional functionally graded tapered microbeams based on Reddy beam theory. *Engin Comput*. <https://doi.org/10.1007/s00366-020-01080-1>
98. Attia MA, Mohamed SA (2020b) Thermal vibration characteristics of pre/post-buckled bi-directional functionally graded tapered microbeams based on modified couple stress Reddy beam theory. *Eng Comput*. <https://doi.org/10.1007/s00366-020-01188-4>
99. Barati A, Hadi A, Nejad MZ, Noroozi R (2020) On vibration of bi-directional functionally graded nanobeams under magnetic field. *Mech Based Des Struct Mach*. <https://doi.org/10.1080/15397734.2020.1719507>
100. Çelik M, Artan R (2020) An investigation of static bending of a bi-directional strain-gradient Euler-Bernoulli nano-beams with the method of initial values. *Microsyst Technol* 26(9):2921–2929
101. Dangi C, Saini S, Lal R, Singh IV (2020) Size dependent FEM model for Bi-directional functionally graded nano-beams. *Mater Today Proc* 24:1302–1311
102. Malik M, Das D (2020) Study on free vibration behavior of rotating bidirectional functionally graded nano-beams based on Eringen's nonlocal theory. *Proc Inst Mech Eng Part L: J Mater Des Appl*. <https://doi.org/10.1177/1464420720929375>
103. Ansari R, Pourashraf T, Gholami R (2015) An exact solution for the nonlinear forced vibration of functionally graded nanobeams in thermal environment based on surface elasticity theory. *Thin-Walled Struct* 93:169–176
104. Ansari R, Pourashraf T, Gholami R, Sahmani S (2017) Post-buckling behavior of functionally graded nanobeams subjected to thermal loading based on the surface elasticity theory. *Meccanica* 52:283–297
105. Ansari R, Gholami R (2016) Size-dependent modeling of the free vibration characteristics of postbuckled third-order shear deformable rectangular nanoplates based on the surface stress elasticity theory. *Compos B Eng* 95:301–316
106. Chu L, Li Y, Dui G (2020) Nonlinear analysis of functionally graded flexoelectric nanoscale energy harvesters. *Int J Mech Sci* 167:105282
107. Ebrahimi F, Hosseini SHS (2020) Effect of residual surface stress on parametrically excited nonlinear dynamics and instability of double-walled nanobeams: an analytical study. *Eng Comput*. <https://doi.org/10.1007/s00366-019-00879-x>
108. Esfahani S, Khadem SE, Mamaghani AE (2019) Nonlinear vibration analysis of an electrostatic functionally graded nanoresonator with surface effects based on nonlocal strain gradient theory. *Int J Mech Sci* 151:508–522
109. Hosseini-Hashemi S, Nazemnezhad R (2013) An analytical study on the nonlinear free vibration of functionally graded nanobeams incorporating surface effects. *Compos B Eng* 52:199–206
110. Saffari S, Hashemian M, Toghraie D (2017) Dynamic stability of functionally graded nanobeam based on nonlocal Timoshenko theory considering surface effects. *Phys B* 520:97–105
111. Sahmani S, Aghdam M, Bahrami M (2015) On the free vibration characteristics of postbuckled third-order shear deformable FGM nanobeams including surface effects. *Compos Struct* 121:377–385
112. Xie B, Sahmani S, Safaei B, Xu B (2020) Nonlinear secondary resonance of FG porous silicon nanobeams under periodic hard excitations based on surface elasticity theory. *Eng Comput*. <https://doi.org/10.1007/s00366-019-00931-w>
113. Gao X-L, Mahmoud F (2014) A new Bernoulli-Euler beam model incorporating microstructure and surface energy effects. *Zeitschrift für angewandte Mathematik und Physik* 65:393–404
114. Gao X-L (2015) A new Timoshenko beam model incorporating microstructure and surface energy effects. *Acta Mech* 226:457–474
115. Gao X-L, Zhang G (2015) A microstructure-and surface energy-dependent third-order shear deformation beam model. *Zeitschrift für angewandte Mathematik und Physik* 66:1871–1894
116. Zhang GY, Gao XL, Bishop JE, Fang HE (2018) Band gaps for elastic wave propagation in a periodic composite beam structure incorporating microstructure and surface energy effects. *Compos Struct* 189:263–272
117. Attia MA, Mahmoud FF (2016) Modeling and analysis of nanobeams based on nonlocal-couple stress elasticity and surface energy theories. *Int J Mech Sci* 105:126–134
118. Attia MA, Mahmoud FF (2017) Size-dependent behavior of viscoelastic nanoplates incorporating surface energy and microstructure effects. *Int J Mech Sci* 123:117–132
119. Zhang L, Wang B, Zhou S, Xue Y (2017) Modeling the size-dependent nanostructures: incorporating the bulk and surface effects. *J Nanomech Micromech* 7:04016012. [https://doi.org/10.1061/\(ASCE\)NM.2153-5477.0000117](https://doi.org/10.1061/(ASCE)NM.2153-5477.0000117)
120. Attia MA (2017a) On the mechanics of functionally graded nanobeams with the account of surface elasticity. *Int J Eng Sci* 115:73–101
121. Attia MA, Rahman AA (2018) On vibrations of functionally graded viscoelastic nanobeams with surface effects. *Int J Eng Sci* 127:1–32
122. Attia MA, Mohamed SA (2018) Pull-in instability of functionally graded cantilever nanoactuators incorporating effects of microstructure, surface energy and intermolecular forces. *Int J Appl Mech* 10:1850091
123. Attia MA, Mohamed SA (2019) Coupling effect of surface energy and dispersion forces on nonlinear size-dependent pull-in instability of functionally graded micro-/nanoswitches. *Acta Mech* 230:1181–1216
124. Abo-Bakr RM, Eltaher MA, Attia MA (2020) Pull-in and free-standing instability of actuated functionally graded nanobeams including surface and stiffening effects. *Eng Comput*. <https://doi.org/10.1007/s00366-020-01146-0>
125. Shanab RA, Attia MA, Mohamed SA (2017) Nonlinear analysis of functionally graded nanoscale beams incorporating the surface energy and microstructure effects. *Int J Mech Sci* 131:908–923
126. Shanab RA, Mohamed SA, Mohamed NA, Attia MA (2020) Comprehensive investigation of vibration of sigmoid and power law FG nanobeams based on surface elasticity and modified

- couple stress theories. *Acta Mech.* <https://doi.org/10.1007/s00707-020-02623-9>
127. Shanab RA, Attia MA, Mohamed SA, Mohamed NA (2020) Effect of microstructure and surface energy on the static and dynamic characteristics of FG Timoshenko nanobeam embedded in an elastic medium. *J Nano Res.* <https://doi.org/10.4028/www.scientific.net/JNanoR.61.97>
128. Attia MA, Shanab RA, Mohamed SA, Mohamed NA (2019) Surface energy effects on the nonlinear free vibration of functionally graded Timoshenko nanobeams based on modified couple stress theory. *Int J Struct Stab Dyn* 19(11):1950127. <https://doi.org/10.1142/S021945541950127X>
129. Hosseini-Hashemi S, Behdad S, Fagher M (2020) Vibration analysis of two-phase local/nonlocal viscoelastic nanobeams with surface effects. *Europ Phys J Plus* 135:190
130. Yin S, Deng Y, Yu T, Gu S, Zhang G (2021) Isogeometric analysis for non-classical Bernoulli-Euler beam model incorporating microstructure and surface energy effects. *Appl Math Model* 89:470–485
131. Yin S, Deng Y, Zhang G, Yu T, Gu S (2020) A new isogeometric Timoshenko beam model incorporating microstructures and surface energy effects. *Math Mech Solids.* <https://doi.org/10.1177/1081286520917998>
132. Gao X-L, Zhang GY (2016) A non-classical Kirchhoff plate model incorporating microstructure, surface energy and foundation effects, *Continuum Mech. Thermodynamics* 28:195–213
133. Attia MA, Mohamed SA (2017) Nonlinear modeling and analysis of electrically actuated viscoelastic microbeams based on the modified couple stress theory. *Appl Math Model* 41:195–222
134. Attia MA (2017b) Investigation of size-dependent quasistatic response of electrically actuated nonlinear viscoelastic microcantilevers and microbridges. *Meccanica* 52:2391–2420
135. Shahba A, Attarnejad R, Hajilar S (2011) Free vibration and stability of axially functionally graded tapered Euler-Bernoulli beams. *Shock Vibr* 18:683–696
136. Hashemian M, Foroutan S, Toghraie D (2019) Comprehensive beam models for buckling and bending behavior of simple nanobeam based on nonlocal strain gradient theory and surface effects. *Mech Mater* 139:103209

Publisher's Note Springer Nature remains neutral with regard to jurisdictional claims in published maps and institutional affiliations.